Processing of CD74 by the intramembrane protease SPPL2a in B cells:

Impact on endosomal trafficking and signaling

Dissertation in fulfillment of the requirement
for the degree “Dr. rer. nat.” at the Faculty of Mathematics
and Natural Sciences at Kiel University

submitted by

Susann Hüttl

Kiel, February 2015

Referee:	Prof. Dr. Paul Saftig
Co-referee:	Prof. Dr. Matthias Leippe
Date of oral presentation:	28th April 2015
Approved for publication:	28th April 2015

Prof. Dr. Wolfgang J.Duschl

(The decan)

I) Table of contents

I) Abbreviations

ADAM	a disintegrin metalloprotease
APC	antigen presenting cell
APP	amyloid precursor protein
BAFF	B cell activating factor
BAFFR	BAFF receptor
BCR	B cell antigen receptor
Blk	B lymphoid kinase
BMDC	bone marrow-derived dendritic cell
CD	cluster of differentiation
CLIP	class II-associated li chain peptide
DAG	diacylglycerol
DAPI	4',6-diamidino-2-phenylindole
DMSO	dimethyl sulfoxide
DNA	deoxyribonucleic acid
DNA-PK	DNA-dependent protein kinase
EBF	early B cell factor
EEA1	early endosomal antigen 1
eEF2	eucaryotic translation elongation factor 2
EGF	epidermal growth factor
ER	endoplasmic reticulum
ERK1/2	extracellular signal-regulated kinase 1/2
FasL	Fas ligand
FCS	fetal calve serum
FITC	fluorescein isothiocyanate
FO	follicular
FoxO1	forkhead box subgroup O 1
GM-CSF	granulocyte macrophage colony-stimulating factor
h	hour
Hck	hemopoietic cell kinase
HEK	human embryonic kidney
HEL	hen-egg lysozyme
HeLa	Henrietta Lacks
HLA	human leukocyte antigen
HSC	hematopoietic stem cell
ICD	intracellular domain
I-CLiP	intramembrane cleaving protease
Ig	immunoglobulin
IL	interleukin
IL-7R	interleukin-7 receptor
IP_3	inositol-(1,4,5)-triphosphate
ITAM	immunoreceptor tyrosine-based activation motif
IVC	individually ventilaged cages

LAMP2	lysosome-associated membrane protein type 2
LBPA	lysobisphosphatidic acid
LIMP2	lysosomal integral membrane protein type 2
LPS	lipopolysaccharide
MAPK	mitogen-activated protein kinase
MEK1/2	mitogen-activated protein/extracellular signal-regulated kinase 1/2
MHCI/MHCII	major histocompatibility complex I/major histocompatibility complex II
MIF	macrophage migration inhibitory factor
min	minutes
mRNA	messenger RNA
mTORC2	mammalian target of rapamycin complex 2
MZ	marginal zone
MIIC	MHCII compartment
NF-κB	nuclear factor κ-light-chain-enhancer of activated B cells
NTF	N-terminal fragment
OVA	ovalbumin
PDK1	phosphoinositide-dependent kinase 1
PIP_2	phosphatidylinositol-(4,5)-bisphosphate
PIP_3	phosphatidylinositol-(3,4,5)-triphosphate
PI3K	phosphoinositide 3-kinase
PLC	phospholipase C
PS	presenilin
PTEN	phosphatase and tensin homolog
PTK	protein tyrosine kinase
RAF	rapidly activated fibrosarcoma
RAG	recombination activating gene
RAS	rat sarcoma
RIP	regulated intramembrane proteolysis
RT	room temperature
RNA	ribonucleic acid
SDH	succinate dehydrogenase
SH2	Src-homology 2
SNARE	soluble N-ethylmaleimide-sensitive-factor attachment receptor
SREBP	sterol regulatory element binding protein
SPP	signal peptide peptidase
SPPL	signal peptide peptidase-like
S1P	site 1 protease
S2P	site 2 protease
TACE	TNFα-converting enzyme
Tfn	transferrin
TfnR	transferrin receptor
TNFα	tumor necrosis factor α
TRAF3	tumor necrosis associated factor receptor 3
T1/T2	transitional 1/transitional 2

1 Introduction

1.1 Regulated intramembrane proteolysis (RIP)

Proteolysis describes the irreversible hydrolysis of peptide bonds of proteins and peptides for the generation of smaller peptides or amino acids and is mediated by peptidases or proteases. The process' benefits for the cell are multifaceted and range from post-translational modifications (e.g. removal of signal peptides) and protein degradation (e.g. lysosomal and proteasomal degradation) to the regulation of cellular processes (e.g. cell cycle regulation, induction of apoptosis). Intramembrane proteolysis represents a specific form of protein degradation. Thereby, an intramembrane-cleaving protease (I-CLiP) catalyzes the hydrolysis of the transmembrane region of its substrate in the plane of a cellular membrane (Wolfe *et al*., 1999). In contrast to conventional proteolysis which takes place in aqueous environments, I-CLiPs reside within the hydrophobic lipid bilayer and mediate hydrolysis of their substrates in a water-excluding environment. Cleavage of transmembrane proteins by I-CLiPs is often embedded within the process of regulated intramembrane proteolysis (RIP) (Brown *et al.*, 2000; Lal & Caplan, 2011). The RIP process starts with the proteolytic processing of the luminal domain of the full-length substrate by one of a variety of proteases, collectively known as ectodomain sheddases (Figure 1).

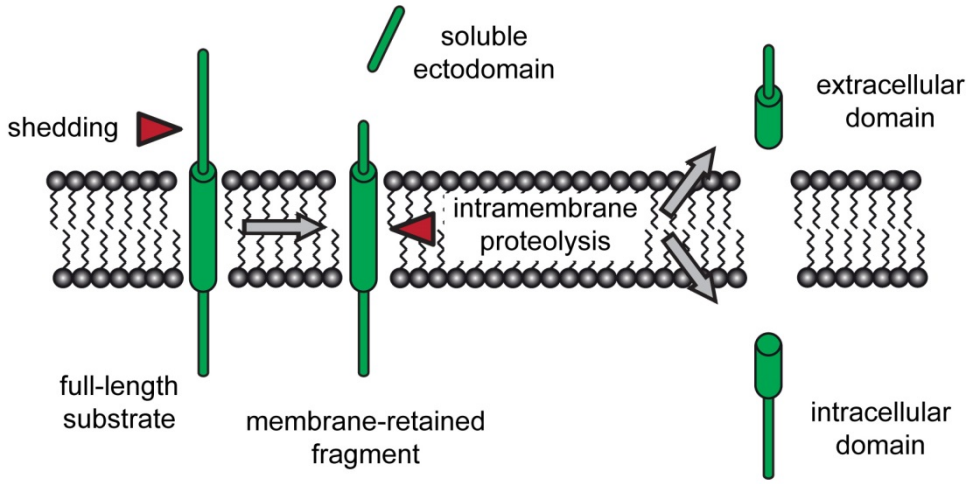

Figure 1. Scheme of the process of regulated intramembrane proteolysis (RIP), exemplified for a single-pass transmembrane protein. RIP starts with the release of the ectodomain of the transmembrane protein by the action of a sheddase. The remaining membrane-bound fragment is further processed by an intramembrane cleaving protease (I-CLiP) resulting in the release of the intracellular domain (ICD) and initiation of a cellular response.

Shedding occurs either constitutively or in a regulated manner and results in the release of the soluble ectodomain. The membrane-retained fragment is now accessible to intramembrane proteolysis by an I-CLiP leading to the release of the intracellular domain (ICD) into the cytoplasm (Figure 1). Finally, the ICD can either translocate into the nucleus and/or initiate signaling events. Furthermore, the ICD can be subjected to further degradation.

1.1.1 Intramembrane cleaving proteases (I-CLiPs)

Several proteases which are capable of mediating the processing of transmembrane proteins have been described (Weihofen & Martoglio, 2003; Wolfe, 2009a, b). Based on their catalytic center, I-CLiPs can be grouped into metallo-, serine and aspartyl proteases (Table 1).

Table 1. List of selected RIP-mediating I-CLiPs. Bold residues are involved in the catalytic activity of the protease. SPP, signal peptide peptidase; SPPL, signal peptide peptidase-like; S2P, site 2 protease. Modified from (Beel & Sanders, 2008; Weihofen & Martoglio, 2003)**.**

Family	I-CLiP(s)	Catalytic motif	Topology of substrates	Selected substrates
Metallo-proteases	S2P	**HE**xx**H**, L**D**G	Transmembrane protein type II	SREBP
Serine proteases	Rhomboids	Gx**S**G, **H**	Transmembrane protein type I	Spitz
Aspartyl proteases	γ-secretase	Y**D**, GxG**D**	Transmembrane protein type I	Notch 1-4 βAPP
"	SPP	"	Transmembrane protein type II	Signal peptides of MHCI, Prolactin
"	SPPL	"	"	Bri2 FasL TNFα

The first protease which was identified as an I-CLiP was the metalloprotease site 2 protease (S2P) (Rawson *et al.*, 1997). S2P is a multispanning membrane protein and contains the classical metalloprotease consensus motif HExxH and the conserved LDG sequence. The

Golgi-resident protease was described to mediate the processing of the sterol regulatory element binding protein (SREBP) within the first transmembrane domain after proteolysis of the luminal domain by the site 1 protease (S1P) (Duncan *et al*., 1998; Sakai *et al*., 1996). Processing of SREBP was described to be essential for the regulation of the cholesterol homeostasis (Brown & Goldstein, 1997).

Rhomboids were first discovered in *Drosophila melanogaster*. They belong to the group of serine proteases and span the membrane of the Golgi and the Endoplasmic Reticulum (ER), respectively, six to seven times (Lemberg, 2013). As one example, Rhomboid-1 catalyzes the release of Spitz, the membrane-bound ligand of the epidermal growth factor (EGF) receptor in *D. melanogaster*, which is finally secreted in order to activate EGF receptors on neighboring cells (Lee *et al.*, 2001).

The most prominent members of the aspartyl protease family are the presenilins (PSs), the active site of the γ-secretase complex, as well as the presenilin homologs signal peptide peptidase (SPP) and the signal peptide peptidase-likes (SPPL) (Voss *et al.*, 2013). Although the sequence homology between PSs and SPP/SPPL proteases is limited, they share two highly conserved active site motifs GxGD and YD, which are localized in two adjacent transmembrane domains and form the catalytic center of the enzyme (Figure 2) (Ponting *et al.*, 2002).

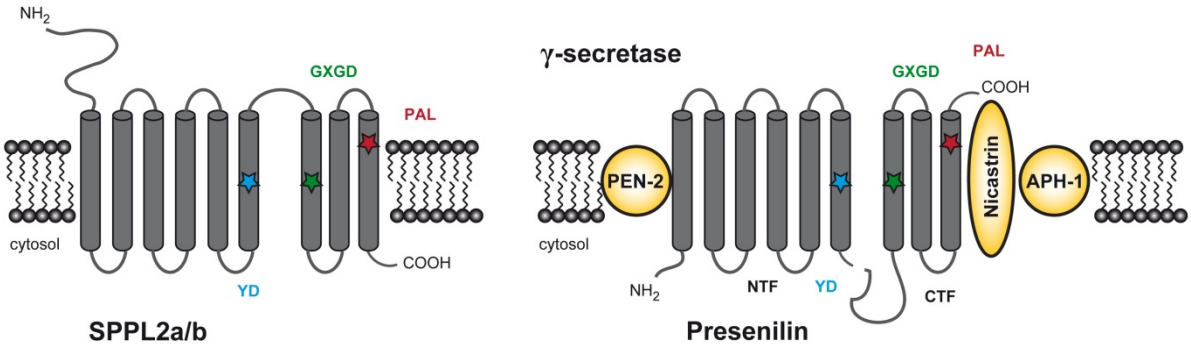

Figure 2. Schematic overview of the topology of SPPL2a/b, members of the SPP/SPPL family, and the presenilins (PSs), the catalytic part of the γ-secretase complex. Both families share the active site motifs YD and GxGD and the PAL sequence which are located in the transmembrane domain six, seven and nine. The active γ-secretase is formed upon complex assembly of PS with nicastrin, the anterior pharynx-defective 1 (APH-1) as well as the presenilin enhancer 2 (PEN-2). Modified from (Fluhrer *et al.*, 2009).

SPP/SPPLs are suggested to be active as monomers or homodimers and do not require the presence of additional interacting proteins for their activity (Nyborg *et al.*, 2004). In contrast, PSs need to assemble with the co-factors nicastrin, the anterior pharynx-defective 1 (APH-1)

as well as the presenilin enhancer 2 (PEN-2) in order to form a catalytically active γ-secretase complex (Edbauer *et al.*, 2003). Additionally, PSs and SPP/SPPLs differ in their substrate specificity. The identified substrates of PSs are type I transmembrane proteins (Haapasalo & Kovacs, 2011), whereas SPP/SPPLs process transmembrane proteins in type II orientation. Accordingly it is not surprising, that the membrane topology of PSs and SPP/SPPLs is reversed (Figure 2) (Friedmann *et al.*, 2004). Despite the fundamental differences with regard to the topology and complex formation, both protease families show a similar cleavage pattern and hydrolyze their substrates at multiple points (Steiner *et al.*, 2008; Wolfe & Selkoe, 2002; Voss *et al.*, 2013).

For the two homologs PS1 and PS2 more than 100 substrates have already been identified (Haapasalo & Kovacs, 2011). Among them is the amyloid precursor protein (APP) which is involved in the pathogenesis of Alzheimer's disease (Haass & Steiner, 2002) as well as the transmembrane receptor Notch whose C-terminal intracellular domain mediates the transcription of proteins regulating cell differentiation upon γ-secretase cleavage (Jorissen & De Strooper, 2010).

SPP cleaves remnant signal peptides resulting from their release by signal peptidases (Lyko *et al.*, 1995). As an example, major histocompatibility complex class I (MHCI) signal peptides are processed by SPP in order to generate binding epitopes for the nonclassical MHCI molecule human leukocyte antigen (HLA)-E for subsequent presentation to natural killer cells (Lemberg *et al.*, 2001).

1.1.2 Signal peptide peptidase like (SPPLs) proteases

In the human as well as murine genome, four SPPL homologs have been identified: SPPL3, which represents an independent subfamily and shows the highest homology to SPP; as well as the SPPL2 subfamily comprised of SPPL2a, SPPL2b and SPPL2c (Figure 3) (Friedmann *et al.*, 2004). The SPPL2 proteases contain a highly glycosylated N-terminus including a signal sequence (Friedmann *et al.*, 2004). SPPL2a and SPPL2b are both synthesized at the ER and sorted via the secretory pathway. Endogenous murine as well as human SPPL2a were shown to be localized in late endosomes/lysosomes (Behnke *et al.*, 2011; Friedmann *et al.*; 2006; Schneppenheim, Hüttl *et al.* 2014), whereas upon overexpression of murine SPPL2a in HeLa cells, the protease was also detectable at the cell surface (Behnke *et al.*, 2011). Lysosomal sorting of SPPL2a highly depends on a C-terminal tyrosine-based sorting motif, which is not present in the SPPL2b protein (Behnke *et al.*, 2011). Overexpressed SPPL2b is primarily

detectable at the plasma membrane (Behnke *et al.*, 2011; Friedmann *et al.*, 2006) and only to a minor extent in the Golgi apparatus (Martin *et al.*, 2008) or endocytic vesicles (Krawitz *et al.*, 2005).

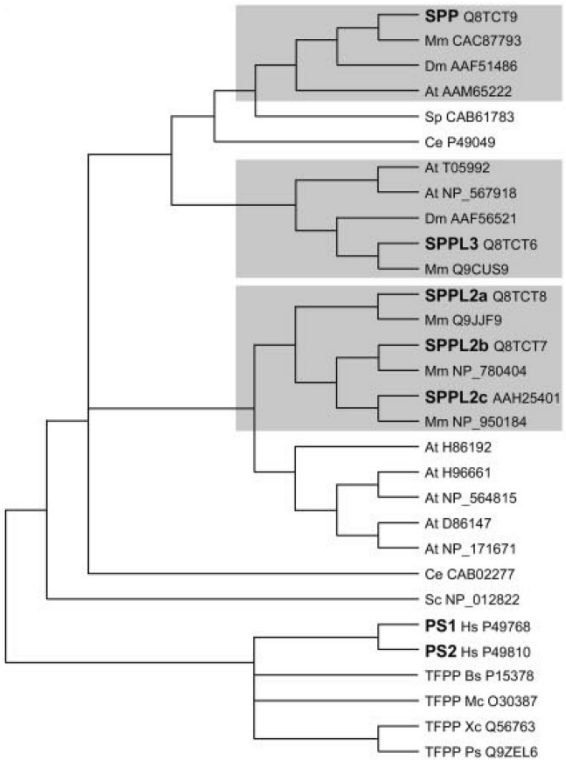

Figure 3. Phylogenetic tree of GxGD aspartyl proteases. Proteins encoded in the human genome are highlighted in bold. *Hs, Homo sapiens; Mm, Mus musculus; Dm, Drosophila melanogaster; At, Arabidopsis thaliana; Sp, Schizosaccharomyces pombe; Ce, Cenorhabditids elegans; Sc, Saccharomyces cerevisiae; Bs, Bacillus subtilis; Ps, Pseudomonas strutzer; Xc, Xanthomonas campestris; Mc, Myxococcus xanthus.* Taken from (Friedmann *et al.*, 2004)**.**

To date, SPPL2c has only poorly been studied and the physiological function of this protease remains unknown. Due to its intron-less structure and its high polymorphism, SPPL2c appears to be a pseudogene (Ponting *et al.*, 2002). Although SPPL2c harbors the characteristic GxGD motif of aspartyl proteases, no substrates have been identified until now.

1.1.2.1 Substrates of SPPL2a and -b

Except for the recently identified substrate cluster of differentiation 74 (CD74), all other substrates known for SPPL2a and SPPL2b were identified in cell-based studies. The first substrate that has been determined to be cleaved by either SPPL2a or -b was the type II transmembrane protein tumor necrosis factor α (TNFα). Processing of the transmembrane region of TNFα by SPPLs is preceded by shedding of the substrates membrane-proximal ectodomain by a disintegrin metalloprotease 17 (ADAM17, also known as TNFα-converting

enzyme (TACE)). By overexpression of TNFα and SPPL2a or -b in HeLa cells, both proteases were shown to cleave the membrane-bound N-terminal fragment (NTF) of TNFα leading to the liberation of the cytoplasmic ICD (Fluhrer *et al.*, 2006; Friedmann *et al.*, 2006). In activated dendritic cells, co-expression of either SPPL2a or -b together with the TNFα NTF leads to the liberation of the TNFα ICD that can translocate to the nucleus and mediate interleukin (IL)-12 production (Friedmann *et al.*, 2006). Intramembrane cleavage of the Fas ligand (FasL), which belongs to the TNF family, is achieved by SPPL2a after ectodomain shedding by ADAM10 (Kirkin *et al.*, 2007). The FasL mediates apoptosis and is involved in the regulation of the immune system via the NF-κB pathway (Li-Weber & Krammer, 2003). Overexpression studies in human embryonic kidney (HEK) 293T cells demonstrated that the membrane-anchored FasL NTF is processed by SPPL2a and that the liberated intracellular FasL domain is able to translocate to the nucleus thereby inhibiting gene transcription (Kirkin *et al.*, 2007). In contrast to TNFα, intramembrane proteolysis of the FasL NTF was shown to be mediated only by SPPL2a under the tested conditions. The third substrate of SPPL2a and -b is Bri2 (Itm2b) whose ectodomain undergoes processing by furin and ADAM10 prior to the cleavage by either SPPL2a or -b (Kim *et al.*, 1999; Kim *et al.*, 2002; Martin *et al.*, 2008). As shown by overexpressing SPPL2a or -b together with Bri2 in HEK 293T cells, SPPL2a- or SPPL2b-mediated intramembrane proteolysis of the membrane-bound NTF of Bri2 leads to the generation of the Bri2 ICD which is released into the cytosol (Martin *et al.*, 2008). To date, the physiological relevance of the Bri2 RIP process is unclear. However, mutations in the stop codon of the Bri2 encoding gene have been shown to cause aggregation of amyloid deposits which are associated with familial British and Danish dementia (Vidal *et al.*, 1999). Recently, two substrates have been added to the substrate list of either SPPL2a or -b. Upon co-expression of SPPL2a or SPPL2b and the corresponding substrate in HEK 293T cells, the transferrin receptor 1 (TfnR1) was cleaved by SPPL2b (Zahn *et al.*, 2013) and TMEM106B by SPPL2a (Brady *et al.*, 2014). Although SPPL2a and -b show 50 % identity and 70 % homology to each other, both proteases have a substrate overlap but do not exclusively have redundant substrate specificities. This also applies to the recently identified substrate CD74 (invariant chain, Ii), which will be introduced in 1.1.2.3.

1.1.2.2 The *in vivo* function of SPPL2a and -b

To understand the *in vivo* function of SPPL2a and -b and to identify new interaction partners of the proteases, mouse models deficient for SPPL2a (*SPPL2a*$^{-/-}$), SPPL2b (*SPPL2b*$^{-/-}$) and

SPPL2a and -b (*SPPL2a*$^{-/-}$ *SPPL2b*$^{-/-}$) were generated (Schneppenheim, Dressel, Hüttl *et al.*, 2013; Schneppenheim, Hüttl *et al.*, 2014). In detail, generation of the SPPL2a-knock-out was accomplished by insertion of a neomycin-cassette into exon 2 of the SPPL2a-encoding gene (Schneppenheim, Dressel, Hüttl *et al.*, 2013). Heterozygote mice for the insertion of a β-galactosidase genetrap in intron 2 of the *SPPL2b* gene were obtained from the CARD Institute (Kumamoto University, Japan) and bred to obtain mice homozygous for the targeted allele (Schneppenheim, Hüttl *et al.*, 2014). SPPL2a SPPL2b double-deficient mice were generated by breeding SPPL2a and -b single-deficient mice. Mice of all three strains are vital and fertile. Detailed analysis of the mice's phenotype showed considerable deficits in the adaptive immune system of *SPPL2a*$^{-/-}$ mice including a reduction of B cells in different lymphatic tissues due to an arrest of the B cell maturation at the transitional 1 (T1) stage in the spleen (Table 2). These phenotypical changes could be attributed to the missing clearance of CD74 which was, in this context, identified as first *in vivo* validated substrate of SPPL2a.

Table 2. Summary of the major phenotypical alterations of *SPPL2a*$^{-/-}$, *SPPL2b*$^{-/-}$ and *SPPL2a*$^{-/-}$ *SPPL2b*$^{-/-}$ mice. APCs, antigen presenting cells.

Mouse strain	Phenotype	Reference
***SPPL2a*$^{-/-}$**	- Reduced tooth enamel formation - Reduced number of B cells in all lymphatic tissues - Developmental arrest of B cells at splenic T1 stage - Reduced numbers of follicular and marginal zone B cells - Impaired B cell function of remaining B cells - Accumulation of endosomal vesicles in B cells - Accumulation of CD74 NTF in APCs - Reduced BCR-mediated Ca^{2+} flux	(Bronckers *et al.*, 2013; Schneppenheim, Dressel, Hüttl *et al.*, 2013)
***SPPL2b*$^{-/-}$**	- Normal tooth enamel formation - No obvious immunological phenotype - No accumulation of endosomal vesicles in B cells - No accumulation of CD74 NTF in APCs	(Schneppenheim, Hüttl *et al.*, 2014)
***SPPL2a*$^{-/-}$ *SPPL2b*$^{-/-}$**	- Phenotype comparable to *SPPL2a*$^{-/-}$	(Schneppenheim, Hüttl *et al.*, 2014)

Interestingly, SPPL2b-deficient mice did not show any obvious phenotypical changes which are related to the immune system. Additionally, ablation of SPPL2b in *SPPL2a*$^{-/-}$ mice did not exacerbate the described immunological alterations in SPPL2a single-deficient mice (Table 2)

(Schneppenheim, Hüttl *et al.*, 2014). This indicates that both proteases seem to have distinct functions *in vivo*.

Beside of its importance in the immune system of mice, SPPL2a is also essential for the formation of dental enamel (Bronckers *et al.*, 2013). *SPPL2a*$^{-/-}$ mice show decolorized incisors that are due to a lowered mineral density and an apparent dysfunction of ameloblasts. Since SPPL2a is expressed in enamel epithelium during the maturation of ameloblasts, a direct role of SPPL2a in tooth enamel formation is possible.

1.1.2.3 CD74 is an *in vivo* validated substrate of SPPL2a

CD74 is a type II transmembrane protein and is expressed in antigen presenting cells (APCs), namely B cells, macrophages and dendritic cells. Murine APCs express two isoforms of CD74, p31 and p41 (p33, p35, p43 and p45 in human). The p31 isoform consists of 217 amino acids with an N-terminal cytosolic domain, a transmembrane domain as well as a luminal domain (Figure 4 A). The p41 isoform results from alternative splicing and contains 64 additional amino acids at its C-terminus (Yamamoto *et al.*, 1985). Since the majority of the CD74 pool in murine APCs is made up of p31, it is always referred to the p31 isoform in this thesis.

CD74 mainly functions as a chaperone in major histocompatibility class II (MHCII)-restricted antigen presentation. Upon its synthesis in the ER, the CD74 MHCII complex follows the endocytic route to late endosomes where CD74 is proteolytically degraded. Moreover, a small fraction of CD74 is transported to the plasma membrane and acts as a receptor for the pro-inflammatory cytokine macrophage migration inhibitory factor (MIF) (Leng *et al.*, 2003). By binding to the extracellular domain of cell surface-localized CD74, MIF induces signal transduction pathways which causes the activation of the extracellular signal-regulated kinases 1 and 2 (ERK1/2), prostaglandin E2 production and cell proliferation. Moreover, binding of MIF to CD74 and its co-receptor CD44 was suggested to induce proliferation of B cells by activation of the the nuclear factor κ-light-chain-enhancer of activated B cells (NF-κB) (Gore *et al.*, 2008; Starlets *et al.*, 2006).

CD74 is processed by cysteine proteases and cathepsins, mainly cathepsin S (CTSS), in specialized late endosomes referred to as MHCII compartments (MIICs) (Figure 4 A) (Matza *et al.*, 2003; Villadangos & Ploegh, 2000). Proteolysis by CTSS removes the class II-associated li chain peptide (CLIP) domain and generates the membrane-bound NTF of CD74. The intramembrane protease SPPL2a was identified as the responsible protease mediating the

final cleavage of this NTF (Figure 4 A) (Beisner et al., 2013; Bergmann et al., 2013; Schneppenheim, Dressel, Hüttl *et al.*, 2013). The first substantial evidence of SPPL2a-mediated cleavage of the CD74 NTF was provided in HeLa cells upon overexpression. Overexpression of the murine p31 isoform of CD74 generates a full-length protein and N-terminal cleavage fragments when detecting CD74 with an antibody directed against the N-terminus of the protein (Figure 4 B). The NTFs are processed upon co-expression of SPPL2a, but not by its catalytically inactive form (Figure 4 B).

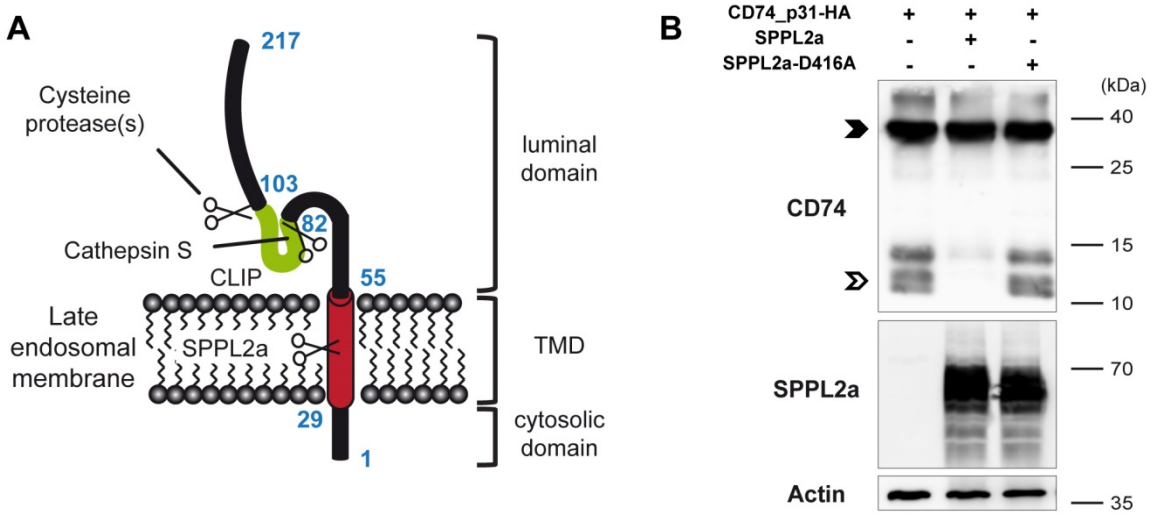

Figure 4. Topology and cleavage pattern of the CD74 protein. (A) The murine p31 isoform of CD74 consists of 217 amino acids (blue numbers) whereas the amino acids 29-55 constitute the transmembrane domain (TMD). In late endosomes, the luminal domain of the protein is processed in a stepwise manner by cysteine proteases as well as cathepsin S liberating the class II-associated li chain peptide (CLIP). Modified from (Matza *et al.*, 2003). (B) The N-terminal fragment (NTF) of CD74 is processed by SPPL2a upon overexpression. HeLa cells were transiently transfected with plasmids encoding the HA-tagged p31 isoform of CD74 as well as SPPL2a or its catalytically inactive form D416A and harvested 48 h post-transfection. After protein isolation, CD74 and SPPL2a were detected by Western Blotting with antibodies directed against the N-termini of the proteins. Full-length CD74 is indicated by a closed, CD74 NTF by an open arrowhead. Actin served as loading control.

Proteolysis of the CD74 NTF was also proven to take place *in vivo*. Analysis of mice deficient for SPPL2a showed that absence of the protease causes an accumulation of CD74 NTF in B cells (Schneppenheim, Dressel, Hüttl *et al.*, 2013) and bone marrow-derived dendritic cells (BMDCs) (Schneppenheim, Hüttl *et al.*, 2014) (Figure 5).

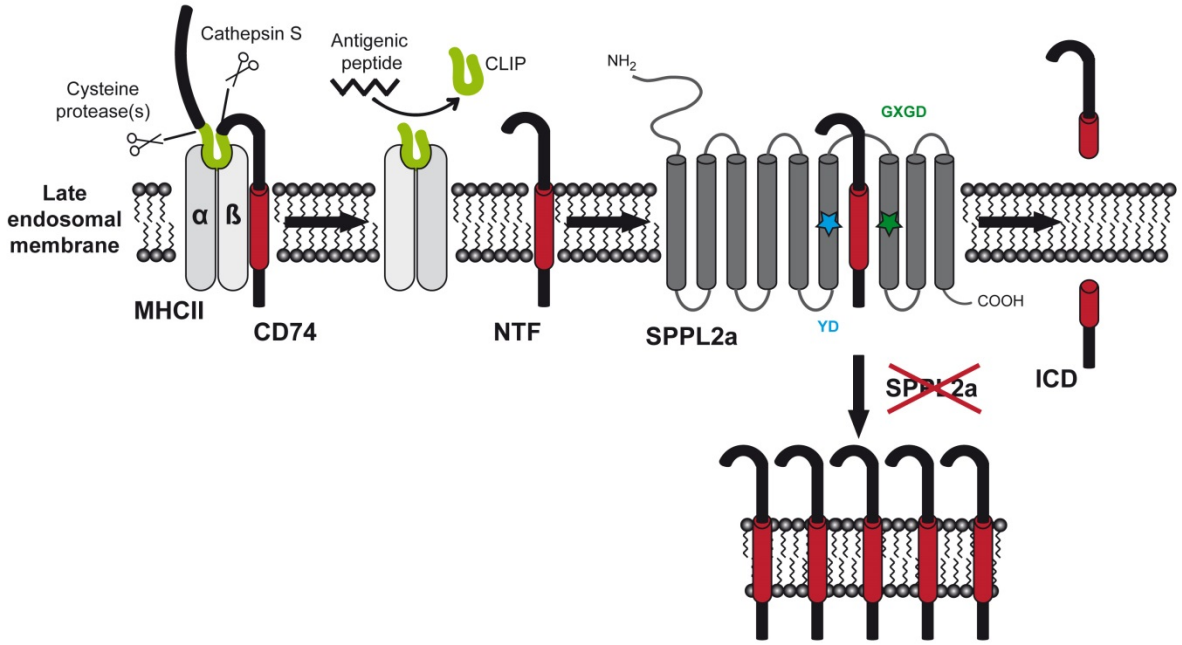

Figure 5. Schematic overview of the processing of the CD74 NTF by SPPL2a. In specialized late endosomes, CD74 and MHCII form a complex thereby masking the peptide binding groove of the MHCII complex by the class II-associated li chain peptide (CLIP) domain of CD74. Stepwise removal of the luminal domain of CD74 by cysteine proteases and cathepsin S leads to the release of the CD74 NTF. The CLIP domain remains bound to MHCII until its replacement by an antigenic peptide. The remaining membrane-bound CD74 NTF is further processed by intramembrane proteolysis mediated by SPPL2a generating the CD74 intracellular domain (ICD). Absence of SPPL2a causes an accumulation of CD74 NTFs in the late endosomal membrane. Modified from (Schneppenheim, Dressel, Hüttl *et al.*, 2013).

Interestingly, CD74 NTF processing by SPPL2b could be shown upon overexpression of both proteins, however, SPPL2b does not mediate the cleavage of CD74 *in vivo* (Schneppenheim, Hüttl *et al.*, 2014). This observation indicates that the substrate preferences of the family members SPPL2a and -b are in principal very similar. However, the differential subcellular localization of SPPL2a (late endosomes/lysosomes) and SPPLb (mainly cell surface) as well as its different tissue expression (SPPL2a ubiquitously expressed except for brain, SPPL2b predominantly expressed in brain and bone marrow) (Behnke *et al.*, 2011; Friedmann *et al.*, 2006; Schneppenheim, Hüttl *et al.*, 2014) might determine their substrates at the physiological level.

1.2 The role of B lymphocytes in the adaptive immune system

The immune system is composed of a variety of effector cells and molecules and can be grouped into the innate and adaptive immunity (Murphy, 2012). In general, both innate and adaptive immunity include the humoral (macromolecule-mediated) and cell-mediated immune response. Innate resistance mechanisms are relatively nonspecific defense mechanisms and are present in every individual. The innate immune response is induced immediately after pathogenic infection and includes antimicrobial peptides, the complement system, natural killer cells and phagocytic cells like macrophages and neutrophils carrying nonspecific pathogen-recognition receptors. In contrast, the adaptive immunity is only present in vertebrates and develops during the lifetime of the individual. Unlike the innate immunity, the adaptive immune response is highly specific and involves the action of antigen-specific lymphocytes, namely B and T lymphocytes. The billions of lymphocytes within the body collectively provide a repertoire of antigen receptors at their cell surface which enables the immune system to recognize and respond to nearly any antigen invading the body. B cells are the principal cellular mediator of the specific humoral immunity in the adaptive immune system. Binding of an antigen to the B cell antigen receptor (BCR) of a B lymphocyte induces the cells proliferation and differentiation into a plasma cell as well as the production of antibodies. Subsequently, secreted antibodies can bind and neutralize pathogens or designate them for destruction by phagocytosis. Due to their essential role in the humoral immunity, a dysregulation of B cells can cause diseases, e.g. autoimmune disorders (Boehmer & Melchers, 2010). In case of an activation of B cells that present a BCR recognizing antigens of the body, autoantibodies are secreted. If this activation persists, an immune response similar to those caused by pathogens is generated against endogenous antigens and leads to autoimmune disorders. Thus, B cell activity needs to be tightly regulated in order to guarantee a healthy immune system.

1.2.1 B lymphocyte development in mice

In order to be capable of antibody secretion, B cells need to differentiate into plasma B cells. The maturation of B lymphocytes involving different B cell stages starts in the bone marrow and finally proceeds in the spleen (Figure 6) (Hardy *et al.*, 2007; Rolink & Melchers, 1996). The differentiation highly depends on signals and cytokines provided by the microenvironment of the developing cells. These signals switch on key genes that direct the

maturation program of the cell. Like T cells and natural killer cells, B cells are derived from common lymphoid progenitor cells, which themselves originate from multipotent hematopoietic stem cells (HSCs) that can also constitute all other blood cells. This early step in B cell maturation involves expression of the IL-7 receptor (IL-7R) that transmits signals mediated by the cytokine IL-7 which is secreted by bone marrow stromal cells (Figure 6). IL-7 signaling promotes the expression of the transcription factors E2A and Early B cell factor (EBF) which in turn drive the expression of pro-B cell-specific proteins, e.g. the recombinases RAG1 and RAG2 encoded by the recombination activating genes (*RAG1* and *RAG2*) (Figure 6). RAG1 and 2 are essential for immunoglobulin (Ig) gene rearrangement, the so called V(D)J recombination, resulting in a high diversity of surface Ig (Alt *et al.*, 1992). This generates a huge receptor diversity which is the hallmark of the adaptive immune system. In brief, Igs are composed of the heavy chain μ and the light chain κ, which are both generated by the random arrangement of different gene segments clustered at a certain genetic locus.

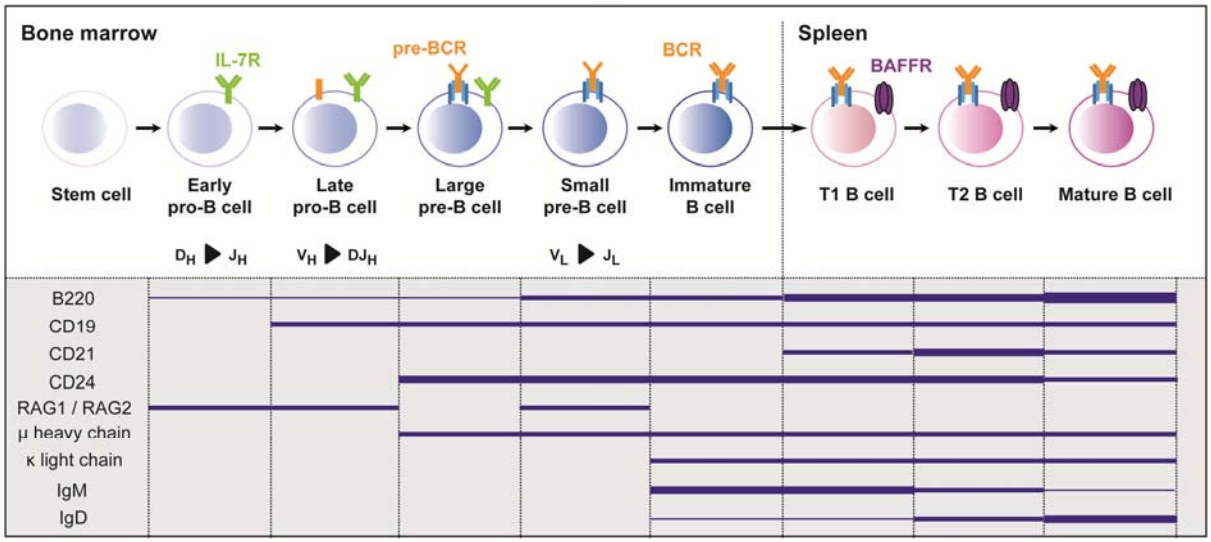

Figure 6. Overview of B lymphocyte development in mice, the expression of characteristic surface and intracellular markers as well as V(D)J recombination. In the bone marrow, B cells develop from hematopoietic stem cells via the pro- and pre-B cell stage (expressing the IL-7 receptor (IL-7R) and the pre-B cell antigen receptor (pre-BCR), respectively) into immature B cells. Meanwhile, the heavy and light chain rearrange by the help of the recombinases RAG1 and 2 leading to the formation of a functional B cell antigen receptor (BCR). Immature B cells translocate to the spleen where they start to express the B cell-activating factor receptor (BAFFR) and differentiate into mature B cells via the transitional 1 and 2 (T1, T2) stage. Expression intensity of the characteristic B cell stage markers B220, CD19, CD21 and CD24 as well as RAG1/RAG2 and the heavy (H) and light (L) chain of the BCR is depicted in blue lines. Rearrangement of the variable (V), diversity (D) and joining (J) gene segments for generation of the BCR is symbolized with arrow heads (Hardy *et al.*, 2007)**.**

The recombination process starts in pro-B cells with the joining of the diversity (D) and joining (J) segment of the heavy chain ($D_H \rightarrow J_H$) followed by the joining of the variable (V) segment ($V_H \rightarrow DJ_H$) (Figure 6) (Roth & Craig, 1998). Expression of a functional heavy chain subsequently allows the formation of the pre-BCR which is characteristic for the next developmental stage, the pre-B cell stage. After arrangement of the light chain by recombining the V and J gene segment ($V_L \rightarrow J_L$), the heavy and light chain can pair generating the complete surface IgM (Roth & Craig, 1998). Finally, IgM associates with the immunoglobulin-associated chains Igα and Igβ to form the BCR allowing the B cell to enter the immature stage (Figure 6). At this developmental stage, the BCR is tested for reactivity to self-antigens. Only non-reactive B cells are able to leave the bone marrow in order to translocate via the blood stream to the spleen. Autoreactive B cells will either be removed by apoptosis, or enter a state of unresponsiveness (anergy) or the self-reactive light chain of the BCR will be replaced by another sequence (receptor editing).

Roughly 10 % of the bone marrow-derived B cells reach the spleen whereas 1-3 % finally differentiate into mature B cells (Melchers *et al.*, 1995). In the follicles of the spleen, the immature B cells proceed their differentiation through the two defined transitional stages, called T1 and T2. Maturing splenic B cell populations can be subdivided by differential expression of the cell surface markers CD21 and CD24 (Figure 6). Signals for the survival and differentiation of B cells are mainly provided by the TNF-family cytokine B cell activating factor (BAFF) which is secreted by follicular dendritic cells (Mackay *et al.*, 2010). BAFF can induce signaling events by binding to three different receptors for BAFF, namely BAFFR, BCMA and TACI whereas the BAFFR is the most prominent one for transitional B cells (Figure 6). At the mature stage, B cells are tested for autoreactivity for a second time, since potential autoantigens are not only present in the bone marrow but also in the periphery. At this checkpoint, self-reactive B cells are eliminated by apoptosis, silenced by anergy or the receptor is edited as described above.

1.2.2 Signaling in developing B cells

1.2.2.1 BCR-mediated signaling

The BCR complex is an important mediator in humoral immunity since the activation of mature B cells and their subsequent antibody secretion depends on the binding of foreign antigens to the receptor complex. Thus, the BCR is required for the later stages of B cell

differentiation. This was experimentally proven by Lam and co-workers who showed that targeted disruption of the BCR in mature B cells inhibits the accumulation of B cells in the periphery, causes a down-regulation of MHCII and finally leads to cell death (Lam *et al.*, 1997). However, BCR-mediated signaling is also essential in early processes of B cell development since inducible deletion of Igβ in immature B cells results in apoptosis of these cells (Meffre & Nussenzweig, 2002). Differentiation of B cells from HSC into mature B cells which are finally capable of being activated by antigens is a tightly regulated process with maturation stage-specific cell decisions. Interestingly, the final cell responses depend on various parameters such as signal strength and duration, subcellular localization of the signal, participation of co-receptors and the expression of downstream effectors (Dal Porto *et al.*, 2004; Harnett *et al.*, 2005; Yankee & Clark, 2000). In developing B cells, activation of the BCR by binding of antigens results in receptor ligation and can initiate signaling events in different downstream branches including the NF-κB, mitogen-activated protein kinase (MAPK) and phosphoinositide 3-kinase (PI3K)/Akt pathway (Figure 7) (Harnett *et al.*, 2005; Kurosaki *et al.*, 2010; Niiro & Clark, 2002). BCR ligation induces tyrosine phosphorylation of the cytoplasmic immunoreceptor tyrosine-based activation motifs (ITAMs) of the BCR-associated molecules Igα and Igβ by Src-related protein tyrosine kinases (PTKs) including Lyn, Fyn and Blk (Figure 7) (Burkhardt, 1991; Clark *et al.*, 1992; Yamanashi *et al.*, 1991). The generated phospho-tyrosine residues in turn serve as docking sites for Src-homology 2 (SH2) domain-containing proteins, such as the PTK spleen tyrosine kinase (Syk) which becomes activated by phosphorylation following binding to the ITAMs (Figure 7) (Hutchcroft *et al.*, 1991; Hutchcroft *et al.*, 1992). Subsequently, activation of the different downstream effectors determines the fate of the cell.

Activation of the phospholipase C (PLC) is essential for BCR-induced activation of the classical NF-κB pathway (Figure 7) (Petro & Khan, 2001). NF-κB describes a family of transcription factors with anti-apoptotic and pro-survival functions (Barkett & Gilmore, 1999). Upon activation of PLC, the phospholipide phosphatidylinositol-(4,5)-bisphosphate (PIP_2) is hydrolyzed into inositol-(1,4,5)-triphosphate (IP_3) and the second messenger diacylglycerol (DAG) driving the release of ER-stored Ca^{2+} into the cytosol and activation of the Ca^{2+}-dependent protein kinase C. Finally, protein kinase C-mediated inactivation of the inhibitor of NF-κB (IκB) allows processing of the NF-κB family member p105 in its transcriptionally active form p50 (NF-κB1) followed by its nuclear translocation together with the family member RelA. In the nucleus, p50/RelA induces the expression of members of the anti-apoptotic Bcl-2 family, such as Bcl-2 and Bcl-X_L (Grumont *et al.*, 1998).

ERK1/2, which belong to the MAPK family, can get activated by protein kinase C as well, but also in a PLC-independent manner through the activation of the MAPKs rat sarcoma protein (RAS) and rapidly activated fibrosarcoma protein (RAF) (Figure 7) (Hashimoto *et al.*, 1998). Upon activation via phosphorylation, ERK1/2 shuttle into the nucleus and induce the activity of transcription factors driving the transcription of pro-proliferative genes. ERK1/2 are essential for proliferation and cell cycle progression in various cell types (Chambard *et al.*, 2007). In B cells, ERK1/2 are required for BCR-induced proliferation at different B cell developmental stages (Richards *et al.*, 2001; Rowland *et al.*, 2010; Yasuda *et al.*, 2008) and the expression of the cell cycle regulator cyclin D (Piatelli *et al.*, 2002).

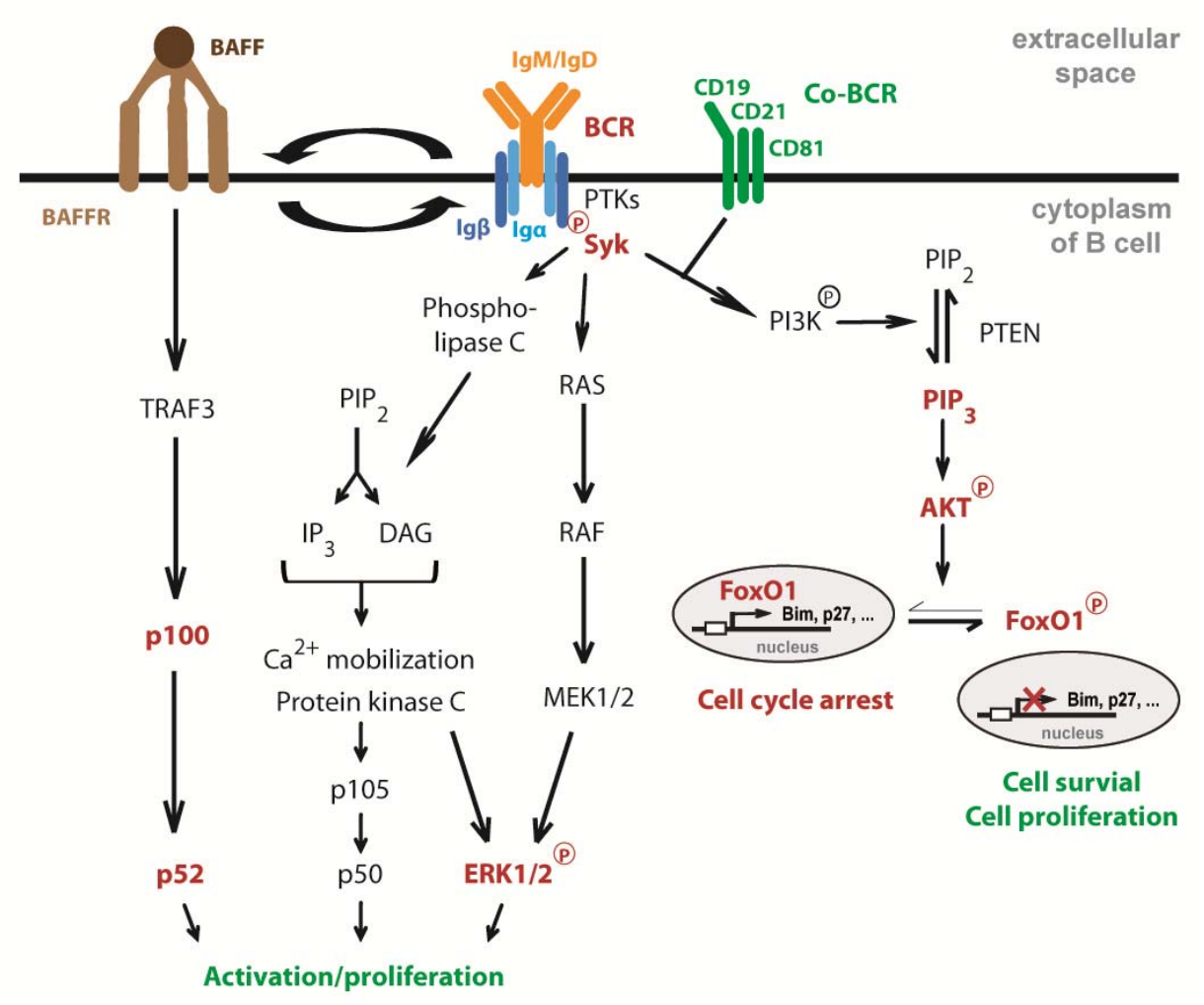

Figure 7. Overview of BCR- and BAFFR-mediated signaling pathways in developing B lymphocytes. Phosphorylation of proteins is indicated by a circled P. BAFF, B cell activating factor; BAFFR, BAFF receptor; BCR, B cell antigen receptor; DAG, diacylglycerol; ERK1/2, extracellular signal-regulated kinase 1/2; FoxO1, forkhead box subgroup O; IP_3, inositol-(1,4,5)-triphosphate; MEK1/2, mitogen-activated/extracellular signal-regulated 1/2; PIP_2, phosphatidylinositol-(4,5)-bisphosphate; PIP_3, phosphatidylinositol-(3,4,5)-triphosphate; PI3K, phosphoinositide 3-kinase; PTEN, phosphate and tensin homolog; PTK, protein tyrosine kinase; RAF, rapidly activated fibrosarcoma; RAS, rat sarcoma; TRAF3, tumor necrosis associated factor receptor 3.

The PI3 and Akt kinases are the most prominent mediators of B cell survival (Fruman *et al.*, 1999; Pogue *et al.*, 2000). Phosphorylated and activated PI3K drives the conversion of PIP_2 into phosphatidylinositol-(3,4,5)-trisphosphate (PIP_3) thereby activating Akt via phosphorylation (Figure 7). The phosphatase and tensin homolog (PTEN) acts as antagonist of the PI3K and is thereby capable to reverse the activity of this survival pathway (Sun *et al.*, 1999). The kinase Akt phosphorylates several downstream targets, including the forkhead box subgroup O (FoxO) family of transcription factors (Szydłowski *et al.*, 2014). In resting B lymphocytes, FoxO resides in the nucleus and drives the transcription of cell cycle regulating genes. Phosphorylation of FoxO by Akt leads to the stabilization of the transcription factor, its cytoplasmic sequestration and subsequent inhibition of gene transcription. Among the FoxO family members, FoxO1 has been implicated in B cell differentiation with unique roles at the different maturation stages (Dengler *et al.*, 2008). FoxO transcription factors were shown to drive the transcription of pro-apoptotic genes such as the ones coding for Bim and p27 (Dijkers *et al.*, 2000; Medema *et al.*, 2000).

1.2.2.2 Tonic ligand-independent BCR-mediated signaling

In addition to the described ligand-induced signaling, the pre-BCR and the BCR are also capable of ligand-independent signaling termed as tonic BCR signaling (Monroe, 2004; Monroe, 2006). The first solid proof was provided by Reth and co-workers. They showed that treatment of B cells with the phosphatase inhibitor pervanadate, which does not lead to BCR ligation, induces a protein phosphorylation pattern similar to that generated by BCR cross-linking (Wienands *et al.*, 1996). It was concluded that a BCR transducer complex exists which is able to constitutively generate basal signals stabilized by the inhibition of tyrosine phosphatases. At a later date it was further shown that the BCR and the associated Igα and Igβ chains need to be targeted to the plasma membrane in order to guarantee tonic signaling (Mielenz *et al.*, 2003). Currently, three models on the basis of existing data are suggested which aim to explain the mechanism underlying tonic BCR signaling: (i) The homotypic pre-BCR-binding model describes the existence of surrogate light chains within the pre-BCR which mediate self-aggregation of pre-BCR complexes (Ohnishi & Melchers, 2003); (ii) The lipid raft compartmentalization model suggests the selective association of the pre-BCR/BCR in signaling-competent lipid rafts (Guo *et al.*, 2000); (iii) The equilibrium model proposes the existence of a dynamic equilibrium of positive and negative regulatory proteins which control

the phosphorylation state of PTKs and the ITAMs of Igα and Igβ (O'Keefe *et al.*, 1996; Sato *et al.*, 1996).

The importance of tonic BCR signaling has for example been shown by the generation of a BCR complex lacking the entire transmembrane and extracellular region of Igα and Igβ (Bannish *et al.*, 2001). Since the Igα/β transmembrane proteins mediate the signal transduction function of the BCR, this mutated BCR complex is not capable of transducing signals into the cell which are generated by BCR cross-linking. Apparently, the basal signaling through this surrogate BCR complex is sufficient to facilitate the pro-B to pre-B cell transition as well as the generation of immature and mature peripheral B cells. Thus, pro-to-pre-B cell and immature-to-mature transition are dependent on tonic signaling. Moreover, ligand-independent signaling regulates receptor editing (Keren *et al.*, 2004). By reducing the level of tonic signaling by applying PI3K inhibitors, an increase in RAG2 levels was observed resulting in new Ig κ chain gene rearrangement. These studies clearly show the relevance of tonic ligand-independent signaling mediated by the BCR for the maturation and survival of developing B cells.

1.2.2.3 BAFFR-mediated signaling

Whereas expression of the BCR starts at the immature B cell stage, the BAFFR is expressed from the splenic T1 B cell stage onwards (Mackay & Schneider, 2009). The major downstream pathway which is triggered by activation of the BAFFR involves the induction of the alternative NF-κB pathway via the degradation of the NF-κB suppressor tumor necrosis associated factor receptor 3 (TRAF3) (Figure 7) (Morrison *et al.*, 2005). This finally allows processing of the NF-κB p100 protein into its transcriptionally active form p52 (NF-κB2) which associates with the family member RelB. The p52/RelB heterodimer translocates into the nucleus and is able to act as a transcription factor driving the activation and proliferation of B cells (Figure 7). One of the p52/RelB target genes encodes the anti-apoptotic protein Bcl-2 which is thought to become upregulated as a response of alternative NF-κB signaling (Claudio *et al.*, 2009; He *et al.*, 2004; Hsu *et al.*, 2002). The requirement for BAFF-mediated survival signals for full maturation of B cells beyond the T1 stage is supported by studies analyzing the effects of BAFF- or BAFFR-deficiency (Miller & Hayes, 1991; Schiemann *et al.*, 2001; Thompson *et al.*, 2001). Ablation of either the BAFF- or BAFFR-encoding gene in mice results in a B cell maturation block at the T1 developmental stage.

1.2.3 B cell subtypes in the murine system

Mature non-activated B cells, further named as naive B cells, can generally be divided into three subsets: Follicular (FO) and marginal zone (MZ) B cells that differentiated in the adult bone marrow via the pathway described in 1.2.1 (Allman & Pillai, 2008; Pillai & Cariappa, 2009) and B-1 B cells. FO B cells are a pool of recirculating B cells localized in the follicles of secondary lymphoid organs such as the spleen, lymph nodes, tonsils and Peyer's patches. This subpopulation is non-proliferating and can persist in the resting state for several months until T cell-dependent activation (1.2.4). In contrast, MZ B cells are located in the MZ of the spleen. Due to their direct connection to the blood stream they represent the major antigen filtering and scavenging area and respond very rapidly to antigen invasion in a T cell-dependent and -independent manner (1.2.4) (Pillai *et al.*, 2005). The signal intensities transduced via the BCR determine the development into either MZ (weak signals) or FO (strong signals) B cells. Besides FO and MZ B cell population, B-1 B cells exist and are abundant in the peritoneal cavity. They account for approximately 5 % of the murine B cells and originate from a different progenitor cell than FO and MZ cells in the fetal liver (Hardy & Hayakawa, 1991). B-1 cells mediate fast T cell-independent immune responses and exhibit a relatively restricted antigen-receptor repertoire.

1.2.4 Activation of B cells

Naive B cells are able to secrete antigen-specific antibodies to combat infections and prevent their spread. The response is initiated upon binding of an antigen to the BCR. The BCR can bind a variety of chemical structures including polysaccharides, proteins as well as whole virus particles and bacterial cells by recognizing epitopes on their cell surface. Upon binding of the pathogenic particle, a T cell-dependent or -independent response can be triggered depending on the type of antigen.

The T cell-dependent immune mechanisms in response to protein antigens involve both BCR-mediated signaling and BCR-mediated internalization of the bound molecule for MHCII-mediated antigen presentation to T cells. During this process, CD74 plays an important role by acting as a chaperone for the assembly and transport of MHCII complexes. Newly synthesized MHCII α and β chains (MHCIIα/β) associate with CD74 in the ER and form a nonameric $\alpha_3\beta_3li_3$ complex. Thereby, the CLIP domain of CD74 masks the peptide binding groove of the MHCII complex and prevents premature binding of antigenic peptides (Figure

8). A dileucine motif at position 7 and 8 of the cytosolic domain of CD74 mediates the transport of the $\alpha_3\beta_3li_3$ complex to specialized late endosomes, so called MHCII compartments (MIICs) (Landsverk *et al.*, 2009; Pieters *et al.*, 1993). Additionally, surface localization of the newly synthesized CD74-MHCII complex followed by rapid internalization via the endocytic pathway has been reported (Figure 8) (Bénaroch *et al.*, 1995; Roche *et al.*, 1993).

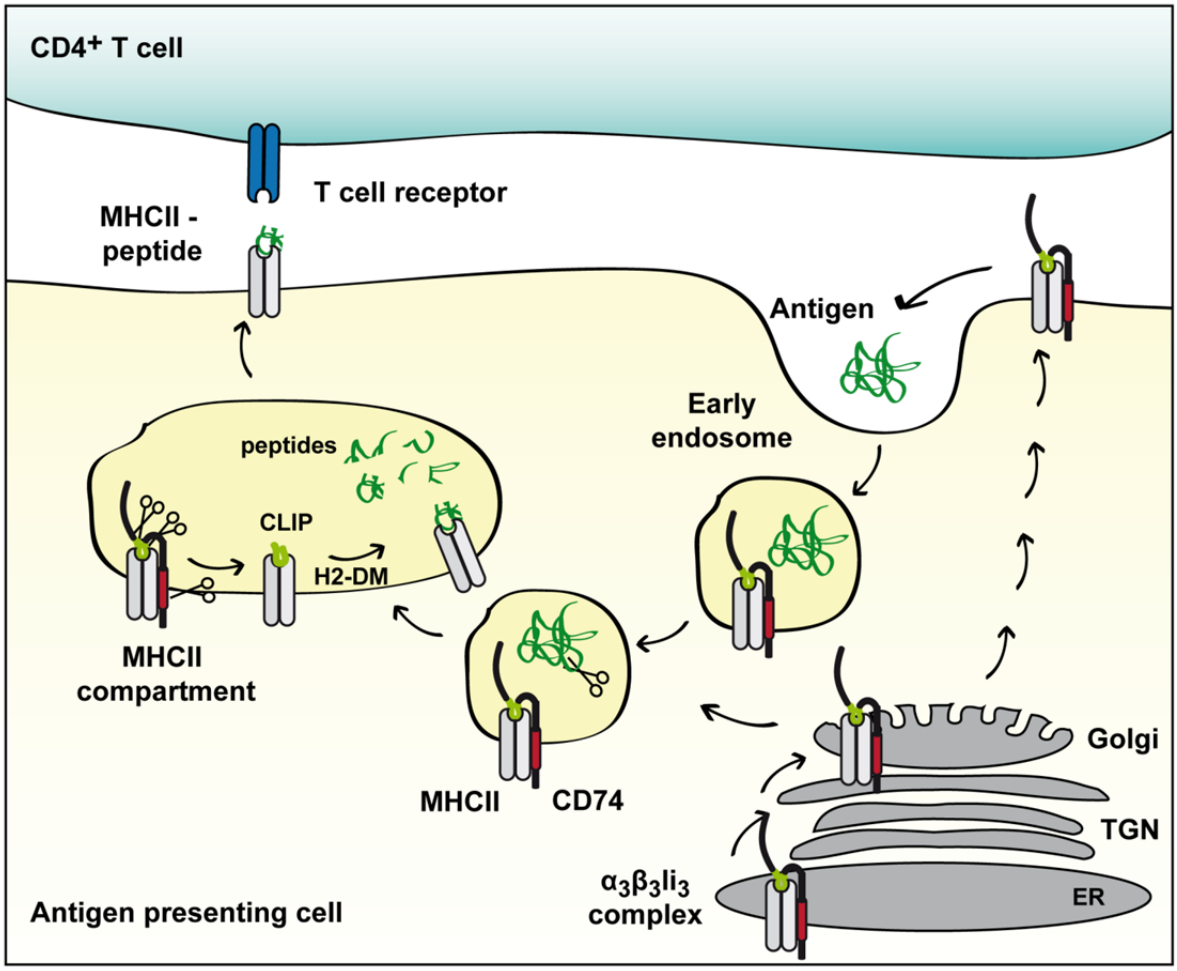

Figure 8. Schematic overview of the MHCII antigen presentation pathway. MHCII α and β chains as well as CD74 assemble in the endoplasmic reticulum (ER) in order to form a nonameric $\alpha_3\beta_3li_3$ complex. Thereby, the class II-associated li chain peptide (CLIP) of CD74 masks the peptide binding groove of MHCII and thus prevents premature binding of peptides. A sorting motif in the cytosolic domain of CD74 guarantees the transport of the $\alpha_3\beta_3li_3$ complex to MHCII compartments via the trans-golgi network (TGN) and the Golgi. In MHCII compartments, the luminal domain of CD74 is processed in a stepwise manner. After removal of the CLIP domain by the chaperone H2-DM, peptides derived from proteolysis of exogenous antigens can be bound by MHCII and are shuttled to the cell surface in order to be presented to the T cell receptor of $CD4^+$ T helper cells. Modified from (Neefjes *et al.*, 2011).

In MIICs, coordinated processing of the luminal domain of CD74 by cysteine proteases as well as cathepsins needs to take place in order to load MHCII complexes with peptides

derived from the internalization and proteolysis of exogenous antigens (Figure 8). The CLIP domain still remains to be bound to the peptide binding groove of the MHCII complex until its release which is mediated by H2-DM (Monji *et al.*, 1994; Vogt & Kropshofer, 1999). Subsequently, antigenic peptides are able to bind to MHCII followed by the translocation of the MHCII-peptide complex to the plasma membrane for presentation to $CD4^+$ T cells via their T cell receptor (Figure 8). As a consequence, cytokines are secreted by the effector T cell initiating the proliferation of the B cell. Additionally, differentiation of the B cell is induced into either an antibody-producing plasma cell or a memory B cell. Memory B cells mediate the immunological memory. They are more sensitive towards antigens than naive B cells and are able to respond rapidly if an antigen is re-exposed to the cell.

In contrast, B cells are also able to respond to antigens directly without the help of T cells. In this case naive B cells can be stimulated by some microbial constituents, such as lipopolysaccharides. However, antibodies induced by microbial antigens in general have lower affinity and are not as functional as those secreted upon T cell help. Moreover, naive B cells activated by the T cell-independent process are not able to differentiate into memory cells.

1.3 The immunological phenotype of SPPL2a-deficient mice

1.3.1 SPPL2a-deficient mice show arrested B cell maturation at the splenic T1 developmental stage

Analysis of the immunological phenotype of SPPL2a-deficient mice revealed that the adaptive immune system of these mice is massively compromised. Major macroscopical differences include a size reduction of secondary lymphoid organs such as spleen and lymph nodes and a reduction of the number of Peyer's patches in *SPPL2a*$^{-/-}$ mice in comparison to wild type control mice (Schneppenheim, 2013). Analysis of the immune cell composition in different lymphatic tissues showed a considerable decrease of B cells in bone marrow, spleen, lymph nodes, blood and the peritoneal cavity (Schneppenheim, Dressel, Hüttl *et al.*, 2013). Interestingly, the amount of pro-/pre- and immature B cells in the bone marrow as well as splenic T1 B cells of *SPPL2a*$^{-/-}$ mice are comparable to wild type mice. The reduction of B cells manifests at the splenic T2 developmental stage indicating an arrest of B cell maturation at the T1 stage (Beisner *et al.*, 2013; Bergmann *et al.*, 2013; Schneppenheim, Dressel, Hüttl *et al.*, 2013). Moreover, functionality of the remaining B cells is considerably impaired with

regard to immunoglobulin secretion upon T cell-dependent and -independent immunization. These functional deficits could clearly been ascribed to the accumulation of CD74 NTF in the absence of SPPL2a. In mice deficient for both SPPL2a and CD74, the CD74 NTF cannot accumulate. Therefore, *SPPL2a*$^{-/-}$ *CD74*$^{-/-}$ mice represent an ideal tool for the identification of CD74 NTF-specific phenotypic alterations of *SPPL2a*$^{-/-}$ mice. SPPL2a CD74 double-deficient mice only show a mild B cell maturation defect starting at the transition from the T2 to the mature developmental stage which is comparable to CD74 single-deficient mice (Schneppenheim, Dressel, Hüttl *et al.*, 2013). This clearly demonstrates that turnover of CD74 NTF is indispensable to guarantee B cell survival and differentiation beyond the T1 developmental stage.

1.3.2 CD74 NTF accumulation in B cells causes impairments of the endocytic system

Besides the considerable defect in B cell maturation, the accumulation of CD74 NTF in B cells induced by SPPL2a-deficiency impairs the endocytic system. In detail, electron microscopical analysis showed that high abundance of CD74 NTF in *SPPL2a*$^{-/-}$ B cells causes an accumulation of intracellular vesicles with mostly low electron density which cannot be detected at that this frequency in wild type B cells (Figure 9). These vesicles were shown to be positive for CD74, LAMP1 and MHCII identifying them as compartments derived from the endocytic system (Schneppenheim, Dressel, Hüttl *et al.*, 2013).

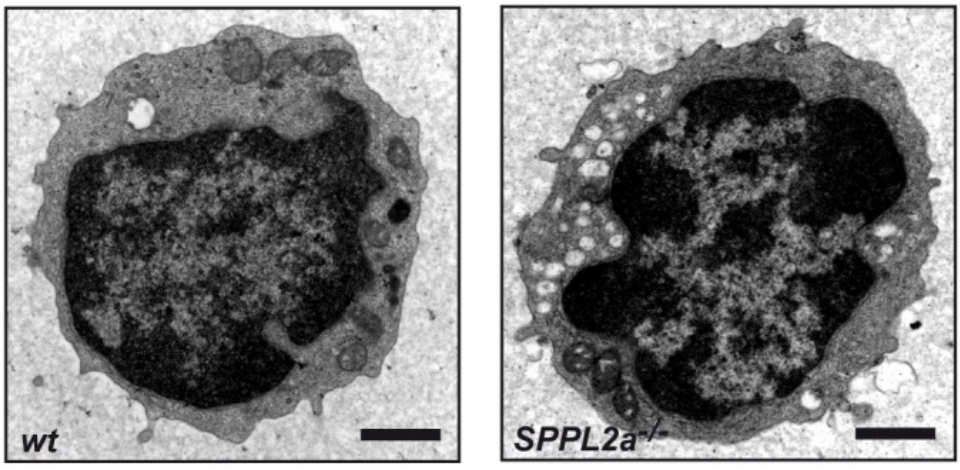

Figure 9. Transmission electron microscopy visualizes disturbances in the endocytic system of SPPL2a-deficient B cells. Cross-sections of splenic IgM^{+} B cells isolated from wild type (*wt*) and *SPPL2a*$^{-/-}$ mice are shown. Scale bar, 1 µm. Taken from (Schneppenheim, Dressel, Hüttl *et al.*, 2013)**.**

Similar to the maturation arrest, the vesicle accumulation observed in SPPL2a-deficient B cells can be restored by additional ablation of CD74 identifying the CD74 NTF as cause for the endocytic impairments. Thus it can be concluded that the NTF of CD74 has the potential to modulate membrane trafficking of the endocytic system. These observations are in accordance with cell culture-based data from Bakke and co-workers who described CD74 as a regulator of endosomal morphology and maturation. In detail, overexpression of CD74 in COS7 cells or cells stably transfected with CD74 and MHCII were identified to induce the formation of enlarged endocytic vesicles due to an increased fusion of endosomes (Nordeng *et al.*, 2002; Stang & Bakke, 1997).

1.4 Aim of the dissertation

CD74, the chaperone for MHCII-mediated antigen presentation, is sequentially processed in late endosomes. Thereby, the intramembrane protease SPPL2a mediates the final clearance of the membrane-bound N-terminal fragment (NTF) of CD74. In mice, deficiency of SPPL2a causes a significant accumulation of CD74 NTF which is associated with a B cell maturation block at the splenic T1 stage and an impairment of the endocytic system by accumulating intracellular vesicles. However, the mechanism underlying this phenotype was not known.

The first major aim of this project was to gain a profound knowledge about how the N-terminus of CD74 influences the functionality of the endocytic system. Therefore, microscopical techniques were applied to characterize the origin of CD74-containing vesicles in cell lines as well as in primary cells. Furthermore, the conduction of trafficking experiments in primary *SPPL2a*$^{-/-}$ B cells should give new insights into the question which trafficking routes are impaired. Additionally, the effect of CD74 NTF accumulation on MHCII homeostasis should be investigated.

In order to understand how SPPL2a deficiency causes the B cell maturation defect, signaling pathways which are associated with B cell survival and differentiation were analyzed in *SPPL2a*$^{-/-}$ B cells. Developing B cells are mainly dependent on signals transmitted by the B cell antigen receptor (BCR) and the B cell activating factor receptor (BAFFR). Therefore, downstream pathways mediated by these two receptors were of interest. By determining the phosphorylation status of downstream kinases in splenic B cells of *SPPL2a*$^{-/-}$ mice, namely. Syk, ERK1/2 and Akt, the activation of BCR-mediated signaling pathways was analyzed. Additionally, the transcription factor FoxO1 as one Akt target as well as distinct downstream cell cycle regulators should be analyzed in SPPL2a-deficient B cells. Finally, the obtained results should help to explain how CD74 NTF accumulation in *SPPL2a*$^{-/-}$ B cells affects the maturation and survival of these cells.

2 Materials and methods

2.1 Materials

2.1.1 Chemicals

Unless stated otherwise, all chemicals were obtained from the companies Sigma-Aldrich (Taufkirchen, Germany), Carl Roth (Karlsruhe, Germany) or Merck (Darmstadt, Germany) with the purity level *pro analysi* (p.a.).
Solutions were prepared in double distilled H_2O (ddH_2O) (Millipore, Schwalbach, Germany) if not stated otherwise. Sterilization of buffers and materials was achieved by autoclaving (Systec DX-150; Systec GmbH, Wettenberg, Germany).

2.1.2 Mouse strains

Mice were kept in a sterile environment in individually ventilaged cages (IVCs) at a room temperature of 19-21 °C, a relative humidity of 45-60 °C and a circadian rhythm of 12 h lightness and 12 h darkness. Animal care and handling were performed in agreement with the guidelines of the Christian-Albrechts-University of Kiel and authorized by the Ministerium für Energiewende, Landwirtschaft, Umwelt und ländliche Räume. Animals of one experimental setup were matched in terms of age and sex.
Generation of *SPPL2a*$^{-/-}$ mice was done by Dr. Bernd Schröder (Biochemical Institute, CAU Kiel) as described previously (Schneppenheim, Dressel, Hüttl *et al.*, 2013). Mice used for this PhD project were backcrossed for ten generations on a C57BL76N *Crl* background.
Mice deficient in CD74 (B6.129S6-*Cd74*^{tm1Liz}/J) were obtained from The Jackson Laboratory (Bar Harbor, Maine) and have been described before (Bikoff *et al.*, 1993).
SPPL2a-CD74 double-deficient mice were generated by the working group of Dr. Bernd Schröder (Biochemical Institute, CAU Kiel) by breeding *CD74*$^{-/-}$ mice with backcrossed *SPPL2a*$^{-/-}$ mice.

2.1.3 Cell lines

As a cell culture system, the two immortalized cell lines were used: Henrietta Lacks (HeLa) cell line (human cervical carcinoma cell line; DSMZ, Braunschweig, Germany), Bal17 cell line (mature mouse B cell lymphoma cell line; kind gift from Dr. Michael Engelke, University Göttingen; Kim *et al.*, 1979).

2.1.4 Bacterial strains

For amplification of plasmids, the bacterial strain *E. coli* XL1-Blue (Stratagene, La Jolla, California) was used with the following genotype: *recA1 endA1 gyrA96 thi-1 hsdR17 supE44 relA1 lac [F´ proAB lacI^{q}ZΔM15 Tn10 (Tet^r)]*.

Amplification of vectors encoding SPPL2a or its inactivate variant SPPL2a-D416A was achieved in the CopyCutter™ EPI400™ Electrocompetent *E. coli strain (Epicentre, Madison, Wisconsin) with the genotype F$^-$ mcrA Δ(mrr-hsdRMS-mcrBC) Φ80dlacZΔM15 ΔlacX74 recA1 endA1 araD139 Δ(ara, leu)7697 galU galK λ$^-$ rpsL (Str^R) nupG trfA tonA pcnB4 dhfr.* This strain is preferentially used for cloning of unstable DNA or DNA coding for toxic proteins. During the replication of CopyCutter E. coli cells, the vector copy number is kept at a low level until amplification of the vector is induced with the CopyCutter Induction Solution leading to high vector copy numbers.

2.1.5 Plasmids

In order to overexpress SPPL2a, SPPL2a-D416A, CD74 or CD74-D6R in HeLa cells, the genes coding for the named proteins were cloned into the multiple cloning site (MCS) of the mammalian expression vector pcDNA3.1/Hygro$^+$ (Life Technologies, Carlsbad, California) (Figure 10, Table 3). This vector allows constitutive high-level expression of genes in a variety of mammalian cells.

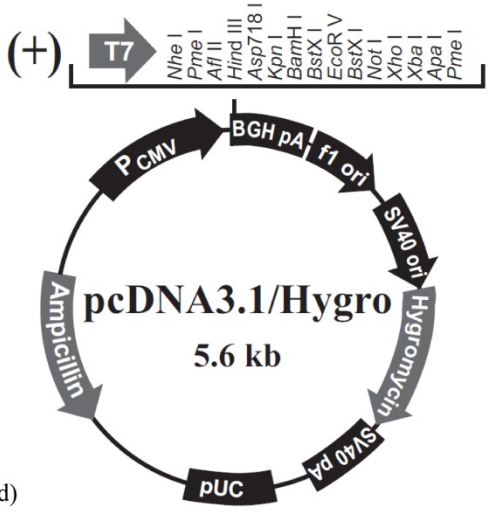

Components:

- **CMV promoter** (bases 209-863)
- **T7 promoter** (bases 863-882)
- **MCS** (bases 895-1010)
- **BGH reverse priming site** (bases 1022-1039)
- **BGH polyadenyltaion signal** (bases 1021-1235)
- **f1 origin** (bases 1298-1711)
- **SV40 promoter** (bases 1776-2100)
- **Hygromycin resistance gene** (bases 2118-3141)
- **SV40 early polyadenylation signal** (bases 3154-3526)
- **pUC origin** (bases 3786-4456, complementary strand)
- **Ampicillin resistance gene** (bases 4601-5461, complementary strand)

Figure 10. Vector map of the mammalian expression vector pcDNA3.1/Hygro$^+$. The vector consists of 5,597 base pairs and includes the components depicted at the left side. BGH, genomic bovine growth hormone gene; CMV, cytomegalo virus; MCS, multiple cloning site; pUC, plasmid University of California; SV, simian virus. The MCS is in the forward (+) orientation. Taken from Life Technologies.com.

Table 3. List of the used expression constructs.

Construct	Encoded protein	Tag	Source
mSPPL2a-Myc-pcDNA3.1/H$^+$	SPPL2a	Myc	Dr. Janna Schneppenheim
mSPPL2a-D416A-Myc-pcDNA3.1/H$^+$	SPPL2a-D416A	Myc	Dr. Janna Schneppenheim
mCD74_p31-HA- pcDNA3.1/H$^+$	CD74	HA	Dr. Bernd Schröder
mCD74_p31-D6R-HA-pcDNA3.1/H$^+$	CD74-D6R	HA	Described in 2.2.1.5.2

2.1.6 Antibodies

The following antibodies were used for indirect immunofluorescence (2.2.2.10), Western Blot (2.2.3.5) and flow cytometric analysis (2.2.3.6):

Table 4. List of the used primary antibodies.

Antibody	Clone	Vendor	Source	Conditions
Actin	JLA20	DSHB	mouse, monoclonal	WB: 1:2000 in 5 % MP
Akt	C67E7	Cell Signaling (Danvers, Massachusetts)	rabbit, monoclonal	WB: 1:1000 in 5 % BSA, FC: 1:200
BAFFR-APC	eBio7H22-E16	eBioscience	rat, monoclonal	FC: 1:200
CD19-PE	1D3	eBioscience	rat, monoclonal	FC: 1:100
CD21-PE	4E3	eBioscience	rat, monoclonal	FC: 1:100
CD24-FITC	30-F1	eBioscience	rat, monoclonal	FC: 1:100
CD24-APC	M1/69	BioLegend	rat, monoclonal	FC: 1:200
CD45R-PE-Cy7	RA3-6B2	eBioscience	rat, monoclonal	FC: 1:200
CD74	IN-1	BD Biosciences (Heidelberg, Germany)	rat, monoclonal	WB: 1:5000 in 5 % MP, IF: 1:200
CD74	P1, aa 2-27	Pineda	rabbit, polyclonal	IF: 1:200
EEA1		Cell Signaling	rabbit, monoclonal	IF: 1:200
EEA1	14/EEA1	BD Biosciences	mouse, monoclonal	IF: 1:500
eEF2	ab33523	Abcam (Cambridge, Great Britain)	rabbit, polyclonal	WB: 1:500 in 5 % MP

ERK1/2	137F5	Cell Signaling	rabbit, monoclonal	WB: 1:1000 in 5 % BSA, FC: 1:200
FoxO1	C29H4	Cell Signaling	rabbit, polyclonal	WB: 1:1000 in 5 % BSA
IgM Alexa Fluor 594	μ chain	Life Technologies	goat, polyclonal	IF: 1:100 1 h 4 °C
IgM-biotin	II741	eBioscience	rat, monoclonal	FC: 1:200
IgM-APC	II741	eBioscience	rat, monoclonal	FC: 1:200
KDEL	C10C3	Enzo Life Sciences (Lörrach, Germany)	mouse, monoclonal	IF: 1:50
LAMP2 (Radons *et al.*, 1992)	2D5	Andrej Hasilik (University Marburg)	mouse, monoclonal	IF: 1:500
LBPA	6C4	Jean Gruenberg	mouse, monoclonal	IF: 1:50
LIMP2 (Zachos *et al.*, 2012)	T2	Pineda	rabbit, polyclonal	IF: 1:500
MHCII	M5/114.15.2	eBioscience	rat, monoclonal	IF: 1:200
MHCIIβ		Willem Stoorvogel (Utrecht University)	rabbit, polyclonal	IF: 1:500
MHCII-APC	M5/114.15.2	eBioscience	rat, monoclonal	FC: 1:200
pAkt (Ser473)	D9E	Cell Signaling	rabbit, monoclonal	WB: 1:1000 in 5 % BSA, FC: 1:200
pERK1/2 (Thr202/Tyr204)	D13.14.4E	Cell Signaling	rabbit, monoclonal	WB: 1:1000 in 5 % BSA, FC: 1:200
pFoxO1 (Ser 256)	C29H4	Cell Signaling	rabbit, polyclonal	WB: 1:1000 in 5 % BSA
PIP_3	Z-B345	Echelon (Salt Lake City, Utah)	mouse, monoclonal	FC: 1:50
pSyk (Tyr519/520)	C87C1	Cell Signaling	rabbit, monoclonal	WB: 1:1000 in 5 % BSA, FC: 1:200
SPPL2a (Behnke *et al.*, 2011)	N-terminus, aa 77-94	Pineda	rabbit, polyclonal	WB: 1:200 in 5 % MP

Syk	D3Z1E	Cell Signaling	rabbit, monoclonal	WB: 1:1000 in 5 % BSA, FC: 1:200
TfnR	ab84036	Abcam	rabbit, polyclonal	IF: 1:200
TfnR-APC (CD71)	R17217	eBioscience	rat, monoclonal	FC: 1:200
β-Tubulin	E7	DSHB	mouse, monoclonal	WB: 1:1000 in 5 % MP

Table 5. List of the used secondary antibodies.

Antibody	Conjugation	Vendor	Source	Conditions
anti-mouse IgG	HRP	Dianova (Hamburg, Germany)	sheep	WB: 1:15000
anti-rabbit IgG	HRP	Dianova	goat	WB: 1:15000
anti-rat IgG	HRP	Dianova	goat	WB: 1:15000
anti-mouse IgG	Alexa Fluor 594	Life Technologies	goat	IF: 1:300
anti-rabbit IgG	Alexa Fluor 488	Life Technologies	goat	IF, FC: 1:300
anti-rabbit IgG	Alexa Fluor 594	Life Technologies	goat	IF: 1:300
anti-rat IgG	Alexa Fluor 488	Life Technologies	goat	IF: 1:300

2.2 Methods

2.2.1 Molecular biology-based methods

2.2.1.1 Isolation of total RNA

Total RNA of freshly isolated splenic $B220^+$ B cells (2.2.2.4) was isolated using the NucluoSpin® RNA Isolation Kit (Macherey-Nagel, Düren, Germany) according to the manufacturer's recommendations. RNA quality was verified by subjecting aliquots of 150ng isolated RNA to agarose gel electrophoresis (2.2.1.4).

2.2.1.2 Determination of nucleic acid concentration

Concentrations of nucleic acids were determined spectro-photometrically at an absorption of 260 nm using the Synergy HT multi detection reader (BioTek, Winooski, Vermont) and

calculated based on the Lambert-Beer law. Purity of the nucleic acid preparation was evaluated by determining the ratio $OD_{260/280}$ which should be at approximately 1.8 for pure DNA and around 2 for pure RNA.

2.2.1.3 First strand cDNA synthesis

Synthesis of first strand cDNA from total RNA templates (2.2.1.1) was achieved by using the RevertAid First Strand cDNA Synthesis Kit (Thermo Scientific, Waltham, Massachusetts). Therefore, 50-250 ng RNA and 1 µl of the supplied random hexamer primer were incubated in nuclease-free water in a total volume of 12 µl for 5 min at 65 °C to break off secondary structures of the RNA template. Reaction buffer, 20 U RiboLock RNase Inhibitor, 0.5 mM dNTP Mix and 200 U RevertAid M-MulV Reverse Transcriptase were added. Subsequently, the mixture was incubated for 5 min at 25 °C followed by 60 min at 42 °C. The reaction was terminated by heating for 5 min at 70 °C. Samples were stored at -80 °C until analysis by qRT-PCR (2.2.1.5.3).

2.2.1.4 Agarose gel electrophoresis

Tris base, acetic acid, EDTA (TAE) buffer

Tris	40 mM
EDTA	1 mM (pH 8.0)
Acetic acid	0.11 % (v/v)

Separation of DNA and RNA was achieved by agarose gel electrophoresis. Therefore, DNA samples were supplemented with Loading Dye (Thermo Scientific), RNA samples with Gel Loading Buffer II (Life Technologies) and loaded onto an agarose gel containing 333 ng/ml ethidium bromide. Dependent on the size of the separated DNA fragments, agarose (SeqKem® LE Agarose, Lonza, Rockland, Maine) concentrations between 0.8 and 2.5 % (w/v) dissolved in TAE buffer were used. Electrophoresis was performed at 120 V in TAE buffer. As size standard, the Gene Ruler 1 kb or 100 bp Plus DNA ladder (Thermo Scientific) were used. Nucleic acids were visualized by using the Gel Jet Imager (Intas, Göttingen, Germany) at a wavelength of 312 nm.

2.2.1.5 Polymerase chain reactions (PCRs)

2.2.1.5.1 Genotyping of mice

Genomic DNA was isolated from mouse tails by incubating the tail (≤ 0.5 cm) in 200 µl DirectPCR® Tail (Peqlab Biotechnologie GmbH, Erlangen, Germany) supplemented with 200 µg/ml proteinase K (Roche, Basel, Switzerland) over night at 56 °C with subsequent inactivation of the enzyme for 45 min at 85 °C. The mice's genotypes were determined by polymerase chain reaction (PCR) using the following oligonucleotides (Sigma-Aldrich):

Table 6. List of oligonucleotides used for genotyping PCRs.

Oligonucleotide	Sequence (5`- 3`)
mSPPL2a-Exon2-Fw	AAA CTC ATT GAA GGA CTT GCT C
mSPPL2a-Exon2-Rv	TTT CTA GGG AAC TTG GAA GTC
mCD74-Geno-Fw	GGC TAG GTC CCA GTG TAG GC
mCD74-wt-Rv	AAT CAG CGC TCA AGG TCA CT
mCD74-ko-Rv	CGC TGA CAG CCG GAA CAC GG

1 µl of the isolated genomic DNA was mixed with 200 nM of each SPPL2a and CD74 primer, respectively, as well as 200 nM dNTPs (Thermo Scientific, Waltham, Massachusetts), 2.5 U DreamTaq DNA Polymerase (Thermo Scientific), DreamTaq Reaction Buffer (Thermo Scientific) and 5 % DMSO in a final volume of 25 µl (Table 7). To detect *CD74*, the Fw as well as both Rv oligonucleotides were used in one reaction (Table 6).

Table 7. Components of a genotyping PCR.

Ingredients	Volume [µl]
Genomic DNA	1
10 x Dream Taq Reaction Buffer	2.5
10 µM oligonucleotide Fw	0.5
10 µM oligonucleotide Rv	0.5
2 mM dNTPs	2.5
Dream Taq Polymerase	0.25
DMSO	1.25
ddH_2O	ad 25 µl

PCR reactions amplifying the genes encoding SPPL2a and CD74 were subjected to the following protocols:

Table 8. Protocol SPPL2a Exon 2 genotyping PCR.

	Temperature	Duration	Number of cycles
Initial Denaturing	95 °C	5 min	
Denaturing	95 °C	15 s	
Annealing	55 °C	30 s	35 x
Extension	72 °C	2 min	
Final extension	72 °C	3 min	

Table 9. Protocol CD74 genotyping PCR.

	Temperature	Duration	Number of cycles
Initial Denaturing	94 °C	3 min	
Denaturing	94 °C	30 s	
Annealing	66 °C	1 min	35 x
Extension	72 °C	1.5 min	
Final extension	72 °C	2 min	

The obtained PCR products were analyzed by agarose gel electrophoresis (2.2.1.4).

2.2.1.5.2 Mutagenesis PCR

Insertion of the D6R mutation into the mCD74_p31-HA-pcDNA3.1/H^+ plasmid was achieved by mutagenesis PCR. Therefore, 10 ng of the template mCD74_p31-HA-pcDNA3.1/H^+ were mixed with 1 x *Pfu* Buffer with $MgSO_4$ (Thermo Scientific), 200 nM dNTP-mix (Thermo Scientific), 2.5 % DMSO, 200 nM of each of the oligonucleotides (Table 2.7) and 1.25 U *Pfu* DNA Polymerase (Thermo Scientific) in a total volume of 50 µl.

Table 10. List of oligonucleotides used for the cloning of mCD74_p31-D6R-HA-pcDNA3.1/H^+.

Oligonucleotide name	Sequence (5'-3')
mCD74-BamHI-Fw-D6R II	GATCGGATCCACGCCACCATGGATGACCAACGCAGGCTCATCTCTAACCATGAACAGTTGCCC
mCD74-HA-XhoI-Rv	GATCCTCGAGTCAAGCGTAGTCTGGGACGTCGTATGGGTACAGGGTGACTTGACCCAGTTC

PCR reactions for insertion of the point mutation and amplification of the mutated gene were subjected to the following protocol:

Table 11. Protocol mutagenesis PCR.

	Temperature	Duration	Number of cycles
Initial Denaturing	95 °C	5 min	
Denaturing	95 °C	30 s	
Annealing	58 °C	30 s	35 x
Extension	72 °C	2 min	
Final extension	72 °C	10 min	

The obtained PCR product was analyzed by agarose gel electrophoresis (2.2.1.4), purified (2.2.1.6) and subjected to enzymatic restriction (2.2.1.7).

2.2.1.5.3 Quantitative real-time PCR (qRT-PCR)

Gene expression was quantified by qRT-PCR using the Universal Probe Library Technology (Roche) and the UPL Set mouse (04 683 641 001). Oligonucleotides and probes were designed using the Assay Design Center (Roche) to amplify intron-spanning regions with an amplicon of <130 bp. Hydrolysis probes were labeled with the reporter dye fluorescein (5' end) and a dark quencher dye (3' end). The following oligonucleotides (Sigma-Aldrich) and hydrolysis probes were used:

Table 12. Oligonucleotides and hydrolysis probes used for qRT-PCR.

mRNA	Oligonucleotides (5'-3')	Probe No
BAFFR	Fw GCCGGACACTGGACATACA Rv GCCAGTATCAGTCCCAGGAG	1
Blk	Fw AAGCTACTGAAGCCCTGCAA Rv TTCTCACTGACCTGCCTCTTG	66
Bim	Fw GGAGACGAGTTCAACGAAACTT Rv AACAGTTGTAAGATAACCATTTGAGG	41
eEF2	Fw GTTGACGTCAGCGGTCTCTT Rv GCACGGATCTGATCTACTGTGA	70
Fgr	Fw TTCCATCCAGGCTGAAGAGT Rv CTGGGGGTTACCAGAGGAC	34
Fyn	Fw GCAATTACGTGGCTCCAGTT Rv GCCAAGTTTTCCAAAGTACCA	58

FoxO1	Fw CTTCAAGGATAAGGGCGACA Rv GACAGATTGTGGCGAATTGA	11
Hck	Fw ACGGAGTTCATGGCCAAA Rv GCTTGCTGCCTTCTTCACTC	40
Ig μ chain (b allele, constant region of the memebrane-bound form)	Fw AGTCCACTGAGGGGGAGGT Rv GAAGGTGGAGGCAGTGGTC	73
Lyn	Fw CCAGGACAGAGATTTCAAACAA Rv TAAGGCCACCACAATGTCAC	6
MHCIIα	Fw CTCTGATTCTGGGGGTCCT Rv ACCATAGGTGCCTACGTGGT	110
MHCIIβ	Fw GTGGTGCTGATGGTGCTG Rv CCATGAACTGGTACACGAAATG	26
p27	Fw GTTAGCGGAGCAGTGTCCA Rv TCTGTTCTGTTGGCCCTTTT	62
RAG1	Fw AGGCCTGTGGAGCAAGGTA Rv GCTCAGGGTAGACGGCAAG	46
RAG2	Fw TGCCAAAATAAGAAAGAGTATTTCAC Rv GGGACATTTTTGATTGTGAATAGG	4
SDH α	Fw TGTTCAGTTCCACCCCACA Rv TCTCCACGACACCCTTCTG	71
TfnR	Fw CCCAAGTATTCTCAGATATGATTTCAA Rv CAGTCCAGCTGGCAAAGATTAT	3
Tubulin α	Fw CTGGAACCCACGGTCATC Rv GTGGCCACGAGCATAGTTATT	88

Samples containing 0.5 µl cDNA (2.2.1.3), 4.5 µl LightCycler 480 Probes Master (Roche), 0.1 µM hydrolysis probe and 0.3 µM of each oligonucleotide in a final volume of 10 µl were analyzed on a Light Cycler 480 Instrument II (Roche). All assays were performed in duplicates. With the exception of *RAG1* and *RAG2*, primer efficiency (E) was calculated for each sample and gene: $E=10^{-1/slope}$. ΔCp (crossing point) was calculated by normalizing the Cp of each assay to the average Cp of the reference genes eEF2, tubulin α and SDH α of the same assay. Finally, ΔΔCp was calculated ($\Delta\Delta Cp=E^{-\Delta Cp}*100$). For *RAG1* and *RAG2*, E was adjusted to a value of 2.

2.2.1.6 Purification of DNA

DNA obtained by mutagenesis PCR product (2.2.1.5.2) was purified from agarose gel slices by using the High Pure PCR Product Purification Kit (Roche) according to the manufacturer's

instructions. Purification of DNA after restriction enzyme digestion (2.2.1.7) was achieved in solution using the same kit.

2.2.1.7 Restriction enzyme digestion

The purified PCR product (2.2.1.5.2, 2.2.1.6) was subjected to restriction enzyme digestion using the enzymes *XhoI* and *BamHI*. Therefore, 25 µl of the purified PCR product were digested in 1 x Buffer G (Thermo Scientific) with 20 U *XhoI* (Thermo Scientific) and 10 U *BamHI* (Thermo Scientific) in a total volume of 50 µl for 2 h at 37 °C. 3 µg of the empty pcDNA3.1/H^+ vector were restricted in the same way with subsequent dephosphorylation with 3 U FastAP (Thermo Scientific) for 15 min at 37 °C followed by heat activation for 5 min at 75 °C. Digestion products were analyzed by agarose gel electrophoresis (2.2.1.4) and purified (2.2.1.6).

2.2.1.8 Ligation

The restriction enzyme generated mCD74-D6R_p31-HA DNA fragment was inserted into the linearized pcDNA3.1/H^+ vector in a total volume of 20 µl containing 1 µl purified and linearized empty vector, 7 µl purified and digested insert as well as 1 Weiss U T4 DNA Ligase (Thermo Scientific) in 1 x T4 DNA Ligase Buffer (Thermo Scientific) for 15 min at RT with subsequent heat inactivation at 75 °C for 5 min. The ligation mixture was directly used for the transformation of electrocompetent *E. coli* XL1-Blue cells (2.2.1.10).

2.2.1.9 Generation of electrocompetent *E. coli* XL1-Blue cells

Luria broth (LB) medium

NaCl	10 g/l
Trypton/pepton	10 g/l
Yeast extract	5 g/l
pH 7.0	

For the generation of electrocompetent *E. coli* XL1-Blue cells an LB agar plate coated with 20 µg/ml tetracyclin was inoculated with a single *E. coli* XL1-Blue colony and grown overnight at 37 °C. Using this culture plate, a single clone was picked and transferred to 50 ml LB medium supplemented with 20 µg/ml tetracyclin, which was cultivated overnight at 37 °C under vigorous shaking. 20 ml of the *E. coli* XL1-Blue overnight culture were used to

inoculate 1 l LB medium supplemented with 20 µg/ml tetracyclin. *E. coli* were grown at 37 °C with vigorous shaking until reaching an OD_{600} of 0.5 - 0.6. Bacteria were recovered by centrifugation (31,000 x g, 15 min, 4 °C). The sediment was washed twice in 250 ml ddH_2O and finally resuspended in 100 ml ice-cold 10 % glycerin. After centrifugation (2,210 x g, 20 min, 4 °C) the bacterial pellet was resuspended in 4 ml 10 % glycerin, divided into 50 µl aliquots on dry ice and directly transferred to -80 °C.

2.2.1.10 Transformation of electrocompetent bacteria

50 µl of electrocompetent bacteria (2.2.1.9) were thawed on ice. After the addition of 2 µl of the ligation mixture (2.2.1.8), bacteria were transferred into a precooled electroporation cuvette (Peqlab, Erlangen, Germany) and electroporated at 2.5 kV, 25 µF and 400 Ω by using the Gene Pulser (BioRad, Munich, Germany). Subsequently, 1 ml pre-warmed LB medium were added and bacteria were grown for 30 min at 37 °C. After sedimentation at 2000 x g for 10 min, bacteria were resuspended in 100 µl LB medium, plated onto an LB agarplate containing 50 µg/ml ampicillin (Sigma-Aldrich) and grown overnight at 37 °C.

2.2.1.11 Amplification and isolation of plasmid DNA

For small-scale amplification, 5 ml LB medium supplemented with 50 µg/ml ampicillin (Sigma-Aldrich) were inoculated with a single bacterial colony by using a sterile toothpick. For medium-scale amplification, 50 µl of corresponding electrocompetent *E. coli* (2.2.1.9) were transformed with 1 ng of plasmid DNA by electroporation (2.2.1.10) and directly added to 100-200 ml LB medium supplemented with 50 µg/ml ampicillin. Bacteria were grown overnight at 37 °C with vigorous shaking. Plasmid DNA was isolated by using the GeneJet Plasmid Miniprep Kit (Thermo Scientific) for small-scale or the Pure Yield Plasmid Midiprep System (Promega, Madison, Wisconsin) for medium-scale isolation according to the manufacturer's instructions.

Amplification of SPPL2a-encoding plasmids was conducted in CopyCutter™ EPI400™ Electrocompetent *E. coli*. After overnight growth at 37 °C with vigorous shaking, amplification of the plasmids was achieved by adding 1 x CopyCutter™ Induction Solution (Epicentre) and an additional incubation at 37 °C for 4 h. Plasmid DNA was isolated as described above.

2.2.1.12 Sequencing of plasmids

The cloned mCD74_p31-HA-pcDNA3.1/H^+ plasmid was sequenced by the company GATC Biotech (Konstanz, Germany) using the CMV-Fw oligonucleotide as starting point. Sequencing reactions were performed according to the chain-termination method (Sanger & Nicklen, 1977). Data were analyzed using the software BioEdit (Ibis Biosciences, Carlsbad, California).

2.2.2 Cell biological methods

2.2.2.1 Culturing of cell lines

Handling of cell lines was carried out under a laminar flow work bench in an aseptic work area.

Dulbecco's Modified Eagle's Medium (DMEM) complete

DMEM with 4500 mg/L glucose, L-glutamine, $NaHCO_3$ and pyridoxine HCL (PAA; Sigma-Aldrich) supplemented with:

FCS (Biochrom, Berlin, Germnany)	10 % (v/v)
Penicillin (Sigma-Aldrich)	100 U/ml
Streptomycin (Sigma-Aldrich)	100 µg/ml

RPMI complete

RPMI-1640 with L-glutamine and $NaHCO_3$ (PAA, Cölbe, Germany; Sigma-Aldrich) supplemented with:

FCS	10 % (v/v)
Penicillin	100 U/ml
Streptomycin	100 µg/ml
β-Mercaptoethanol (Life Technologies)	50 µM

HeLa cells were cultured in 10 cm culture dishes at 37 °C and 5 % CO_2 in DMEM complete. Cells were passaged twice a week at a confluence of approximately 80 % by detaching the cells with accutase (PAA; eBioscience, San Diego, California) and seeding them onto a new cell culture dish with a dilution factor of 1:10.

Bal17 B lymphoma cells were cultured in suspension in 75 cm^2 cell culture flasks with hydrophobic surface at 37 °C and 5 % CO_2 in RPMI complete. Cells were passaged every second to third day by replacing approximately 90 % of the cell suspension by fresh medium.

2.2.2.2 Determination of cell number

In order to determine the number of viable cells, cells were stained with the dye trypan blue which is absorbed by dead cells. Therefore, an appropriate dilution of cells was mixed with trypan blue (0.4 %, Life Technologies) in a dilution of 1:2. Cells were counted by using the C-Chip Neubauer Improved Disposable Hemocytometer (NanoEnTek Inc, Seoul, Korea). Calculation was done according to the manufacturer's instructions.

2.2.2.3 Transfection of mammalian cells

Phsophate buffered saline (PBS)

NaCl	137 mM
Na_2HPO_4	10 mM
KCl	2.7 mM
KH_2PO_4	1.8 mM
pH 7.4	

HeLa cells were transfected with the TurboFect Transfection Reagent (Thermo Scientific). Cells were seeded onto 6-well cell culture plates in order to reach a confluence of approximately 70 % at the day of transfection. For transfection, a total amount of 2 µg DNA was diluted in 200 µl DMEM. In the case of transfecting CD74-encoding plasmid only, 1 µg of empty pcDNA3.1/H^+ vector were added to guarantee equal DNA amounts. After adding 4 µl TurboFect Transfection Reagent, the mixture was incubated for 15 min at room temperature and pipetted drop wise onto the cells. Media was replaced by fresh DMEM complete 5 h after transfection. Cells were typically harvested 48 h post transfection with a cell scraper in PBS supplemented with Complete Protease Inhibitor Cocktail (Roche) and washed once in the same buffer by centrifugation (210 x g, 10 min, 4 °C). Cells were pelleted and stored at -20 °C until use. For the purpose of indirect immunofluorescence, cells were seeded onto coverslips one day prior to transfection. Transfection was carried out as described above.

2.2.2.4 Isolation of primary B cells

MACS buffer

EDTA	2 mM
BSA (Albumin fraction V) in PBS	0.5 % (w/v)

$B220^+$ B cells were isolated by positive selection from murine spleens by using the magnetic-activated cell sorting (MACS®) system (Miltenyi Biotec, Bergisch-Gladbach, Germany). To obtain a single cell suspension, spleens were cut into pieces and passed through a 100 µm cell strainer (BD Bioscience) in 15-45 ml of MACS buffer. Splenocytes were collected by centrifugation (210 x g, 10 min, 4 °C) and resuspended in 630 µl MACS buffer. After addition of 70 µl B220 MicroBeads, cell suspension was incubated for 15 min at 4 °C with subsequent pelleting (210 x g, 10 min, 4 °C) and recovery in 500 µl MACS buffer. An LS column was inserted into the MACS Separator and equilibrated by rinsing with 3 ml MACS buffer. The cell suspension was applied onto the prepared column and unlabeled cells which passed through were collected. Columns were washed three times with 3 ml MACS buffer. After removal of the LS column from the separator, magnetically labeled cells were flushed out in 5 ml MACS buffer by applying a plunger. The obtained cells were further used for qRT-PCR (2.2.1.5.3), Lysotracker staining (2.2.2.11) or Western Blot analysis (2.2.3.4).

For indirect immunofluorescent staining of B cells, total splenic B cells were isolated untouched by negative selection using the Pan B cell isolation Kit (Miltenyi Biotec). Therefore, the cell number of the splenocyte suspension was determined and cells were resuspended in 40 µl MACS buffer per 10^7 total cells. After addition of 10 µl Pan B Cell Biotin-Antibody Cocktail per 10^7 total cells, cell suspension was incubated for 10 min at 4 °C. 30 µl cold MACS buffer and 20 µl Anti-Biotin MicroBeads per 10^7 cells were added and incubated for additional 15 min at 4 °C. An LD column was placed in the magnetic field of the MACS Separator and rinsed with 2 ml MACS buffer. The cell suspension was applied onto the column following two washing steps with 2 ml MACS buffer each. Thereby, unlabeled cells corresponding to the Pan B cell fraction were collected. Cells were directly used for staining by indirect immunofluorescence (2.2.2.10). Purity of the obtained B cells was assessed by flow cytometric analysis after labeling the cells with anti-IgM-APC or anti-CD45R-PE-Cy7, respectively (2.2.3.6.1). Purity was determined to be between 80 and 90 %.

Blocking of SPPL2a activity was achieved by applying SPPL inhibitors. Therefore, freshly isolated wild type splenocytes were cultivated overnight at 37°C in RPMI 1640 complete in the presence of 10 µM $(Z\text{-}LL)_2$-ketone (Peptanova) and 1 µM inhibitor X (EMD Millipore).

2.2.2.5 Generation of bone marrow-derived dendritic cells (BMDCs)

BMDCs were generated according to (Lutz *et al.*, 1999) with some modifications. Therefore, cells were isolated from the red bone marrow of tibia and femur of a mouse by flushing the bones with a 27G cannula (BD Biosciences) with cold PBS (PAA). Bone marrow cells were filtered through a 100 µm cell strainer to obtain a single cell suspension. After centrifugation (210 x g, 10 min, 4 °C), the number of viable cells was determined by trypan blue staining (2.2.2.2). 5 x 10^6 cells were seeded per 10 cm culture dish designed for suspension cells in 10 ml RPMI complete supplemented with 20 ng/ml murine granulocyte-macrophage colony-stimulating factor (mGM-CSF, Immunotools, Friesoythe, Germany) and cultured at 37 °C and 5 % CO_2. Three days after the isolation, 10 ml RPMI complete supplemented with 20 ng/ml mGM-CSF were added. At day six, 10 ml culture medium were withdrawn, the contained cells pelleted by centrifugation (210 x g, 10 min, RT), resuspended in 10 ml RPMI complete + 10 ng/ml mGM-CSF and added to the culture dish. Eight days after cell isolation, BMDCs were stimulated with 1 µg/ml *Escherichia coli*-lipopolysaccharide (L8274, Sigma-Aldrich) for 24 h or left unstimulated. For indirect immunofluorescence (2.2.2.10), adherent as well as suspension cells were used.

2.2.2.6 Enrichment of immature B cells

Iscove's Modified Dulbecco's Medium (IMDM) complete

IMDM with GlutaMAX™ (Life Technologies) supplemented with:

FCS	10 % (v/v)
Penicillin	100 U/ml
Streptomycin	100 µg/ml
β-Mercaptoethanol	50 µM
non-essential amino acids (Sigma-Aldrich)	1 x

In order to enrich immature $B220^+$ IgM^+ B cells according to (Rowland, Leahy, *et al.*, 2010), red bone marrow cells were isolated from femurs, tibias and brachiums of mice as described in 2.2.2.5 and cultivated in IMDM complete in the presence of 5 ng/ml IL-7 (BioLegend, San Diego, California) for 4 days at 37 °C and 5 % CO_2. At day 4, cells were washed twice in

PBS and cultured overnight in fresh complete IMDM without IL-7 prior to flow cytometric analysis.

2.2.2.7 Electron microscopy

The morphology of the intracellular IgM-containing vesicles in primary splenic B cells was analyzed by electron microscopy after internalization of IgM MicroBeads. Therefore, splenocytes were labeled and isolated by positive selection in MACS buffer using IgM MicroBeads and LS columns of the MACS cell separation system according to the manufacturer's recommendations and as described for $B220^+$ sorting in 2.2.2.4. Isolation was carried out strictly at 4°C to avoid any internalization of the IgM-labeled BCR complexes. Isolated cells were resuspended in pre-warmed RPMI complete and internalization of the Microbead-BCR complex was allowed for 20 min at 37°C. Subsequently, cells were fixed in 4 % PFA and 0.1 % glutaraldehyde in 0.1 M phosphate buffer, pH 7.4 in suspension for 90 min at room temperature, transferred to 2 % PFA in 0.1 M phosphate buffer, pH 7.4 and stored at 4 °C until further processing. Further processing of fixed cells was carried by Dr. Michaela Schweizer, ZMNH Hamburg. For postembedding immunogold labeling, small pieces of cryoprotected B cell pellets (2.3 M sucrose) were mounted on specimen holders and immersed in liquid nitrogen. Ultrathin sections (70 nm) were cut according to (Slot & Geuze, 2007) and collected on Carbon-Formvar-coated copper grids (Science Services GmbH, Munich, Germany). Sections were examined in an EM902 (Zeiss, Oberkochen, Germany) and pictures were taken with a MegaViewIII digital camera (A. Tröndle).

2.2.2.8 BCR stimulation with IgG/IgM

For the purpose of inducing signaling cascades downstream of the BCR, BCR was cross-linked by anti-IgG/IgM. For analysis of signaling events by immunoblotting, an adequate amount of $B220^+$ B cells (2.2.2.4) was resuspended in 500 µl RPMI complete and incubated for 15 min at 37 °C and 5 % CO_2. BCR stimulation was performed for 5 min at 37 °C after adding $F(ab)'_2$ goat anti-mouse IgG/IgM (H+L) (Dianova) at a final concentration of 10 µg/ml. A negative control was left untreated. Thereafter, cells were collected immediately by centrifugation (210 x g, 10 min, 4 °C) and washed once in PBS supplemented with 1 x Complete Inhibitor Cocktail (Roche) and PhosphoStop Phosphatase Inhibitor Cocktail (Roche). The cell pellet was stored at -20 °C until protein extraction (2.2.3.1).

For flow cytometric analysis, an adequate amount of splenocytes (freshly isolated or treated overnight with SPPL inhibitors, 2.2.2.4) or immature $B220^+$ IgM^+ B cells (2.2.2.6) were transferred in 500 µl PBS and equilibrated to 37 °C for 15 min in a CO_2 incubator. BCR stimulation was carried out as described above. Immediately after stimulation, cells were fixed by the addition of 1.5 ml 5 % paraformaldehyde (PFA) for 20 min on ice. Analysis of pERK, pAkt and pSyk levels was carried out as described in 2.2.3.

2.2.2.9 Endocytosis assays

2.2.2.9.1 Ovalbumin-FITC endocytosis assay

To examine the efficiency of fluid-phase cargo degradation an Ovalbumin (OVA) endocytosis assay was performed. Murine spleens were cut into pieces and passed through a 100 µm cell strainer in an adequate amount of MACS buffer. Splenocytes were collected by centrifugation (210 x g, 10 min, 4 °C) and recovered in 10 ml MACS buffer. From now on, cells were kept on ice unless otherwise described. Cell number was determined (2.2.2.2) and adjusted to 1.6×10^8 cells / ml in RPMI complete after an additional centrifugation step (210 x g, 10 min, 4 °C). 2.4×10^7 cells were pulsed in an 1.5 ml reaction tube with 250 µg/ml OVA-FITC (Life Technologies) in RPMI complete in a final volume of 600 µl for 30 min at 37 °C and 5 % CO_2. Additionally, as a negative control 0.4×10^7 cells were incubated in 250 µg/ml OVA-FITC and RPMI complete in a final volume of 100 µl for 30 min on ice. As far as possible, samples were protected from light. After the pulse, cells were washed three times in ice cold PBS by centrifugation (210 x g, 10 min, 4 °C). The negative control was recovered in 100 µl ice cold RPMI complete and 200 µl ice cold PBS and transferred to a 96-well round bottom tissue culture plate on ice. Pulsed cells were resuspended in 600 µl prewarmed RPMI complete and divided into six 100 µl aliquots onto a 96-well round bottom tissue culture plate and chased for 0 and 0.5, 1.5, 3, 6 and 24 h at 37 °C and 5 % CO_2. At the mentioned time points, the 100 µl sample was transferred to the 96-well round bottom tissue culture plate on ice and the chase was stopped by adding 200 µl ice cold PBS. After 6 h of chase, the collected samples were pelleted by centrifugation (210 x g, 10 min, 4 °C) and labeled with anti-CD45R-PE-Cy7, anti-CD21/35-PE and anti-CD24-APC for 30 min at 4 °C. Erythrocytes were lysed by incubation in 1 x FACS Lysing Solution (BD Biosciences) for 10 min at RT. After an additional washing step in MACS buffer, samples were subjected to flow cytometric analysis using the FACSCanto and the FACSDiva Software. B cells were gated into the subpopulation T1 ($B220^+$ $CD21^{low}$ $CD24^{high}$) and non-B cells ($B220^-$). The median

fluorescence intensity (MFI) of the FITC channel of the two subpopulations was determined. The 24 h sample was analyzed in the same way the day after. The MFI of the negative control was subtracted from the MFI of all time points and the MFIs were normalized to the 0 min time point of each genotype.

2.2.2.9.2 Transferrin-Alexa Flour 488 recycling assay

RPMI + penicillin/streptomycin (P/S)

RPMI-1640 with L-glutamine and $NaHCO_3$ (PAA) supplemented with:

Penicillin	100 U/ml
Streptomycin	100 µg/ml

Kinetics of endosome recycling was examined by a Transferrin recycling assay. Murine spleens were cut into pieces and passed through a 100 µm cell strainer in 15-45 ml of MACS buffer. Splenocytes were collected by centrifugation (210 x g, 10 min, 4 °C) and recovered in 10 ml MACS buffer. From now on, cells were kept on ice unless stated otherwise. The cell number was determined (2.2.2.2) and adjusted to 1.6 x 10^8 cells / ml in RPMI complete after an additional centrifugation step (210 x g, 10 min, 4 °C). 4.8 x 10^6 cells were serum-deprived for 3 h in RPMI + P/S at 37 °C and 5 % CO_2 in a 6 cm cell culture dish in a final volume of 5 ml. Cells were washed once in 500 µl Earle's balanced salt solution (EBSS; Sigma-Aldrich) by centrifugation (210 x g, 10 min, 4 °C). Binding of Transferrin was achieved by incubating the cells with 200 µg/ml Transferrin-Alexa Flour 488 (Life Technologies) in 1 ml EBSS at 4 °C for 30 min in 1.5 ml reaction tube. As far as possible, samples were protected from light. Thereafter, 200 µl of the cell suspension was washed three times with cold PBS, resuspended in 200 µl and pipetted onto a 96-well round bottom cell culture plate on ice. The remaining cells were allowed to endocytose the labeled Transferrin for 1 h at 37 °C and 5 % CO_2 and subsequently washed three times with ice cold PBS. Cells were recovered in 800 µl prewarmed RPMI + P/S, divided into eight 100 µl aliquots onto a 96-well round bottom tissue culture plate and chased for 0, 5, 10, 20, 30, 60, 120 and 180 min at 37 °C and 5 % CO_2. At the mentioned time points, 100 µl cell suspension was transferred to the 96-well round bottom tissue culture plate on ice and the chase was stopped by adding 200 µl ice cold PBS. After finishing the chase, the samples were pelleted by centrifugation (210 x g, 10 min, 4 °C) and labeled with anti-CD45R-PE-Cy7, anti-CD21/35-PE and anti-CD24-APC for 30 min on ice in MACS buffer. After erythrocyte lysis (2.2.2.9.1), samples were subjected to flow cytometric analysis using the FACSCanto™ and the FACSDiva Software (BD Biosciences). Data were

further processed using the FlowJo software (Tree Star). B cells were gated into the subpopulation T1 ($B220^{+}$ $CD21^{low}$ $CD24^{high}$) and the MFI of the FITC channel of each subpopulation was determined. MFI of the negative control was subtracted from MFI of each time point and the MFI were normalized to the 0 min time point of each genotype.

2.2.2.9.3 IgM endocytosis assay

In order to examine the kinetics of BCR internalization, an IgM endocytosis assay was established. Splenocytes (2.2.2.4) were incubated with biotin-conjugated anti-mouse IgM (II/41, eBioscience) for 30 min on ice diluted 1:200 in MACS buffer. Cells were washed twice in 1 x PBS, resuspended in 600 µl prewarmed RPMI complete and transferred onto a 96-well round bottom cell culture plate in six 100 µl aliquots. Endocytosis of the antibody-BCR complex was allowed for 0, 2, 5, 10, 20 and 30 min by incubation at 37 °C. Internalization was stopped immediately by transferring the sample to a 96-well round bottom tissue culture plate on ice and subsequent addition of 200 µl ice cold PBS. Finally, cells were stained with streptavidin-APC along with anti-CD21/35-PE, anti-CD24-FITC and anti-CD45R-PE-Cy7 in MACS buffer for 30 min on ice. After erythrocyte lysis (2.2.2.9.1), cells were analyzed flow-cytometrically using the FACSCanto™ and the FACSDiva Software (BD Biosciences). Data were further processed using the FlowJo software (Tree Star). The MFI of the APC channel was determined for T1 B cells normalized to the MFI of the 0 min time point of each genotype.

2.2.2.10 Indirect immunofluorescence

Permeabilization buffer I

Saponin	0.2 % (w/v)
in PBS	

Permeabilization buffer II

Saponin	0.2 % (w/v)
Glycin	0.12 % (w/v)
in PBS	

Blocking buffer

Saponin	0.2 % (w/v)
FCS	10 % (v/v)
in PBS	

Embedding medium

Mowiol 4-88 (EMD Millipore)	17 % (v/v)
Glycerol	33 % (v/v)
DABCO (Sigma-Aldrich)	20 mg/ml
DAPI (Sigma-Aldrich)	1 µg/ml
in PBS	

In order to analyze the subcellular localization of proteins, indirect immunofluorescence was performed in different cell types. HeLa cells were already cultured on coverslips (2.2.2.3) prior to transfection. Suspension cells required to be cultured on coated coverslips in order to adhere. Therefore, coverslips placed into cell culture dishes were coated overnight in 100 µg/ml poly-L-lysine (Sigma-Aldrich) and washed twice with ddH_2O for 1 h before use. Total splenic B cells isolated by using the Pan B Cell Isolation Kit (2.2.2.4) or Bal17 cells were seeded onto poly-L-lysine coated coverslips in RPMI + P/S and allowed to adhere for 1 h at 37 °C and 5 % CO_2. Adherend BMDCs (2.2.2.5) harvested by accutase treatment were combined with BMDCs in suspension and cultured on poly-L-lysine coated coverslips in RPMI + P/S as well. Cells were washed three times in PBS and fixation was performed in 4 % PFA for 20 min at room temperature. After three washing steps in PBS, cells were permeabilized in permeabilization buffer I for 10 min at room temperature. Residual free aldehyde groups of fixative PFA were saturated by incubation in permeabilization buffer II for 10 min at room temperature. In order to saturate any nonspecific binding sites, cells were incubated for 1 h in blocking buffer. Immunocytochemical stainings were performed overnight at 4 °C by placing the coverslips upside down in the respective primary antibodies (Table 4) diluted in blocking buffer in a wet chamber. After five washing steps in permeabilization buffer I, the coverslips were incubated with the respective fluorophor-conjugated secondary antibodies (Table 5) diluted 1:300 in blocking buffer for 1 h at room temperature. Coverslips were washed five times in permeabilization buffer I and twice in ddH_2O before mounting them on glass slides in embedding medium which contained 4-,6-diamidino-2-phenylindole (DAPI) for visualization of nuclei by intercalation with DNA.

For visualization of endocytosed BCR by indirect immunofluorescence, splenic $B220^+$ B cells (2.2.2.4) were adhered to poly-L-lysine coated coverslips as described above. Cells were cooled down and the medium was replaced by ice cold RPMI complete containing 10 µg/ml Alexa Flour 594-conjugated goat anti-mouse IgM (Life Technologies). Staining of the surface-localized BCR was performed for 30 min at 4 °C followed by two washing steps with ice cold PBS. Subsequently, cells were resuspended in pre-warmed RPMI complete and internalization of the IgM-BCR complex was allowed for 30 min at 37 °C. Cells were washed three times with ice cold PBS, fixed with 4 % PFA for 20 min and further processed as described above. Representative pictures of cells were acquired by using an FV1000 confocal laser scanning microscope (Olypmus) equipped with an U Pan S Apo 100 x oil immersion objective (N.A. 1.40) and the Olympus Fluoview Software. Images were further processed with the Adobe Photoshop software.

2.2.2.11 Visualization of acidic organelles by LysoTracker®

Acidic organelles were visualized by live cell imaging of cells stained with LysoTracker®. Therefore, an Imaging Dish 1.0 (145 µm cover glass bottom, zell-kontakt GmbH, Nörten-Hardenberg, Germany) was coated overnight in 100 µg/ml poly-L-lysine (Sigma-Aldrich) as described in 2.2.2.10. $B220^+$ cells (2.2.2.4) were resuspended in 2 ml RPMI + P/S, seeded onto the Imaging Dish and allowed to adhere for 30 min at 37 °C and 5 % CO_2. LysoTracker® Red DND-99 (Life Technologies) was added at a final concentration of 0.5 µM and the cells were cultured for additional 50 min. Thereafter, cells were washed five times with PBS and covered with 1 ml RPMI + P/S. Photographs of live cells were taken with an FV1000 confocal laser scanning microscope (Olympus) equipped with an U Plan S Apo 100 x oil immersion objective (N.A. 1.40) and the Olympus Fluoview Software. Pictures were further processed with the Adobe Photoshop software.

2.2.3 Biochemical methods

2.2.3.1 Protein extraction

Lysis buffer

Tris-HCl, pH 7.4	50 mM
NaCl	150 mM
Triton X-100	1 % (w/v)
SDS	0.1 % (w/v)
Complete Protease Inhibitor Cocktail (Roche)	1 x
Pefabloc® SC Protease Inhibitor (Carl Roth)	4 mM
Pepstatin A (Sigma-Aldrich)	0.5 mg/ml

Radioimmunoprecipitation assay (RIPA) buffer

Tris-HCl, pH 7.6	25 mM
NaCl	150 mM
NP40 (Sigma-Aldrich)	1 % (v/v)
Sodium deoxycholate (Merck)	1 % (w/v)
SDS	0.1 % (w/v)
EDTA	4 mM
Complete Protease Inhibitor Cocktail (Roche)	1 x
Pefabloc® SC Protease Inhibitor	4 mM

Pepstatin A	0.5 mg/ml

Cell pellets were thawed on ice and resuspended in an adequate volume of the respective buffer. For the detection of CD74 and SPPL2a, lysis buffer was used. Cell pellets for the detection of tyrosine kinases, p100/p52 and Bcl-2 were lysed in RIPA buffer. Cell lysis was achieved by incubation on ice for 1 h and a sonication step (level 4, 20 s, 4 °C; Branson Sonifier 450, Emerson Industrial Automation, Danbury, Connecticut). Cell debris was collected by centrifugation (10,000 x g, 10 min, 4 °C) and the protein containing supernatant was transferred into a new reaction tube. Immediately, protein concentration was determined (2.2.3.2).

2.2.3.2 Determination of protein concentration

Protein concentration of cell lysates was determined by using the bicinchoninic acid (BCA) Protein Assay Reagent (Thermo Scientific) according to the manufacturer's recommendations. For the generation of the standard curve, bovine serum albumin standards (Thermo Scientific) with a concentration ranging from 0 to 2 mg/ml were used. After measuring the absorption at 562 nm by using the Synergy HT multi detection reader (BioTek), the protein concentration of each sample was determined based on the generated standard curve. Protein lysates were processed immediately for SDS-PAGE (2.2.3.3).

2.2.3.3 SDS polyacrylamide gel electrophoresis (SDS-PAGE)

2.2.3.3.1 Tris-Glycine SDS-PAGE

SDS loading dye		SDS electrode buffer	
Tris-HCl pH 6.8	125 mM	Glycine	0.193 M
DTT	100 mM	Tris	25 mM
Glycerin	10 % (v/v)	SDS	0.1 %
SDS	1 % (w/v)		

Stacking gel buffer		Separating gel buffer	
Tris	0.5 M	Tris	1.5 M
SDS	0.4 % (w/v)	SDS	0.4 % (w/v)
pH 6.8		pH 8.8	

For size-dependent separation of proteins, typically Tris-Glycine SDS-PAGE was performed (Laemmli, 1970). Therefore, 10-20 µg of protein were denatured for 5 min at 56 °C (detection of SPPL2a) or 10 min at 95 °C (other proteins) in 1 x SDS loading dye. Samples were loaded onto an Tris-Glycine SDS-PAGE with separating gels containing 7.5, 10 or 12.5 % polyacrylamide (Table 13) depending on the molecular weight of the analyzed protein.

Table 13. **Ingredients of Tris-Glycine SDS polyacrylamide gels.**

Stock solution		**Stacking gel**	**7.5 % separating gel**	**10 % separating gel**	**12.5 % separating gel**
Stacking gel buffer	(ml)	1.35	-	-	-
Separating gel buffer	(ml)	-	2.6	2.6	2.6
30 % acrylamide (Rotiphorese® Gel 30 (37,5:1))	(ml)	1.75	2.5	3.3	4.2
ddH_2O	(ml)	3.1	4.8	4.0	3.1
Ammoniumpersulfate 10 % (w/v) in ddH_2O	(µl)	60	60	60	60
TEMED	(µl)	30	30	30	30

The electrophoretic separation of proteins was achieved in 1 x SDS electrode buffer at 80-120 V by using the Mini-PROTEAN® Electrophoresis System (BioRad). As molecular weight marker, the PageRuler Plus Prestained Protein Ladder (Thermo Scientific) and the PageRuler Broad Range Unstained Protein Ladder (Thermo Scientific) were used.

2.2.3.3.2 Tris-Tricine SDS-PAGE

<u>3 x Gel buffer</u>

Tris	3 M
HCl	1 M
SDS	0.3 % (w/v)
pH 8.45	

<u>2 x SDS loading dye</u>

Tris-HCl, pH 6.8	75 mM
DTT	20 mM
Glycerin	20 % (v/v)
SDS	2 % (w/v)
Coomassie Blue G-250	0.05 % (w/v)

Anode buffer		Cathode buffer	
Tris	100 mM	Tris	100 mM
HCl	22.5 mM	Tricin	100 mM
pH 8.9		SDS	0.1 % (w/v)
		pH ~8.25	

For an optimal resolution of proteins smaller than 30 kDa, especially the NTFs of CD74, Tris-Tricine-SDS-PAGE was performed (Schägger, 2006). 20 µg of protein were heated for 10 min at 95 °C in loading dye in a final volume of maximal 15 µl. Samples were loaded onto a Tris-Tricine-SDS-PAGE consisting of a separating gel of 16 % acrylamide, an intermediate gel of 10 % and a stacking gel of 4 % acrylamide (Table 14). The electrophoretic separation of proteins was achieved at 40–80 V by using the Mini-PROTEAN® Electrophoresis System (BioRad) whereas anode buffer was added as the lower electrode buffer and cathode buffer as the upper electrode buffer. As molecular weight marker, the Spectra Multicolor Low Range Protein Ladder was used.

Table 14. Ingredients of Tris-Tricine SDS polyacrylamide gels.

Stock solution		4 % stacking gel	10 % intermediate gel	16 % separating gel
50 % acrylamide (16, 6:1; AppliChem, Darmstadt, Germany)	(ml)	-	-	3.29
30 % acrylamide (37, 5:1)	(ml)	1.37	3.18	-
2 % Bisacrylamide (Applichem)	(ml)	0.091	0.261	0.338
3 x gel buffer	(ml)	2.5	3.33	3.33
Urea	(g)	-	-	3.6
ddH_2O	(ml)	ad 10	ad 10	ad 10
Ammoniumpersulfate 10 % (w/v) in ddH_2O	(µl)	75	50	33.3
TEMED	(µl)	7.5	10	10

2.2.3.4 Western Blotting

2.2.3.4.1 Western Blotting of Tris-Glycine SDS gels

Transfer buffer

Glycin	192 mM
Tris	25 mM
Methanol	20 % (v/v)

The transfer of proteins from Tris-Glycine SDS gels onto a nitrocellulose membrane (Whatman® Protran® nitrocellulose membrane, 0.2 µm pore size, Whatman GmbH, Dassel, Germany) was achieved by semi-dry blotting using a Trans-Blot® SD Semi-Dry Transfer Cell (BioRad). Therefore, the Tris-Glycine SDS gel, nitrocellulose membrane and four gel blotting papers (Whatman® gel blotting paper, Whatman GmbH, Dassel, Germany) were equilibrated in transfer buffer for a few minutes and mounted in the following order onto the transfer cell: anode, two sheets of gel blotting paper, nitrocellulose membrane, Tris-Glycin-SDS gel, two sheets of gel blotting paper, cathode. Transfer was performed for 2 h at 65 mA per membrane.

2.2.3.4.2 Western Blotting of Tris-Tricine SDS gels

Electrode buffer

Tris	300 mM
Acetic acid	100 mM
pH 8.6	

The semi-dry transfer of proteins from Tris-Tricine-SDS gels onto a nitrocellulose membrane was also performed with a Trans-Blot® SD Semi-Dry Transfer Cell (BioRad). The Tris-Tricine SDS gel, nitrocellulose membrane and four gel blotting papers (Whatman® gel blotting paper, Whatman GmbH, Dassel, Germany) were equilibrated in electrode buffer for a few minutes and mounted onto the transfer cell as described in 2.2.3.4.1. Transfer was performed for at least 17 h at 20 mA per membrane.

2.2.3.5 Immunodetection of Western Blots

TBS-T		Blocking buffer	
NaCl	137 mM	Milk powder	5 % (w/v)
Tris	25 mM	in TBS-T	
KCl	2,7 mM		
Tween 20	0,1 % (v/v)		

Primary antibody dilution buffer	
BSA	5 % (w/v)
in TBS-T	

In order to reduce unspecific antibody binding, the nitrocellulose membrane was immersed for at least 1 h at room temperature in blocking buffer under gentle agitation. Thereafter, the membrane was incubated with the corresponding primary antibodies (Table 4) over night at 4 °C in blocking buffer with the exception of the antibodies obtained from Cell Signaling, which were diluted in primary antibody dilution buffer.

Afterwards, the membrane was washed three times for 10 min in TBS-T at room temperature under gentle agitation. Incubation with the corresponding horseradish peroxidase (HRP)-coupled secondary antibodies (Table 5) diluted 1:15000 in blocking buffer was performed for 1 h at room temperature under mild shaking. Subsequently, the membrane was washed three times for 10 min in TBS-T and the HRP activity was detected by using the Amersham ECL Advance Western Blotting Detection Reagent (GE Healthcare, Uppsala, Sweden) and the ImageQuant LAS 4000 (GE Healthcare). Signal intensities were quantified using the ImageJ software.

2.2.3.6 Flow cytometric analysis

2.2.3.6.1 Detection of surface and intracellular proteins

To quantify surface as well as total protein levels of TfnR, IgM and MHCII in B cells, permeabilized and non-permeabilized cells were analyzed by flow cytometry. Surface expression was examined by staining splenocytes (2.2.2.4) with APC-conjugated antibodies against TfnR, IgM and MHCII, respectively, along with the CD markers CD21/35-PE, CD24-

FITC and CD45R-PE-Cy7 (Table 4) in MACS buffer for 30 min on ice. Eyrthrocytes were lysed (2.2.2.9.1) followed by washing and recovery of cells in MACS buffer.

In order to stain for total proteins, splenocytes were fixed and permeabilized in Fix/Perm buffer (BD Biosciences) for 20 min on ice. After two washing steps in Perm/Wash buffer (BD Biosciences) cells were stained for total TfnR, IgM and MHCII, respectively, along with the above mentioned surface markers for 30 min in Fix/Perm buffer and resuspended in MACS buffer. Cells were subjected to flow cytometric analysis using the FACSCanto^{TM} and the FACSDiva Software (BD Biosciences). Data were further processed using the FlowJo software (Tree Star).

2.2.3.6.2 Analysis of kinase activation

Staining buffer

BSA	0.5 %
in PBS	

In order to analyze signaling events initiated by the BCR, the phosphorylation status of the kinases Syk, ERK1/2 and Akt was determined by flow cytometry. Therefore, BCR signaling was initiated in total splenic cells and immature B220^{+} IgM^{+} B cells in 500 µl PBS (2.2.2.8). After immediate fixation of the cells for 20 min on ice by the addition of 1.5 ml 5 % PFA, the cells were pelleted by centrifugation (210 x g, 10 min, 4 °C) and permeabilized in 500 µl 90 % methanol for 10 min on ice. After washing the cells twice in 500 µl PBS, they were incubated for 10 min on ice in 600 µl staining buffer, divided into six 100 µl aliquots and transferred onto a 96-well round bottom tissue culture plate. Cells were stained simultaneously for the CD-markers CD21/35-PE, CD24-APC and CD45R-PE-Cy7 as well as either pERK1/2, ERK1/2, pAkt, Akt, pSyk and Syk (Table 4) for 1 h on ice in staining buffer. After a washing step in staining buffer, the primary antibodies directed against the different kinases were detected with a goat anti-rabbit Alexa Fluor 488 IgG (Table 5) antibody diluted 1:300 in staining buffer for 30 min on ice. Subsequently, the cells were washed once in staining buffer, resuspended in MACS buffer and analyzed using the FACSCanto^{TM} and the FACSDiva Software (BD Biosciences). Data were further processed using the FlowJo software (Tree Star). The cells were gated into the T1 subpopulation (B220^{+} CD21^{low} CD24^{high}) or B220^{+} IgM^{+} B cells. MFI for the FITC-channel was determined and the ratio of

phosphorylated versus total kinase was calculated. The obtained ratios were normalized to the unstimulated wild type ratios.

2.2.3.6.3 Analysis of PIP_3 level

Staining buffer

BSA	1 %
Saponin	0.2 %
in PBS	

For the analysis of intracellular PIP_3 levels, BCR signaling was initiated in splenocytes as described in 2.2.2.8. Subsequently, the cells were fixed in a final concentration of 1.5 % PFA in PBS for 10 min, washed once in PBS and permeabilized for 10 min in staining buffer. The cells were first stained with biotinylated anti-PIP_3 (Echelon Biosciences) in staining buffer for 30 min on ice followed by two washing steps in the same buffer. Detection of PIP_3 was achieved by incubation with streptavidin-APC (eBioscience) in staining buffer for 30 min on ice along with staining of surface markers with CD21/CD35-PE, CD24-FITC and CD45R-PE-Cy7. After washing in staining buffer and resuspension in MACS buffer, cells were subjected to flow cytometric analysis using a FACSCanto^{TM} and the FACSDiva Software (BD Biosciences). Data were further processed using the FlowJo software (Tree Star). The cells were gated into the T1 subpopulation ($B220^+$ $CD21^{low}$ $CD24^{high}$). MFI for the FITC-channel was determined and the value of each sample was normalized to the unstimulated wild type sample.

3 Results

3.1 CD74 and its role in endosome morphology and endocytic trafficking

3.1.1 CD74 overexpression leads to the formation of enlarged vesicles

The potential of CD74 to control the endosomal system with respect to vesicle size and abundance has been shown in overexpression studies (Nordeng *et al.*, 2002; Stang & Bakke, 1997) as well as in primary splenic B cells of SPPL2a-deficient mice (1.3) (Schneppenheim, Dressel, Hüttl *et al.*, 2013). In order to characterize the described vesicles caused by high abundance of CD74 in more detail, the effects of CD74 overexpression were analyzed microscopically in a cell culture-based assay. Therefore, HeLa cells were transiently transfected with the HA-tagged murine p31 isoform of CD74 and analyzed by indirect immunofluorescence. CD74-overexpressing cells were characterized by an accumulation of enlarged vesicles (Figure 11 A).

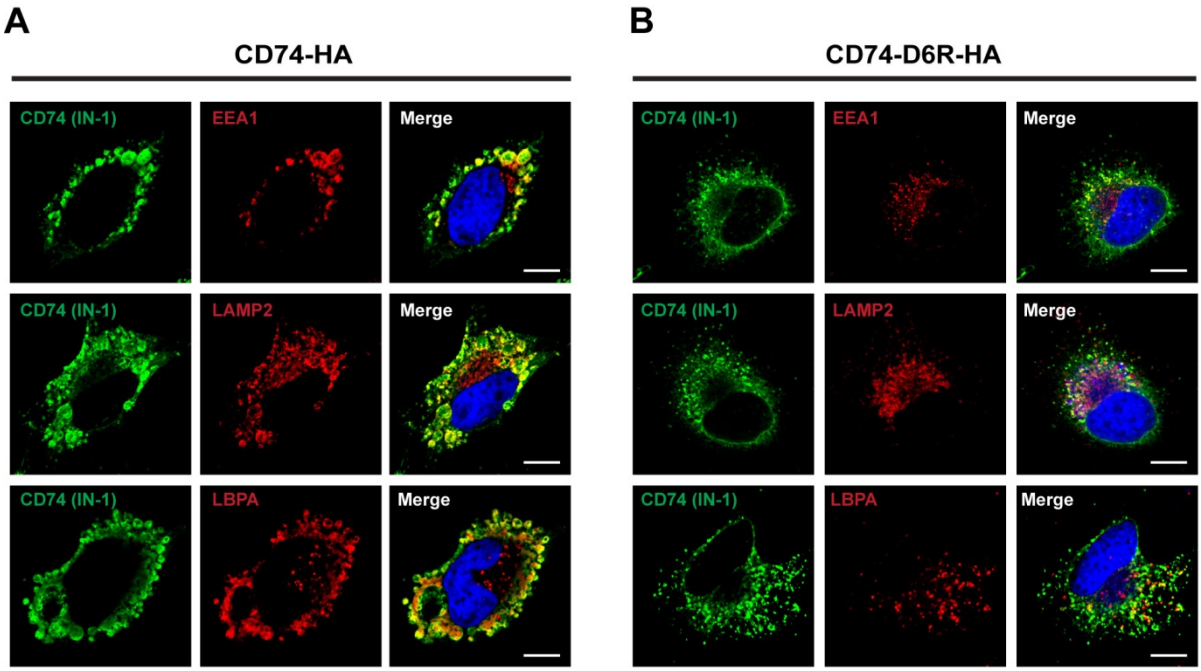

Figure 11. Overexpression of CD74 in HeLa cells induces the formation of enlarged endocytic vesicles, whereas a D6R mutation abolishes this effect. HeLa cells were transiently transfected with plasmids coding for the HA-tagged CD74 p31 isoform (A) or the mutant CD74-D6R (B). Cells were fixed 24 h post-transfection, permeabilized and stained by indirect immunofluorescence for CD74 using an antibody against an epitope of the N-terminus (IN-1) detecting the N-terminal fragment as well as full-length CD74 (Alexa Fluor 488, green). EEA1, LAMP2 and LBPA (Alexa Fluor 594, red) served as markers for early endosomes and lysosomes, respectively. Nuclei were visualized by staining of DNA with DAPI (blue). Co-localization is indicated by yellow staining (merge). Scale bar, 10 µm.

These vesicles were derived from the endocytic system evidenced by co-localization of CD74 with the early endosomal marker early endosomal antigen 1 (EEA1) as well as the late endosomal/lysosomal markers lysosome-associated membrane protein type 2 (LAMP2) and lysobisphosphatidic acid (LBPA). Interestingly, a mutant form of CD74 with a positively charged arginine instead of a negatively charged aspartate at amino acid position six (referred to as CD74-D6R) abolished the formation of enlarged endocytic vesicles (Figure 11 B). Additionally, the mutant CD74-D6R showed an altered subcellular localization compared to wild type CD74. Only a minor amount of CD74-D6R was found in EEA1-positive vesicles. This mutant partially localized to late endosomes and lysosomes, as revealed by the co-localization with LAMP2 and LBPA. These results are in line with data published by Bakke and co-workers. They identified the negative net charge of the CD74 cytoplasmic tail as the main cause of the enlarged vesicle formation (Nordeng *et al.*, 2002). The insertion of the D6R mutation generates an uncharged cytoplasmic tail inhibiting enhanced vesicle size. The N-terminus of CD74 could therefore be shown to play a crucial role in the homeostasis of the endocytic system.

3.1.2 Inhibition of SPPL2a in a B cell line causes accumulation of CD74 NTF in endocytic vesicles

The overexpression of proteins does not necessarily mimic the physiological conditions of endogenous proteins in the cell. Due to the fact that HeLa cells do not express endogenous CD74, a different cell system was chosen to study the effects of CD74 accumulation. Therefore, the mature mouse B cell lymphoma line Bal 17 was used. In order to investigate the effects of CD74 NTF accumulation on endosome morphology in Bal17 cells, SPPL2a activity was blocked using the SPP/SPPL inhibitor $(Z\text{-}LL)_2$ ketone (Weihofen *et al.*, 2000). As observed after indirect immunofluorescent staining, endogenous CD74 was mainly detected in the ER due to co-localization with proteins containing the ER retention motif KDEL (Figure 12 A). Only minor fractions of CD74 were present in lysosomes (positive for lysosomal integral membrane protein type 2 (LIMP2)) and MIICs (positive for MHCII). This observation can be explained by rapid processing and clearance of CD74 in MIICs after successful translocation of MHCII complexes to these organelles. Thus, under steady-state conditions, CD74 appears to be mainly localized in the ER. Upon inhibition of SPPL2a by $(Z\text{-}LL)_2$ ketone, CD74 was primarily detected in late endosomes/lysosomes as well as in MIIC compartments (Figure 12 B).

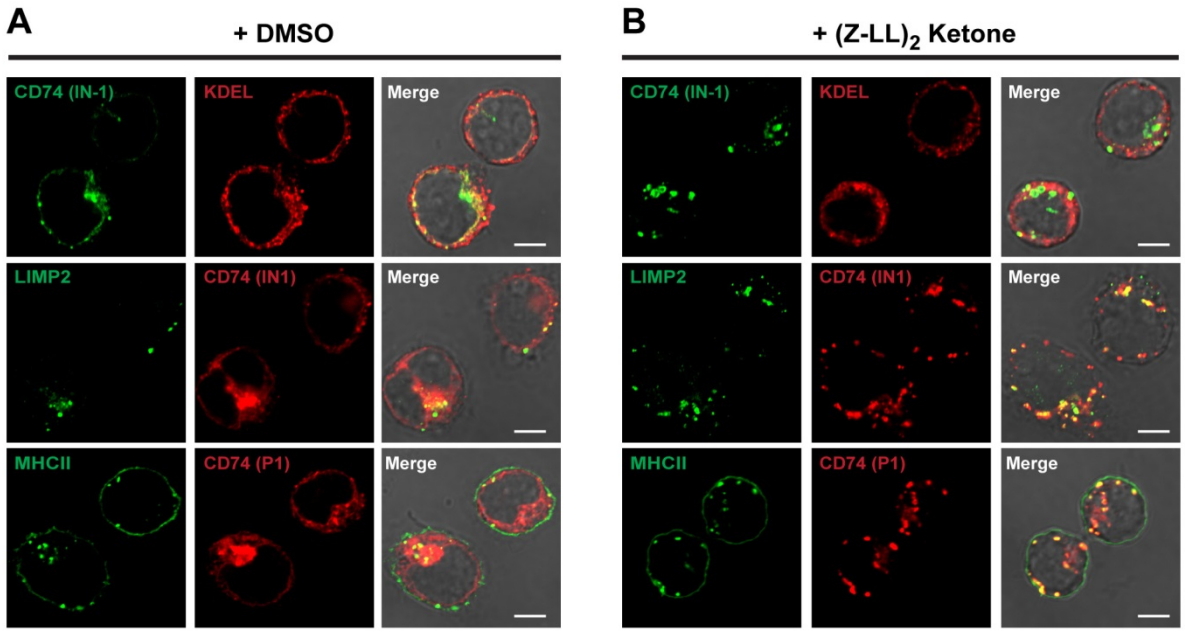

Figure 12. Accumulating CD74 NTF in endocytic vesicles upon SPPL2a inhibition in Bal17 cells. Representative pictures show the subcellular localization of CD74 in Bal17 cells upon SPPL2a inhibition by indirect immunofluorescence. Bal17 cells were treated overnight with DMSO (A) as control or 10 µM of the SPP/SPPL inhibitor $(Z\text{-}LL)_2$ ketone (B), fixed, permeabilized and stained for CD74 (clone IN-1 or Pineda 1 (P1), both directed against an epitope of the N-terminus of CD74). Co-staining was performed using antibodies against the ER retention motif KDEL as ER marker or the marker for lysosomes and MIICs, LIMP2 and MHCII, respectively. Corresponding secondary antibodies coupled to either Alexa Fluor 488 (green) or 594 (red) were used. Morphology of the cells was visualized by bright field. Co-localization is indicated by yellow staining (merge). Scale bar, 4 µm.

Since CD74 was visualized with antibodies directed against an epitope of the N-terminus of the protein, both full-length as well as accumulating CD74 N-terminal fragments (NTFs) were detected. Treatment of Bal17 cells with $(Z\text{-}LL)_2$ ketone did not influence the level of full-length protein but led to a massive increase of CD74 NTF as revealed by Western Blotting of protein lysates of DMSO- and inhibitor-treated Bal17 cells (Figure 13).

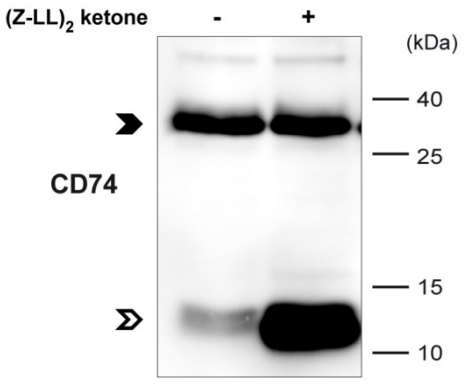

Figure 13. Inhibition of SPPL2a by $(Z\text{-}LL)_2$ ketone induces an accumulation of CD74 NTF in Bal17 cells. Bal17 cells were incubated with 10 µM of the SPP/SPPL inhibitor $(Z\text{-}LL)_2$ ketone for 6 h at 37 °C. CD74 was detected in protein lysates by Western Blotting with anti-CD74 IN-1 directed against the N-terminus of the protein. Full-length CD74 is indicated by a closed arrowhead, CD74 NTF by an open arrowhead.

This is in line with previous studies where it was shown that SPPL2a-deficiency has no influence on the abundance of full-length CD74 (Schneppenheim, Dressel, Hüttl *et al.*, 2013; Schneppenheim, Hüttl *et al.*, 2014). Thus, the CD74 signal in LIMP2- and MHCII-positive compartments observed by indirect immunofluorescence (Figure 12 B) mainly represents the NTFs of CD74. In $(Z\text{-}LL)_2$ ketone-treated Bal17 cells, ER presence of CD74 was not detectable with the applied excitation settings (Figure 12 B), possibly due to the low abundance of full-length CD74 in the ER compared to high amounts of CD74 NTF in vesicular structures. These observations indicate that inhibition of SPPL2a in Bal17 cells leads to an accumulation of CD74 NTF in vesicles derived from the endocytic system. In contrast to the enlarged endocytic vesicles of CD74-overexpressing HeLa cells (Figure 11), the size of CD74 NTF-containing vesicles of $(Z\text{-}LL)_2$ ketone-treated Bal17 cells were comparable to wild type vesicles.

3.1.3 Accumulation of CD74 NTF in primary antigen presenting cells of *SPPL2a*$^{-/-}$ mice

Having identified the CD74 NTF-containing vesicles of Bal17 B cells after SPPL2a inhibition as compartments derived from the endocytic system, the effects of a complete knock-out of SPPL2a on the endosomal system was examined in primary antigen presenting cells (APCs). In order to study the consequences of CD74 NTF accumulation on the endocytic system in primary SPPL2a-deficient cells, subcellular localization of CD74 was analyzed in BMDCs by indirect immunofluorescence. BMDCs were differentiated from red bone marrow cells for eight days with granulocyte macrophage colony-stimulating factor (GM-CSF) and finally stimulated with lipopolysaccharide (LPS) overnight. In wild type BMDCs, CD74 was exclusively found to co-localize with proteins containing the ER-retention motif KDEL rather than with the early endosomal and late endosomal/lysosomal markers EEA1 and LAMP2 (Figure 14 A). The detected CD74 in the ER most likely represents full-length protein due to a rapid turnover of CD74 cleavage products in late endosomes/lysosomes. In comparison, in BMCDs generated from SPPL2a-deficient mice, CD74 NTF was found in vesicular structures which were partially positive for EEA1 and positive for LAMP2 (Figure 14 B). According to the aforementioned results (3.1.2) the signals obtained in *SPPL2a*$^{-/-}$ cells by labeling with an antibody directed against the N-terminus of CD74 should primarily represent the distribution of the CD74 NTF. There was no detectable difference in the distribution of CD74 between unstimulated BMDCs and cells stimulated with LPS. In conclusion, the absence of SPPL2a in BMDCs causes an accumulation of CD74 NTF in late endosomal/lysosomal compartments.

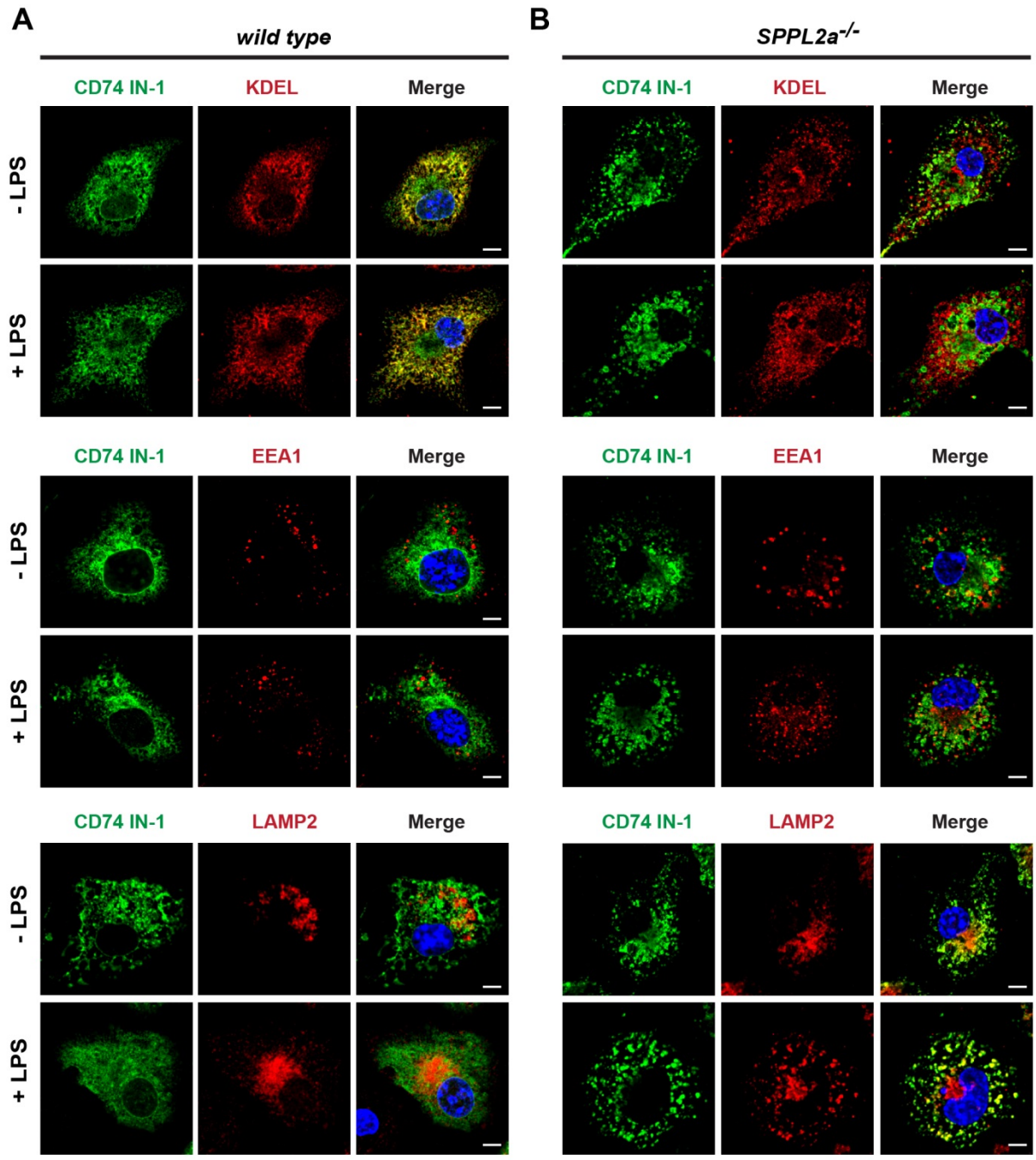

Figure 14. In *SPPL2a*$^{-/-}$ BMDCs, the accumulated CD74 NTF is localized in late endosomes/lysosomes. Representative pictures show *wild type* (A) and *SPPL2a*$^{-/-}$ BMDCs (B) after indirect immunofluorescence staining of the cells. BMDCs were differentiated from bone marrow cells with GM-CSF for 8 days and stimulated with LPS overnight or left unstimulated. Cells were adhered to poly-L-lysine coated coverslips, fixed, permeabilized and stained for CD74 (clone IN-1, Alexa Fluor 488 secondary antibody, green) and KDEL, EEA1 or LAMP2 (Alexa Fluor 594 secondary antibody, red). Nuclei were visualized by staining of DNA with DAPI (blue). Co-localization is indicated by yellow staining (merge). Scale bar, 5 µm.

Since the phenotype of SPPL-deficient mice is most pronounced in B cells with respect to their maturation block and the alterations in the endosomal system (1.3), the following experiments will focus on primary B cells. As explained in the introduction, SPPL2a-deficient

splenic B cells show an extensive accumulation of vesicles. To evaluate the role of the accumulating CD74 NTF in the process of vesicle generation, subcellular localization of CD74 in splenic primary B cells was analyzed by indirect immunofluorescence. A commonly used tool to isolate primary B cells from different organs is the Magnetic Activated Cell Sorting (MACS®) Technology (Miltenyi Biotec). Here, total splenic B cells derived from wild type and *SPPL2a*$^{-/-}$ mice were isolated by negative depletion. Staining for CD74 with an antibody against the N-terminus of the protein revealed a diffuse and widespread localization of CD74 in the cytoplasm of wild type splenic B cells (Figure 15 A). CD74 only partially co-localized with early (EEA1)/late endosomes as well as lysosomes (LAMP1, LIMP2). MHCII β chain (MHCIIβ) as part of the MHCII complex was mainly located at the cell surface, but also partially in intracellular vesicles.

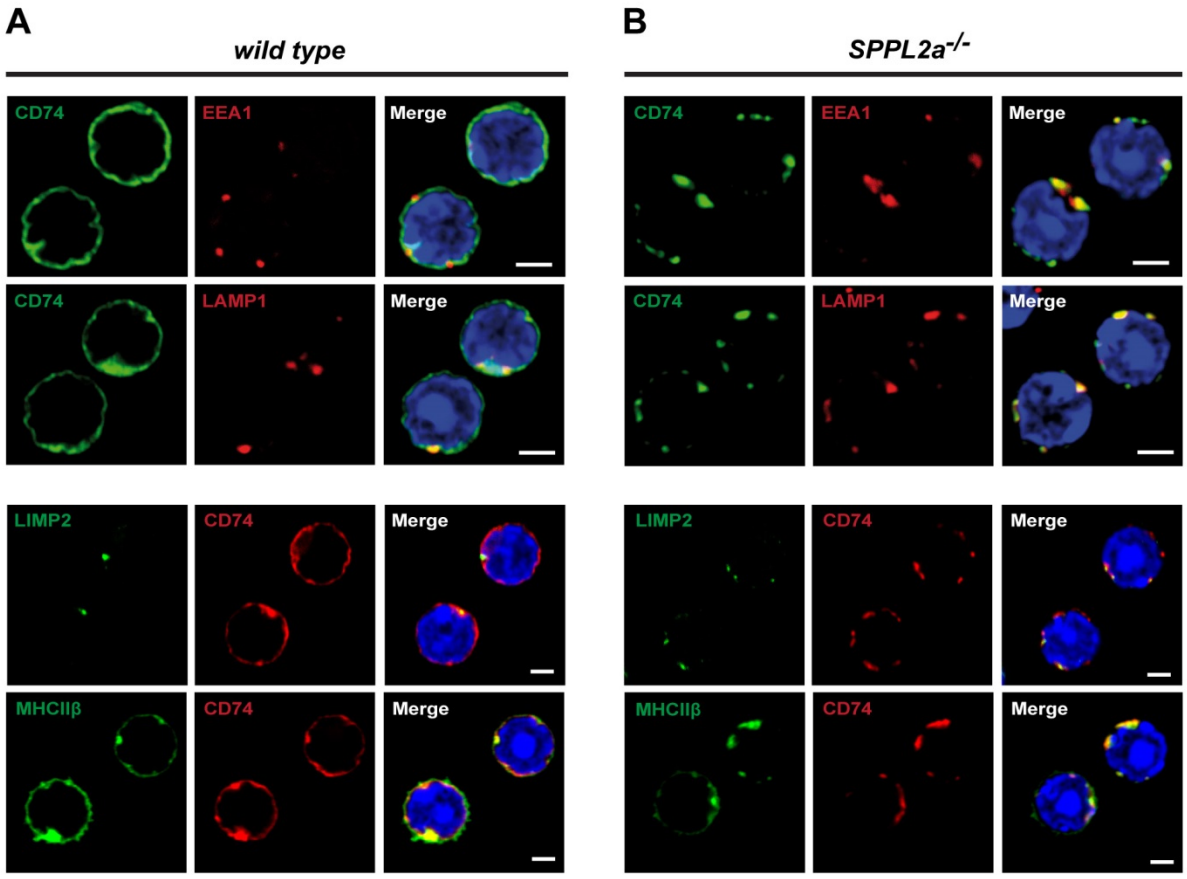

Figure 15. In SPPL2a-deficient B cells, CD74 NTF localizes to endocytic vesicles. Representative pictures of total splenic B cells of *wild type* (A) and *SPPL2a*$^{-/-}$ mice (B) stained by indirect immunofluorescence are shown. Cells were adhered to poly-L-lysine coverslips, fixed and permeabilized. CD74 was detected with an antibody against the N-terminus of the protein (IN-1). Markers for early endosomes (EEA1), late endosomes/lysosomes (LAMP1, LIMP1) as well as MIICs (MHCIIβ) were used for co-staining. Alexa Flour 488 (green) or 594 (red)-coupled secondary antibodies were used as indicated. Nuclei were visualized by staining of DNA with DAPI (blue). Co-localization is indicated by yellow staining (merge). Scale bar, 2 µm.

In these vesicles, co-localization with CD74 could be seen which is in accordance with the interaction of MHCII and CD74 during the transport of MHCII complexes from the ER to late endosomes (Figure 15 A). In contrast, CD74 of SPPL2a-deficient B cells resided in vesicular structures and showed a high degree of co-localization with EEA1, LIMP1, LAMP2 and MHCIIβ (Figure 15 B). In summary, SPPL2a-deficiency in B cells leads to an accumulation of CD74 NTF in vesicles derived from the endocytic system. These data provide strong evidence that an impaired turnover of CD74 NTF leads to disturbances within the endocytic pathway.

3.1.4 Impaired MHCII homeostasis in *SPPL2a*$^{-/-}$ B cells

Due to its function as a chaperone for MHCII, CD74 directly interacts with MHCII complexes via its CLiP domain (Bijlmakers *et al.*, 1994; Freisewinkel *et al.*, 1993; Romagnoli & Germain, 1994). In order to assess whether CD74 NTF accumulation in abundant vesicles disturbs MHCII homeostasis, total and surface amounts of MHCII were examined by flow cytometry. Therefore, splenocytes isolated from wild type and *SPPL2a*$^{-/-}$ mice were stained for MHCII either without permeabilization to visualize surface MHCII molecules or with prior fixation and permeabilization of cells in order to detect both surface and intracellular proteins. Co-staining for the B cell-specific surface markers CD21, CD24 and B220 allowed gating for T1, T2 and mature B cell subpopulations due to differential expression of these markers (Figure 16).

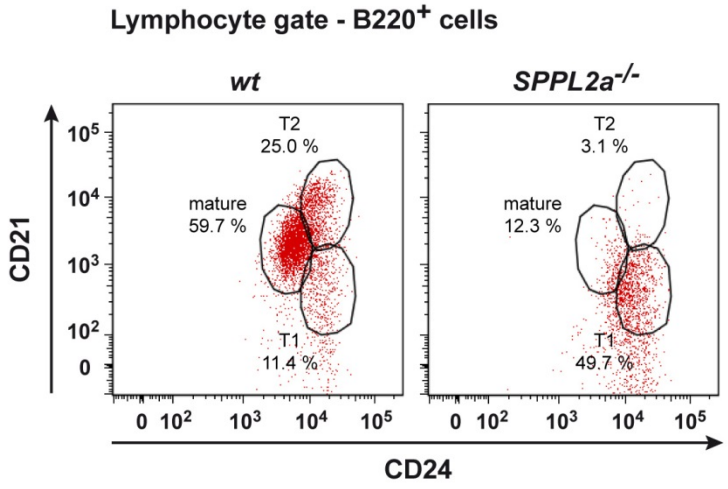

Figure 16. Gating scheme for the analysis of splenic B cell subsets by flow cytometry. In order to distinguish between the different splenic B cell populations, splenocytes isolated from wild type (*wt*) and *SPPL2a*$^{-/-}$ mice were stained for the surface markers CD21, CD24 and B220. B cells can be classified flow cytometrically into T1 (B220^{+} CD21^{low} CD24^{high}), T2 (B220^{+} CD21^{high} CD24^{high}) and mature (B220^{+} CD21^{low} CD24^{low}) B cells.

Flow cytometric analysis revealed significantly increased MHCII levels at the cell surface of SPPL2a-deficient B cells throughout all developmental stages in the spleen (T1, T2 and mature B cells) when compared to the corresponding wild type control (Figure 17). This effect was even more pronounced when analyzing total MHCII levels. MHCII was elevated up to a factor of three. As a result, both surface as well as intracellular MHCII levels are significantly up-regulated in splenic *SPPL2a*$^{-/-}$ B cells.

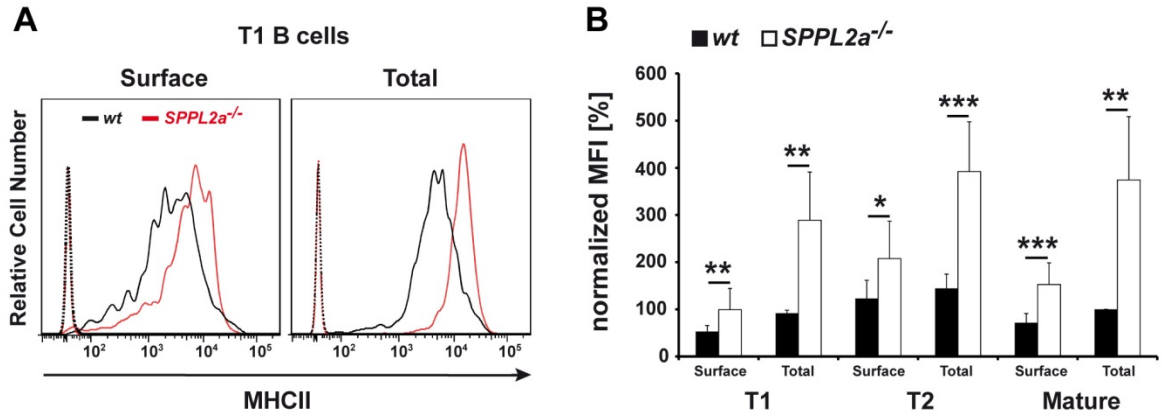

Figure 17. Splenic *SPPL2a*$^{-/-}$ B cells show elevated surface and intracellular MHCII levels. Surface MHCII of wild type (*wt*) and *SPPL2a*$^{-/-}$ splenocytes was detected by staining viable cells whereas total amounts of MHCII were visualized after fixation and permeabilization of splenocytes. Cells were co-stained for the surface markers CD21, CD24 and B220. Median fluorescence intensities (MFI) for the MHCII signal were determined flow cytometrically for T1 (B220^{+} CD21^{low} CD24^{high}), T2 (B220^{+} CD21^{high} CD24^{high}) and mature (B220^{+} CD21^{low} CD24^{low}) B cells. Data are shown as histogram of one representative experiment (A) or as mean of MFI ± standard deviation (SD) after normalization to the total MHCII value of mature wild type cells, n = 5 per genotype, three independent experiments (B). Respective isotype controls are shown as dashed lines. ***, $P < 0.001$; **, $P < 0.01$; *, $P < 0.05$; unpaired, two-tailed Student's *t*-test.

The observed elevated MHCII levels can either be caused by dysregulation at the mRNA or protein level. Subsequently, transcription of the MHCIIα and -β-encoding genes was examined. One representative gene variant for each MHCII chain was analyzed: MHCIIα H2-Aa and MHCIIβ H2-DMb1. For both genes, transcript levels were found to be down-regulated in *SPPL2a*$^{-/-}$ splenic B220^{+} B cells as compared to the wild type (Figure 18). However, these changes were not statistically significant. Taken together, SPPL2a-deficiency in B cells causes increased MHCII protein levels indicating the ability of accumulating CD74 NTF to disturb MHCII homeostasis.

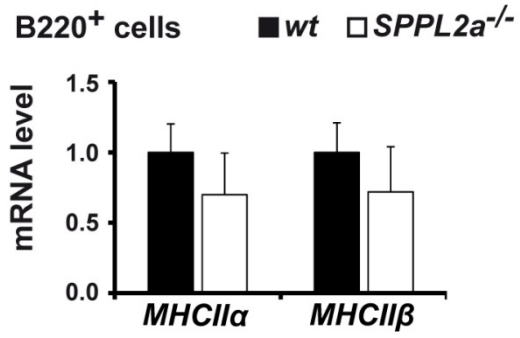

Figure 18. Unaltered MHCIIα and -β mRNA levels in *SPPL2a*$^{-/-}$ B cells. Splenic B220^{+} B cells were isolated from wild type (*wt*) and *SPPL2a*$^{-/-}$ mice. After total RNA extraction and first strand cDNA synthesis, mRNA levels were determined by qRT-PCR using gene-specific primers and the Universal Probe Library Technology (Roche). Data are shown as mean ΔΔCp ± SD after normalization to the wt ΔΔCp, n = 3 per genotype, three independent experiments.

3.1.5 *SPPL2a*$^{-/-}$ B cells show modulated transferrin recycling and reduced cellular transferrin receptor levels

The previous experiments clearly show that accumulating levels of either full-length CD74 or CD74 NTF have a high potential to disturb the morphology of the endocytic system in B cells (1.3, 3.1.3). With the intention to investigate the specific role of CD74 NTF on endocytic trafficking events, the transferrin (Tfn) recycling pathway was analyzed in *SPPL2a*$^{-/-}$ B cells (Figure 19). The Tfn recycling pathway is ubiquitously used by all different cell types due to the requirement of iron. Tfn is an iron-binding blood-plasma glycoprotein responsible for maintaining the iron homeostasis of the cell by transporting iron into the cell (Mayle *et al.*, 2012). In this assay, splenocytes were incubated with Alexa Fluor-coupled human Tfn-Fe^{3+} (Tfn-488) at 4 °C to allow binding of Tfn to the Tfn receptor (TfnR) at the plasma membrane (Figure 19).

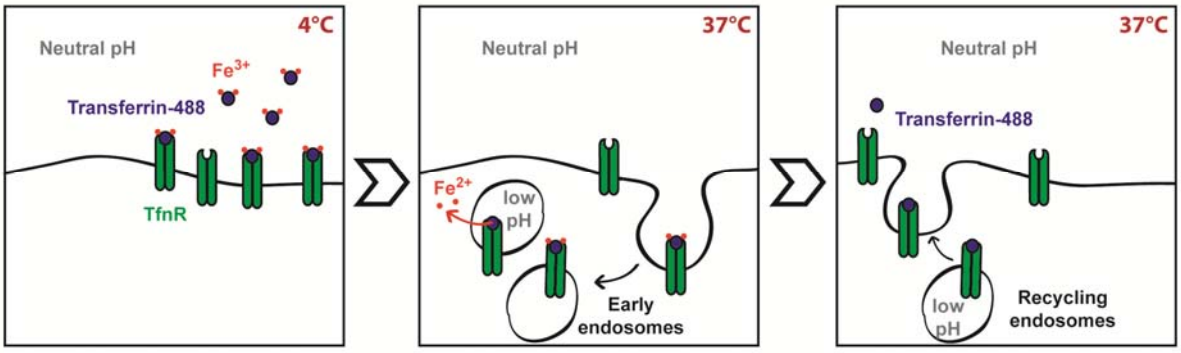

Figure 19. Scheme of the established Tfn recycling assay. Binding of Alexa Fluor 488-coupled Tfn-Fe^{3+} to the TfnR of splenocytes is allowed for 30 min at 4 °C. During a pulse of 1 h at 37 °C, the complex of Tfn-Fe^{3+} and TfnR internalizes via receptor-mediated endocytosis to early and recycling endosomes where the Fe^{3+} dissociates due to the acidic pH. Fe^{3+} is reduced to Fe^{2+} and transported into the cytosol. The apo-Tfn remains bound to the TfnR and is recycled to the plasma membrane where it is finally released from its receptor. The release of recycled Tfn, detectable by a decrease of fluorescence, was monitored during a 0 to 180 min chase period by flow cytometry.

This complex was allowed to internalize into endocytic vesicles via receptor-mediated endocytosis for 1 h at 37 °C where Fe^{3+} was released due to the low pH. After removal of surface-bound Tfn-488 by washing of the cells, the recycling of the complex composed of Tfn-488 and TfnR was monitored during a chase of 0 to 180 min at 37 °C. The amount of recycled and released Tfn thereby correlated with the reduction of fluorescence signal. Staining for the B cell specific surface markers CD21, CD24 and B220 prior to flow cytometric analysis allowed gating for the T1 B cell subpopulation.

The total amount of endocytosed Tfn-488 directly after the pulse was determined in wild type as well as *SPPL2a*$^{-/-}$ T1 B cells. The amount of internalized Tfn was found to be comparable for both analyzed genotypes (Figure 20) providing an optimal basis to evaluate the recycling efficiency of internalized Tfn-488 in wild type and SPPL2a-deficient B cells.

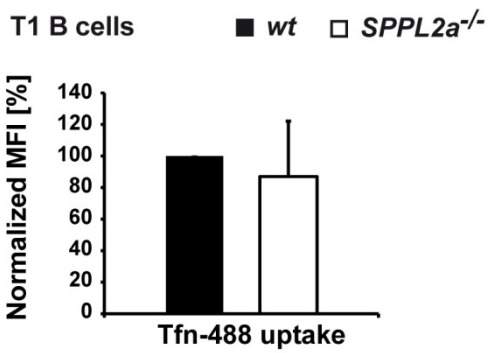

Figure 20. Wild type (*wt*) and *SPPL2a*$^{-/-}$ T1 B cells internalize comparable amounts of Tfn-488. Alexa Fluor 488-coupled Tfn was allowed to bind to the Tfn receptor of wt and *SPPL2a*$^{-/-}$ splenocytes for 30 min at 4 °C. After a pulse at 37 °C for 1 h splenocytes were stained for CD21, CD24 and B220 and analyzed by flow cytometry. MFI of Tfn-488 was determined for the T1 B cell population ($B220^{+}$ $CD21^{low}$ $CD24^{high}$). Data is presented as mean of MFIs ± SD after normalization to wt samples, n = 4 per genotype; four independent experiments.

The capacity to recycle endocytosed Tfn-488 was assessed using a Tfn recycling assay as described in Figure 19. In T1 B cells of wild type and *SPPL2a*$^{-/-}$ mice, the internalized cargo was efficiently recycled due to the exponential decrease of fluorescence (Figure 21 A). The kinetics of Tfn recycling were mostly comparable in B cells of both genotypes. However, approximately 80 % of the internalized Tfn-488 has already been released from wild type cells after 30 min of chase. In comparison, *SPPL2a*$^{-/-}$ T1 B cells showed a slight, but not significant, reduction in recycling velocity with approximately 60 % of recycled Tfn-488 after 30 min of chase. Furthermore, the amount of remaining intracellular Tfn-488 after 180 min of chase was found to be significantly increased in T1 B cells of SPPL2a-deficient mice indicating an increased retention of endocytosed Tfn-488 in these cells. Tfn-488 recycling was also analyzed in B220-negative ($B220^{-}$) cells (Figure 21 B). In non-B cells, no difference in comparison to wild type cells was observed in Tfn recycling capacity suggesting a B cell-specific retention of internalized Tfn in *SPPL2a*$^{-/-}$ mice.

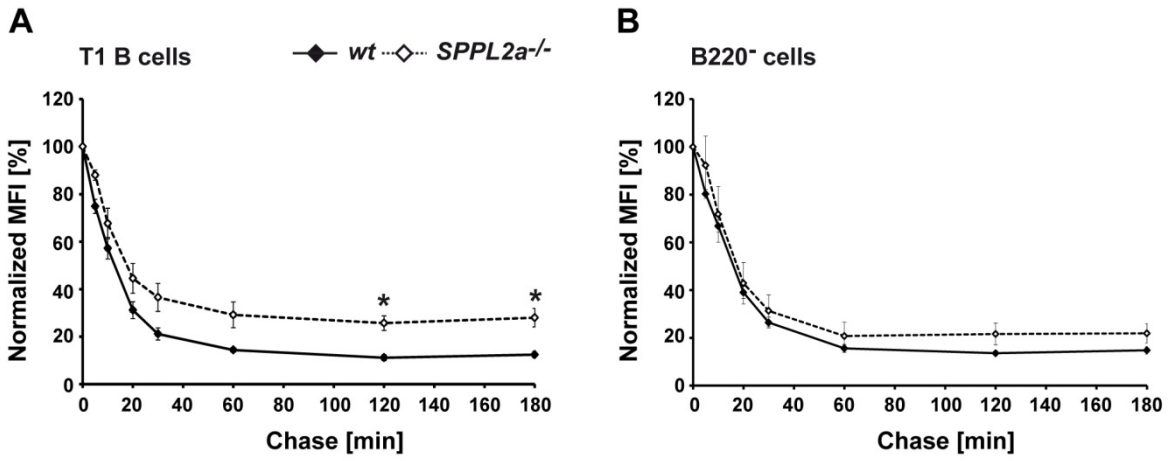

Figure 21. *SPPL2a*$^{-/-}$ T1 B cells show a retention of endocytosed transferrin (Tfn). The recycling of diferric Alexa Flour 488-coupled Tfn (Tfn-488) was monitored over time by flow cytometric analysis. Splenocytes of wild type (*wt*) and *SPPL2a*$^{-/-}$ mice were serum-deprived for 3 h and subsequently incubated with 200 µg/ml Tfn-488 for 30 min at 4 °C. Cells were pulsed for 1 h at 37 °C in the presence of Tfn-488 followed by the removal of surface-bound Tfn-488 by washing of cells. During a chase of 0 to 180 min at 37 °C the release of Tfn was monitored by flow cytometry after staining of cells with CD21, CD24 and B220 to allow gating for T1 B cells (B220^{+} CD21^{low} CD24^{high}) as well as non-B cells (B220^{-}). MFIs of Tfn-488 of T1 B cells (A) and non-B cells (B) was determined for each genotype and sample and normalized to the value of 0 min. Mean of normalized MFI ± standard error of the mean (SEM), n = 3 per genotype; three independent experiments. *, $P < 0.05$; unpaired, two-tailed Student's *t*-test.

In order to clarify whether the retention of internalized TfnR which was observed in SPPL2a-deficient B cells is caused by an altered cellular distribution of the receptor, the amount of surface and total TfnR was quantified by flow cytometry. Splenocytes of wild type and SPPL2a-deficient mice were stained for TfnR along with CD21, CD24 and B220 either without or after permeabilization of cells to detect surface and total levels of TfnR, respectively. T1 as well as mature *SPPL2a*$^{-/-}$ B cells showed reduced TfnR surface levels when compared to the corresponding subpopulation of wild type B cells (Figure 22). Interestingly, this effect was even more pronounced when analyzing the total TfnR level indicating that surface as well as intracellular TfnR levels of T1 and mature *SPPL2a*$^{-/-}$ B cells are similarly reduced. The amount of TfnR in T2 B cells of SPPL2a-deficient mice were not significantly altered, however a tendency towards reduced TfnR levels was observed. TfnR levels in total splenic B cells (B220^{+}) of wild type and *SPPL2a*$^{-/-}$ mice were found to be comparable.

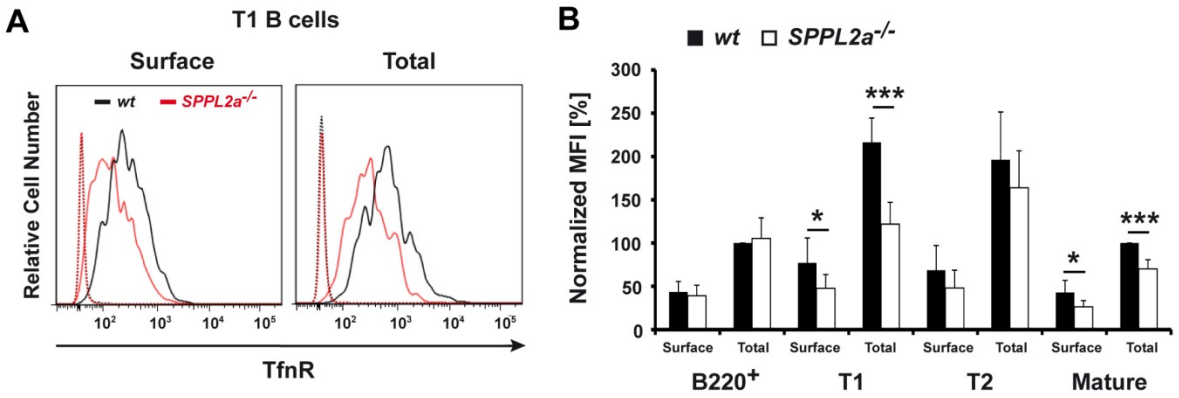

Figure 22. Surface and total levels of TfnR are reduced in T1 and mature B cells of *SPPL2a*$^{-/-}$ mice. TfnR levels were analyzed by flow cytometry. Splenocytes of wild type (*wt*) and SPPL2a-deficient (*SPPL2a*$^{-/-}$) mice were either directly stained for TfnR in combination with the B cell surface markers CD21, CD24 and B220 (surface) or staining was performed after fixation and permeabilization of the cells (total). MFI for surface and total TfnR levels were determined for B220^{+}, T1 (B220^{+} CD21^{low} CD24^{high}), T2 (B220^{+} CD21^{high} CD24^{high}) and mature (B220^{+} CD21^{low} CD24^{low}) B cells by flow cytometry. Data are shown as histogram of one representative experiment (A) or as mean of MFI ± SD, n = 6 per genotype from five independent experiments (B). MFIs of T1, T2 and mature B cells of each experiment were normalized to the total value of mature wild type cells; MFIs of B220^{+} B cells were normalized to the total MFIs of wild type B220^{+} cells. Respective isotype controls are depicted as dashed lines. ***, P < 0.001; *, P < 0.05; unpaired, two-tailed Student's *t*-test.

To examine whether the reduced TfnR levels in *SPPL2a*$^{-/-}$ B cells are caused by alterations in gene transcription, the mRNA level of the TfnR-endocing gene (*TfnR*) was determined by qRT-PCR (Figure 23). Since isolation of T1, T2 and mature B cells by fluorescence activated cell sorting would only yield low amounts of cells, gene transcription was examined in B220^{+} cells. Splenic B220^{+} B cells isolated from SPPL2a-deficient mice showed up-regulated *TfnR* mRNA levels compared to the wild type. However, due to high experimental variability, no significant changes emerged which is in line with the results obtained by flow cytometry.

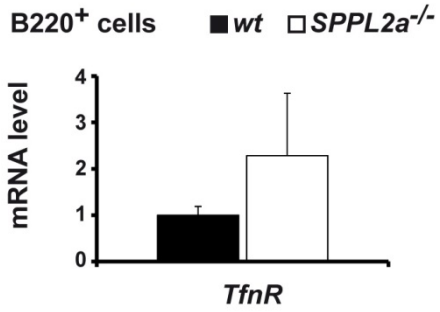

Figure 23. Transcription of the *TfnR* gene is not significantly different in wild type (*wt*) and SPPL2a-deficient (*SPPL2a*$^{-/-}$) splenic B cells. Total RNA was isolated from splenic B220^{+} B cells of wild type and *SPPL2a*$^{-/-}$ mice. After first strand cDNA synthesis, *TfnR* mRNA levels were determined by qRT-PCR using the Universal Probe Library Technology and gene specific primers. Data are shown as mean of ΔΔCp ± SD after normalization to the wt ΔΔCp values, n = 3, three independent experiments.

To visualize potential cellular rearrangements of the receptor by microscopical imaging, the subcellular localization of the TfnR was investigated in total splenic B cells of wild type and

SPPL2a-deficient mice by indirect immunofluorescence. In wild type B cells, the TfnR was mostly present in vesicular structures partially co-localizing with CD74 (Figure 24). The localization of TfnR did not seem to be grossly altered in *SPPL2a*$^{-/-}$ B cells (Figure 24). Additionally, the accumulating CD74 NTF was, to a certain extent, present in TfnR-containing endosomes in both wild type and SPPL2a-deficient B cells.

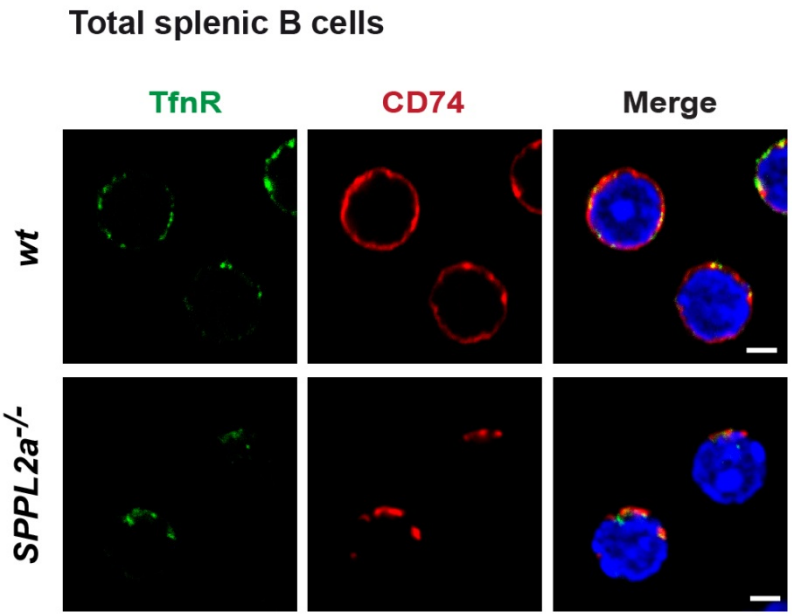

Figure 24. Subcellular localization of the TfnR appears to be unaltered in SPPL2a-deficient B cells. Total splenic B cells of wild type (*wt*) and *SPPL2a*$^{-/-}$ mice were isolated by negative depletion. B cells were adhered to poly-L-lysine coated coverslips prior to fixation and permeabilization. CD74 (clone IN-1, Alexa Fluor 594, red) and TfnR (Alexa Fluor 488, green) were visualized by indirect immunofluorescence. Nuclei were visualized by staining of DNA with DAPI (blue). Co-localization is indicated by yellow staining (merge). Scale bar, 2 µm.

Taken together, these results illustrate that the cellular levels of TfnR are reduced in SPPL2a-deficient T1 and mature B cells without obviously affecting the subcellular localization of the receptor. Tfn recycling kinetics were not significantly altered in *SPPL2a*$^{-/-}$ T1 B cells with the exception that SPPL2a-deficient T1 B cells show an increased intracellular retention of Tfn.

3.1.6 Degradation of endocytosed ovalbumin is delayed in *SPPL2a*$^{-/-}$ B cells

Besides the uptake of cargo molecules by receptor-mediated endocytosis, internalization of molecules can also take place by fluid-phase endocytosis. To assess the functional consequences of CD74 NTF accumulation and the accompanied accumulation of endocytic vesicles on endocytic trafficking, the degradation of a fluid-phase cargo was monitored in an

endocytosis assay (Figure 25). Therefore, splenocytes of wild type and SPPL2a-deficient mice were allowed to internalize the fluorescein isothiocyanate (FITC)-coupled ovalbumin (OVA-FITC). During a pulse period of 30 min, OVA-FITC should reach compartments of the endocytic system. During a chase period of up to 24 h, OVA-FITC is delivered to lysosomes and degraded leading to a reduction of fluorescence signal which can be monitored by flow cytometry. Subsequent staining of the cells for the B cell markers CD21, CD24 and B220 allowed gating and analysis of the different B cell subpopulations of the spleen.

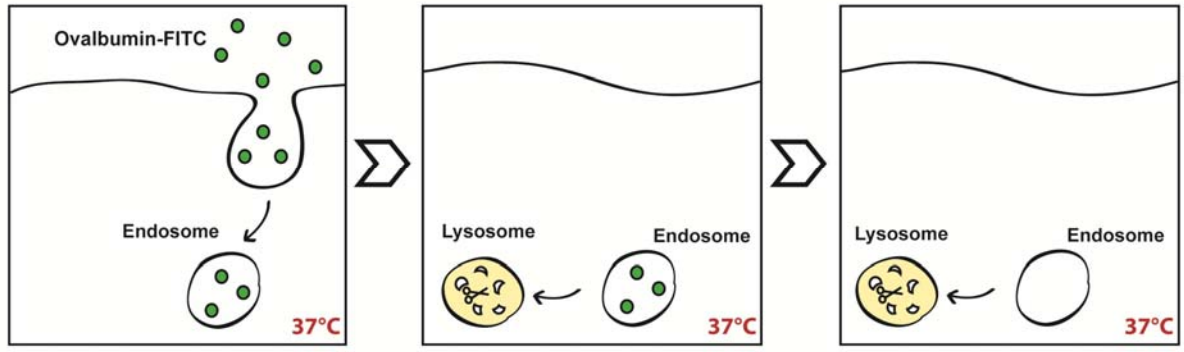

Figure 25. Scheme of the established ovalbumin degradation assay. Cells are pulsed with 250 µg/ml FITC-coupled ovalbumin (OVA-FITC) for 30 min at 37 °C. Meanwhile, OVA-FITC is taken up by the cell via fluid-phase endocytosis and transported through the endocytic pathway. During the chase (0-24 h), OVA-FITC reaches the lysosome where its degradation can be monitored by flow cytometry due to a decrease of fluorescence signal.

To evaluate the functionality of the experimental set-up, the OVA-FITC degradation assay was performed in the presence of inhibitors of lysosomal acidification (Bafilomycin) or lysosomal proteases (leupeptin/pepstatin/E-64d). In control (DMSO/ethanol-treated) T1 B cells of wild type mice, OVA-FITC was efficiently degraded over time (Figure 26). In the presence of Bafilomycin, fluorescence of OVA-FITC decreased during the first 30 min of chase, comparable to control cells. However, fluorescence did not diminish further over time indicating an effective inhibition of OVA-FITC degradation by inhibiting lysosomal acidification and thus shifting the lysosomal pH. Addition of the protease inhibitor cocktail had a similar effect. Fluorescence signal did not decrease by more than 30 % during the whole chase, pointing to a successful blockage of OVA degradation by inhibition of lysosomal proteases. Thus, the OVA-FITC signals were stabilized by inhibiting lysosomal acidification or proteases highlighting a lysosome-specific degradation of OVA. The assay therefore represents a suitable readout to analyze the turnover of OVA-FITC in late endosomes/lysosomes.

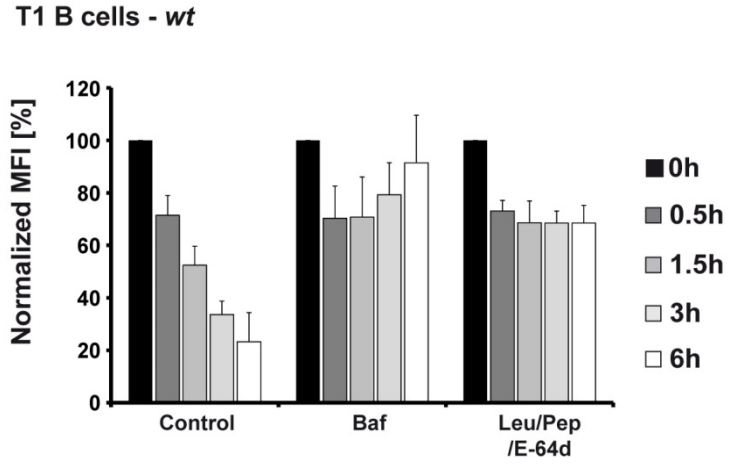

Figure 26. The degradation of OVA-FITC can be blocked by the inhibition of lysosomal acidification and lysosomal hydrolases. OVA-FITC degradation in wild type (*wt*) T1 B cells was monitored in the presence of either DMSO/ethanol (control), 40 nM Bafilomycin (Baf) or a cocktail of 100 µM Leupeptin (Leu), 1 µg/ml Pepstatin A (Pep) and 50 µM E-64d. Prior to the pulse with 250 µg/ml OVA-FITC for 30 min at 37 °C, splenocytes were pre-incubated in medium supplemented with the respective inhibitors for 2 h. Cells were washed and subjected to a chase at 37 °C for various time points between 0 and 6 h. Cells were stained for CD21, CD24 and B220 and MFI of the FITC-channel was determined by flow cytometry for the T1 B cell population ($B220^{+}$ $CD21^{low}$ $CD24^{high}$). Mean of MFI ± SD, n = 2 per genotype; two independent experiments. MFIs of the different time points were normalized to the 0 h time point.

The amount of OVA-FITC that was internalized by wild type and SPPL2a-deficient T1 B cells after a pulse of 30 min was determined (Figure 27). Both wild type and *SPPL2a*$^{-/-}$ T1 B cells internalized equal amounts of OVA-FITC.

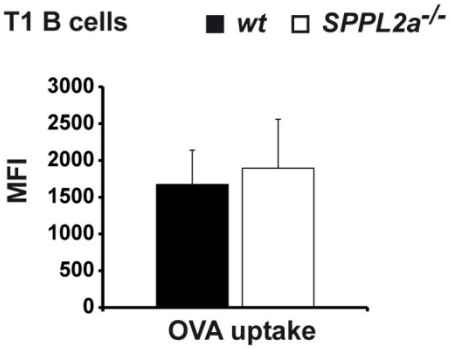

Figure 27. Wild type (*wt*) and *SPPL2a*$^{-/-}$ T1 B cells endocytose comparable amounts of OVA-FITC. Wt and *SPPL2a*$^{-/-}$ splenocytes were allowed to internalize OVA-FITC (250 µg/ml) for 30 min at 37 °C. Cells were washed and stained for CD21, CD24 and B220. The amount of endocytosed OVA-FITC was quantified by flow cytometry by determining the MFI of the FITC-channel for the T1 B cell population ($B220^{+}$ $CD21^{low}$ $CD24^{high}$). Mean of MFI ± SD, n = 3 per genotype; three independent experiments.

During the chase, T1 B cells of wild type and *SPPL2a*$^{-/-}$ mice showed a time-dependent exponential decrease in fluorescence, indicating efficient degradation of OVA-FITC (Figure 28 A). Interestingly, the cargo degradation was significantly decelerated in *SPPL2a*$^{-/-}$ T1 B cells clearly visible between 1.5 and 6 h of chase. However, the overall amount of degraded ovalbumin after 24 h was comparable in both genotypes. No difference in the degradation rate

was detectable in non-B cells (B220$^-$) of wild type and SPPL2a-deficient mice (Figure 28 B), restricting the observed defect to B cells only.

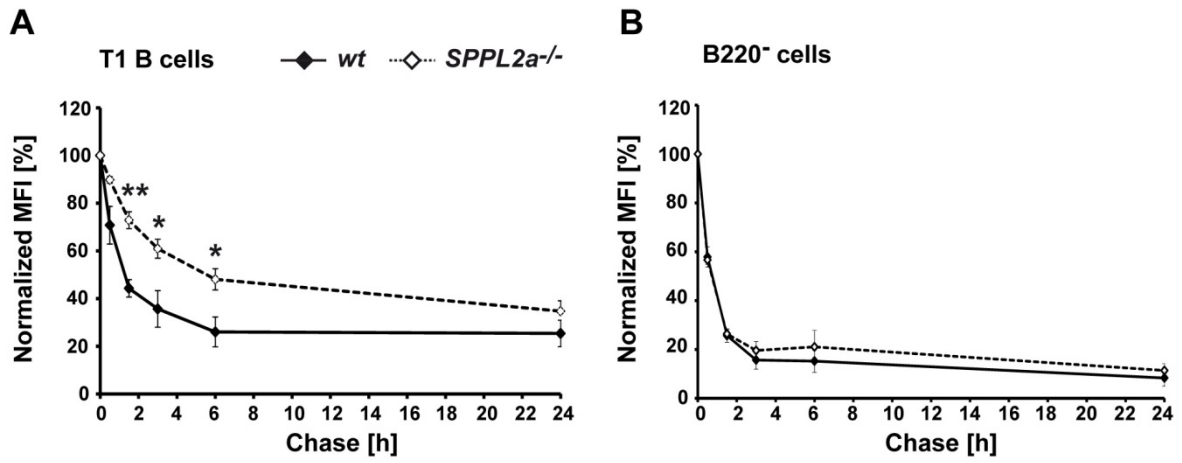

Figure 28. SPPL2a-deficient T1 B cells show a decelerated degradation of the fluid-phase cargo ovalbumin. Splenocytes isolated from wid type (*wt*) and *SPPL2a*$^{-/-}$ mice were pulsed with 250 µg/ml FITC-coupled ovalbumin (OVA-FITC) for 30 min at 37 °C. After washing, cells were chased for 0 - 24 h at 37 °C and subsequently stained for the B cell surface markers CD21, CD24 and B220. Degradation of OVA-FITC was monitored flow cytometrically in T1 B cells (B220$^+$ CD21^{low} CD24^{high}; A) and non-B cells (B220$^-$; B). The MFI of the FITC-channel was determined and normalized to the 0 h value separately for each genotype. Mean of normalized MFI ± SEM, n = 3 per genotype, three independent experiments. **, $P < 0.01$; *, $P < 0.05$; unpaired, two-tailed Student's *t*-test.

The delayed OVA-FITC degradation in *SPPL2a*$^{-/-}$ B cells could for instance be caused by a slowed transport of the endocytosed cargo to lysosomal compartments or a potential increase of the lysosomal pH which could negatively affect the activity of lysosomal hydrolases. In order to rule out that an altered lysosomal pH in *SPPL2a*$^{-/-}$ B cells is responsible for the slowed degradation of OVA-FITC, lysosomal acidification was analyzed by LysoTracker Red staining. LysoTracker is a cell permeable dye which specifically stains acidic organelles (Zhang *et al.*, 1994). B220$^+$ B cells were isolated from the spleen of wild type and SPPL2a-deficient mice by positive selection (MACS sorting system). The obtained viable splenic B220$^+$ B cells were stained with LysoTracker and analyzed by live cell imaging using confocal microscopy. In wild type B220$^+$ B cells, prominent vesicular acidic organelles were detectable in almost every cell (Figure 29). By comparison, size and number of acidic vesicles seemed to be similar in *SPPL2a*$^{-/-}$ B cells. In addition, fluorescence intensity of the LysoTracker staining was comparable in wild type and SPPL2a-deficient B cells. This argues against an obvious increase in lysosomal pH as a potential cause for the decelerated degradation of OVA-FITC in *SPPL2a*$^{-/-}$ B cells.

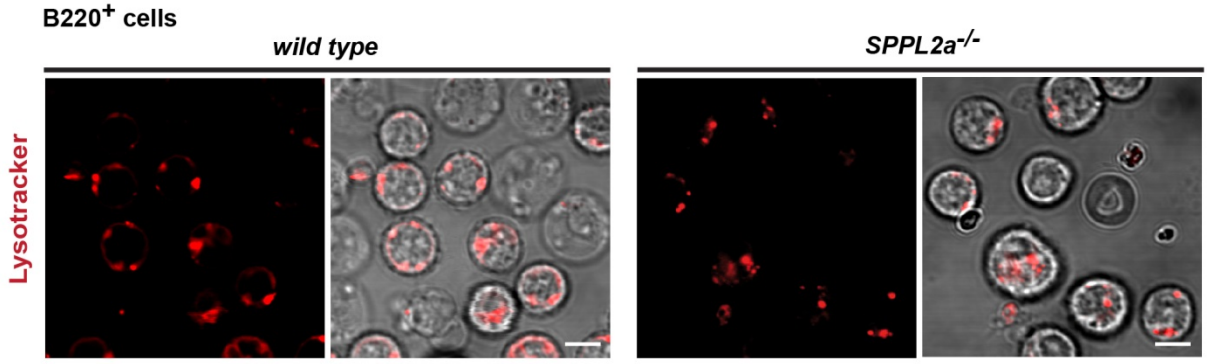

Figure 29. Lysosomal acidification is not obviously altered in *SPPL2a*$^{-/-}$ B cells. Splenic *wild type* and *SPPL2a*$^{-/-}$ B220^{+} B cells were adhered to poly-L-lysine coated glass bottom imaging dishes. Acidic organelles were visualized by staining of cells with 0.5 µM LsyoTracker® Red DND-99 for 50 min at 37 °C. Representative pictures of two independent experiments are shown. Scale bar, 5 µm.

To investigate the role of the accumulating CD74 NTF for the OVA-FITC degradation process, the uptake assay was expanded to B cells of SPPL2a-CD74 double-deficient mice. In these mice, no accumulation of CD74 NTF can take place, but CD74-independent effects of SPPL2a-deficiency still occur (Schneppenheim, Dressel, Hüttl *et al.*, 2013). Interestingly, the observed slowed cargo degradation in SPPL2a-deficient B cells was alleviated in *SPPL2a*$^{-/-}$ *CD74*$^{-/-}$ T1 B cells to the level of *CD74*$^{-/-}$ cells (Figure 30 A). Meanwhile, T1 B cells of CD74 single-deficient mice already showed a slightly, but not significantly altered OVA-FITC degradation when compared to the wild type. Calculation of the intracellular half-life of endocytosed OVA-FITC clearly reveals the magnitude of the degradation defect in *SPPL2a*$^{-/-}$ B cells. Whereas wild type as well as CD74-deficient and SPPL2a-CD74 double-deficient B cells degraded 50 % of the cargo in a maximum of 2 h, *SPPL2a*$^{-/-}$ T1 B cells required more than 4 h (Figure 30 B). These observations provide clear evidence that accumulating CD74 NTF causes significant disturbances in trafficking events within the endocytic route. Accordingly, turnover of CD74 NTF by SPPL2a is essential for maintaining the functionality of the endocytic system.

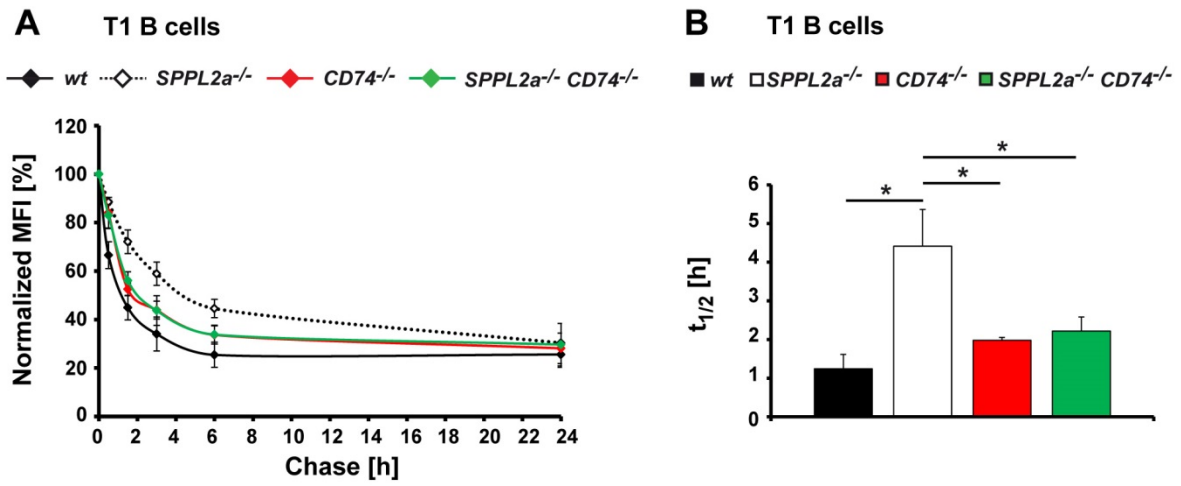

Figure 30. Delayed OVA-FITC degradation in *SPPL2a*$^{-/-}$ B cells can be rescued by additional ablation of CD74. (A) OVA-FITC degradation assay was performed as described before with splenocytes of wild type (*wt*), *SPPL2a*$^{-/-}$, *CD74*$^{-/-}$ and *SPPL2a*$^{-/-}$ *CD74*$^{-/-}$ mice. In brief, 250 µg/ml OVA-FITC was allowed to be internalized into splenocytes for 30 min at 37 °C. Cells were washed followed by a chase for 0-24 h at 37 °C. After staining for CD21, CD24 and B220, MFI for the FITC channel was determined flow cytoemetricly for the T1 B cell subpopulation (B220^{+} CD21^{low} CD24^{high}). Mean of normalized MFI ± SEM, n = 3 per genotype; three independent experiments. (B) The intracellular OVA half-life was calculated for the data set of (A) by non-linear regression. Mean of $t_{1/2}$ ± SD, n = 3 per genotype; three independent experiments. *, P < 0.05; One-way ANOVA with Newman-Keuls posthoc testing.

3.2 Role of SPPL2a-mediated cleavage of CD74 in BCR signaling

3.2.1 BaffR signaling is impaired in SPPL2a-deficient B cells

Besides the described impairments in the endocytic system, accumulation of CD74 NTF in SPPL2a-deficient B cells causes a block in B cell maturation at the T1 stage. In order to study the detailed underlying mechanism, signaling pathways which have been implicated in B cell differentiation and survival were analyzed. Mainly, signals transmitted via the BCR and signals provided by the cytokine BAFF and its receptor BAFFR are critical for the maturation and survival of B cells and the transition from the T1 to the T2 developmental stage (Miller & Hayes, 1991; Schiemann *et al.*, 2001; Thompson *et al.*, 2001). Initially, surface as well as total BAFFR levels were analyzed by flow cytometry in different splenic B cell subpopulations. Throughout all splenic developmental stages (T1, T2 and mature) and in total splenic B cells ($B220^{+}$) a considerable reduction of BAFFR surface expression was observed in SPPL2a-deficient cells when compared to the corresponding wild type cells (Figure 31). Additionally, total BAFFR levels were similarly reduced in all different B cell stages of *SPPL2a*$^{-/-}$ mice. This indicates that surface as well as intracellular BAFFR levels are equally reduced in SPPL2a-deficient B cells.

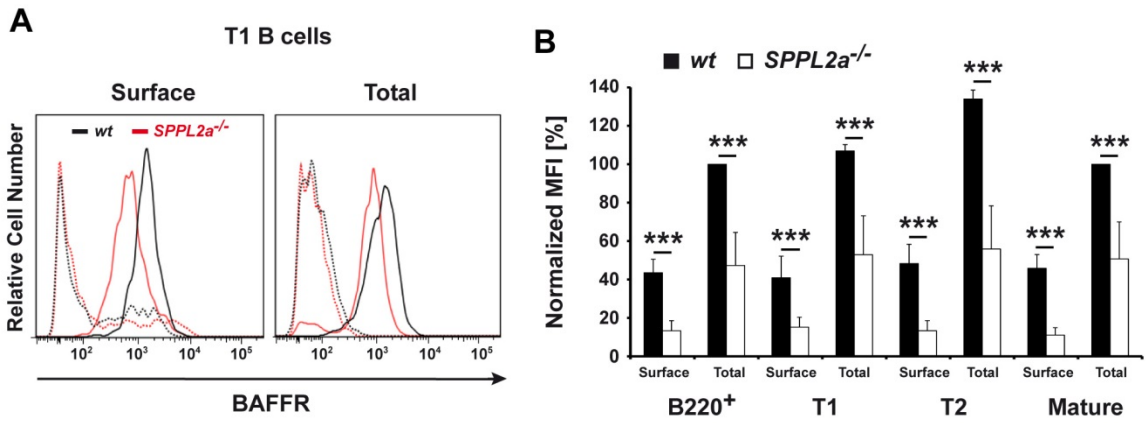

Figure 31. Reduced BAFFR levels in SPPL2a-deficient splenic B cells. Splenocytes of wild type (*wt*) and *SPPL2a*$^{-/-}$ mice were stained for the BAFFR without or after permeabilization along with the surface markers CD21, CD24 and B220. MFI of surface and total BAFFR levels were determined for $B220^{+}$, T1 ($B220^{+}$ $CD21^{low}$ $CD24^{high}$), T2 ($B220^{+}$ $CD21^{high}$ $CD24^{high}$) and mature ($B220^{+}$ $CD21^{low}$ $CD24^{low}$) B cells. Data are shown as histogram of one representative experiment (A) or as mean of MFI ± SD, n = 6 per genotype, five independent experiments (B). MFIs for T1, T2 and mature cells of each experiment were normalized to the total value of mature wild type cells; MFIs for $B220^{+}$ cells were normalized to the total MFI of wild type $B220^{+}$ cells. (A) Respective isotype controls are indicated as dashed lines. ***, $P < 0.001$; unpaired, two-tailed Student's *t*-test.

A reduction in protein level could be due to decreased gene expression or increased protein degradation. By performing qRT-PCR, mRNA levels of the *BAFFR* were analyzed in splenic B220$^+$ B cells of wild type and *SPPL2a*$^{-/-}$ mice. *BAFFR* mRNA of SPPL2a-deficient B cells was found to be comparable to wild type cells (Figure 32). Since no changes were detectable at the transcript level, an increased protein turnover is likely to account for the diminished surface and intracellular BAFFR levels in SPPL2a-deficient B cells.

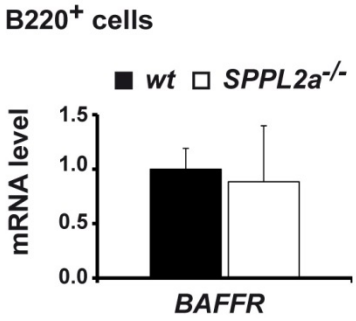

Figure 32. Transcription level of the *BAFFR* gene is not altered in *SPPL2a*$^{-/-}$ B220$^+$ B cells. Total RNA was isolated from splenic B220$^+$ B cells of wild type (*wt*) and SPPL2a-deficient (*SPPL2a*$^{-/-}$) mice. After first strand cDNA synthesis, *BAFFR* mRNA levels were determined by qRT-PCR using the Universal Probe Library Technology and gene specific primers. Data are shown as mean of ΔΔCp ± SD after normalization to the wt, n = 3, three independent experiments.

Initiation of the BAFFR signaling cascade is obligatory to provide essential survival signals for B cells in order to promote differentiation from the T1 to the T2 maturation stage (Mackay & Schneider, 2009). Stimulation of the BAFFR primarily activates the alternative NF-κB pathway leading to the processing of p100 to p52. p52 finally acts as transcription factor and enhances the synthesis of anti-apoptotic proteins (Do *et al*., 2000; Mackay *et al*., 2010; He *et al.*, 2004; Hsu *et al*., 2002). In order to prove whether the reduction of BAFFR surface levels has an impact on downstream signaling, the protein levels of p100 and its processed form p52 were analyzed by Western Blotting. The transcriptionally active form p52 was present in comparable amounts in splenic B220$^+$ B cells of both genotypes (Figure 33). This observation indicates that the constitutive activation of the alternative NF-κB pathway is not significantly affected by the reduced BAFFR surface expression. However, splenic B220$^+$ B cells of *SPPL2a*$^{-/-}$ mice showed reduced amounts of the precursor p100 when compared to wild type cells.

The NF-κB precursor p100 is synthesized upon induction of BCR-mediated tonic signaling that directly links BCR and BAFFR signaling pathways (Stadanlick *et al.*, 2008). Thus, diminished p100 levels could point to an impaired tonic BCR signaling which is in turn essential for the survival of B cells (Kurosaki *et al.*, 2010; Monroe, 2004; Monroe *et al*., 2006). Therefore, signaling mediated by the BCR was analyzed.

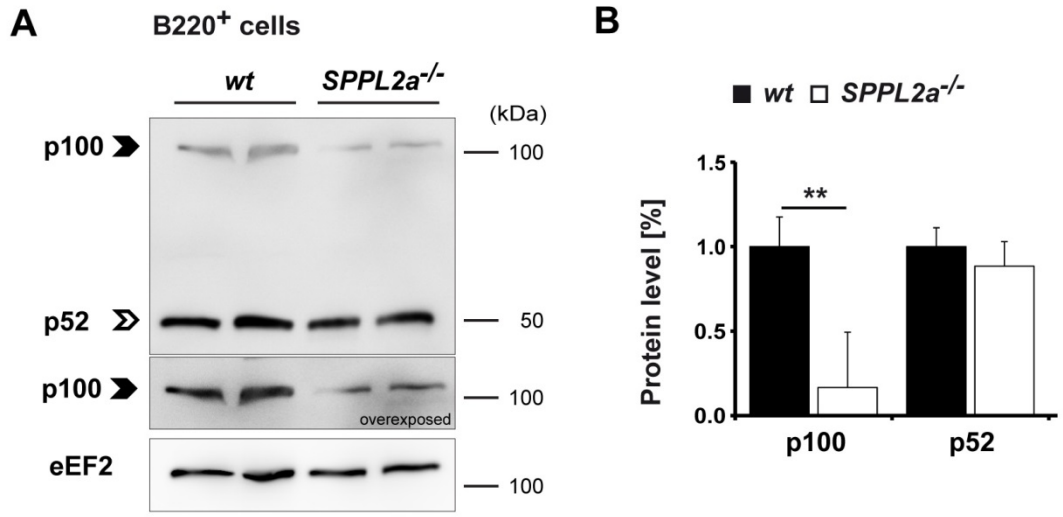

Figure 33. Reduced p100 protein levels in *SPPL2a*$^{-/-}$ B cells. (A) Total cell lysates of wild type (*wt*) and *SPPL2a*$^{-/-}$ splenic B220^{+} B cells were analyzed by Western Blotting using an antibody against p100/p52. p100 is indicated by a closed, p52 by an open arrowhead. eEF2 served as loading control. Data of two mice per genotype are shown. (B) Western Blots were quantified by densitometric analysis. Data are shown as mean ± SD after normalization to wild type values, n = 5 per genotype, two independent experiments. **, $P < 0.01$; unpaired, two-tailed Student's *t*-test.

3.2.2 *SPPL2a*$^{-/-}$ B cells exhibit reduced activation of the tyrosine kinase Syk upon BCR stimulation

The BCR regulates a multiplicity of B cell fate decisions, e.g. survival, proliferation and differentiation (Niiro & Clark, 2002). Upon BCR ligation and phosphorylation of ITAMs in the cytoplasmic tail of the BCR subunits Igα and Igβ, activation of the kinase Syk by phosphorylation is regarded as one of the initial steps of BCR signaling (Hutchcroft *et al.*, 1991). To investigate the capacity of SPPL2a-deficient B cells to transmit signals via the BCR, activation of Syk was analyzed. Therefore, basal (tonic) phosphorylation of Syk as well as phosphorylation upon BCR stimulation was measured in B220^{+} B cells by Western Blotting using an antibody against the phosphorylated form of Syk as well as an antibody detecting total Syk. Cross-linking of the BCR of splenic B220^{+} cells from wild type mice with anti-IgG/IgM for five minutes triggered an obvious increase of phosphorylated and thus activated Syk (Figure 34 A). In comparison, only a minor activation of Syk was observed in *SPPL2a*$^{-/-}$ B220^{+} cells upon BCR ligation. Basal levels of pSyk were comparable in B220^{+} B cells of both genotypes. Densitometric analysis of Western Blots confirmed these observations (Figure 34 B). However, the observed changes were not significant. This might be due to the divergent B cell populations that have been analyzed for wild type and *SPPL2a*$^{-/-}$ mice. Sorting for B220^{+} B cells from spleen results in the isolation of all different splenic B

cell populations including T1, T2 as well as mature B cells. Due to the B cell maturation defect of SPPL2a-deficient mice at the T1 stage, *SPPL2a*$^{-/-}$ B220^{+} B cells primarily comprise T1 B cells, whereas B220^{+} B cells isolated from wild type mice include all splenic B cell subpopulations. Flow cytometric analysis provides an ideal tool to examine protein levels in specifically gated B cell subpopulation. For this reason, a flow cytometry-based assay for the analysis of phosphorylated kinases was established. BCR cross-linking in splenocytes was achieved with anti-IgG/IgM as described above. Subsequently, cells were fixed and permeabilized. The detection of kinases was accomplished by staining with primary antibodies specific for their phosphorylated forms or antibodies detecting the total kinase levels, followed by staining with an Alexa Fluor 488-coupled secondary antibody. Simultaneous staining for the cell surface markers CD21, CD24 and B220 allowed gating for the different B cell subpopulations. Application of this procedure to compare the Syk phosphorylation status displayed a significant reduction of Syk activation upon BCR stimulation for T1 B cells of SPPL2a-deficient mice (Figure 34 C) whereas basal levels of phosphorylated Syk were comparable in wild type and *SPPL2a*$^{-/-}$ T1 B cells.

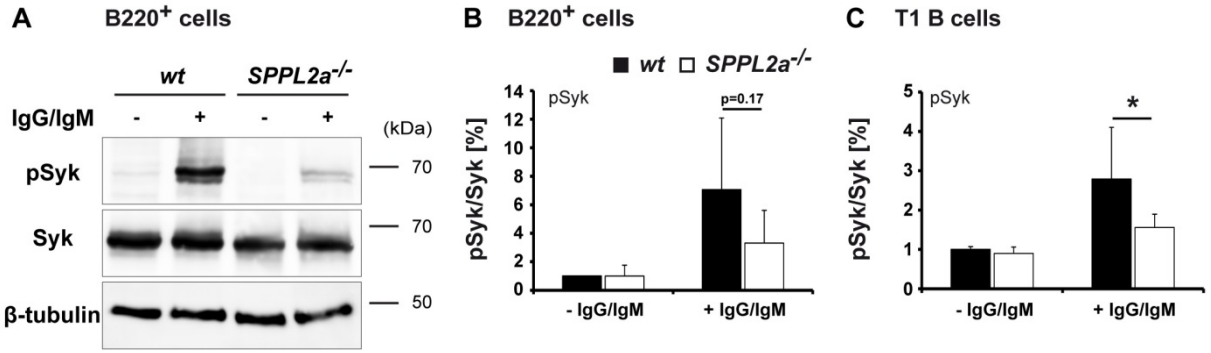

Figure 34. Reduced activation of Syk in B cells of SPPL2a-deficient mice. (A) Splenic B220^{+} B cells of wild type (*wt*) and SPPL2a-deficient (*SPPL2a*$^{-/-}$) mice were stimulated with 10 µg/ml anti-IgG/IgM for 5 min to induce BCR signaling or left unstimulated. Cells were lysed and analyzed by Western Blotting using antibodies against pSyk and total Syk. Equal protein loading was confirmed by using β-tubulin. One representative Western Blot of n = 3 per genotype is shown. (B) Respective densitometric analysis of pSyk/Syk of (A). Data are depicted as mean ± SD, n = 5 per genotype, five independent experiments. (C) wild type and *SPPL2a*$^{-/-}$ splenocytes were stimulated as described above, fixed and permeabilized. Subsequently, cells were stained for pSyk or Syk along with the cell surface markers CD21, CD24 and B220. For the detection of pSyk and Syk, an Alexa Fluor 488-coupled secondary antibody was used. T1 cells (B220^{+} CD21^{low} CD24^{high}) were analyzed by flow cytometry by determining the MFI for the Alexa Fluor 488 channel. Data are shown as mean of MFI ratios ± SD after normalization of pSyk/Syk ratios to the ratios of the unstimulated wild type sample, n = 6, three independent experiments. *, $P < 0.05$; unpaired, two-tailed Student's *t*-test.

Altogether, these observations strongly demonstrate that *SPPL2a*$^{-/-}$ B cells show a diminished signal transmission via the BCR complex.

3.2.3 *SPPL2a*$^{-/-}$ B cells show reduced PI3K/Akt signaling but unaffected activation of the MAPK pathway

To assess the consequences of modified Syk activation in *SPPL2a*$^{-/-}$ B cells on downstream pathways, putative impairments within the MAPK and PI3K/Akt pathway were analyzed. Stimulation of the BCR with anti-IgG/IgM led to an increase of the phosphorylated and thus activated form of the MAPKs ERK1/2 in wild type B220^{+} B cells when compared to unstimulated cells (Figure 35 A and B).

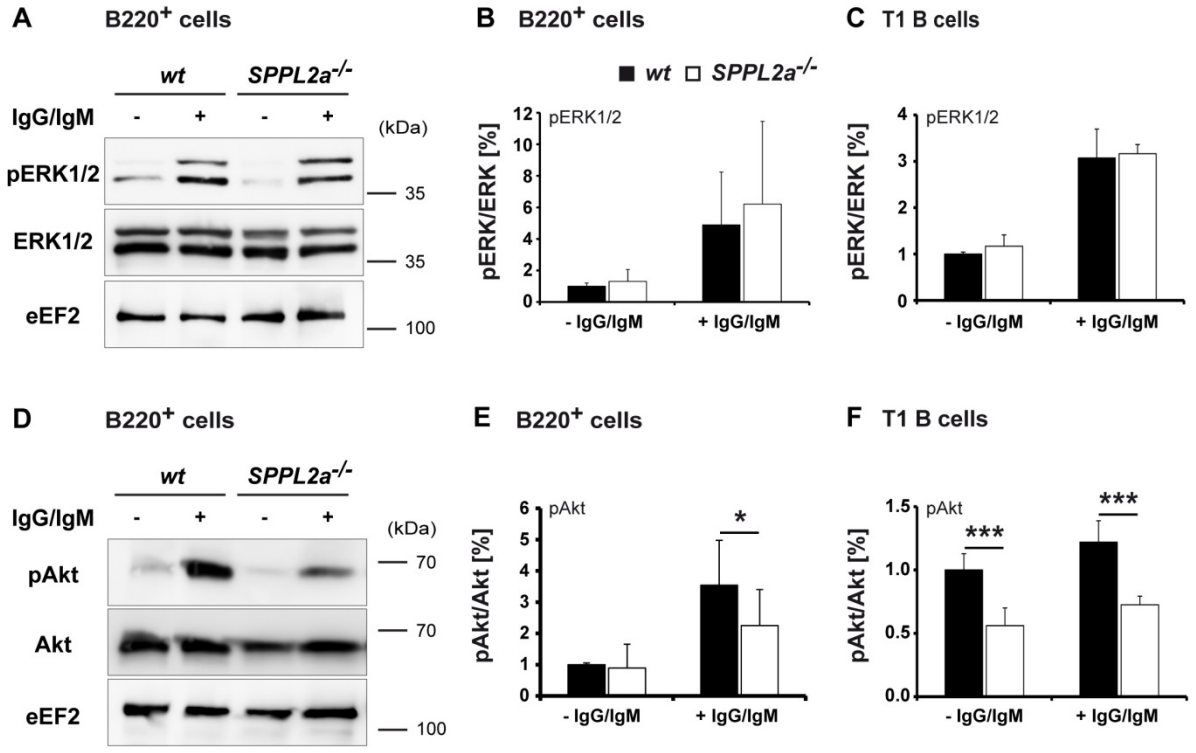

Figure 35. In *SPPL2a*$^{-/-}$ B cells, activation of the kinase Akt is impaired whereas phosphorylation of ERK1/2 appears to be unaffected. Western Blotting (A, D) and respective densitometric analysis (B, E) of ERK1/2 and Akt phosphorylation in splenic B220^{+} B cells isolated from wild type (*wt*) and *SPPL2a*$^{-/-}$ mice. BCR signaling was induced by stimulating the cells for 5 min with 10 µg/ml anti-IgG/IgM. Total cell lysates were used for Western Blot analysis. Equal protein loading was confirmed by eEF2. Data are shown as mean ± SD, n = 10 per genotype, eight-nine independent experiments. (C, F) pERK/ERK and pAkt/Akt levels of T1 B cells (B220^{+} CD21^{low} CD24^{high}) of wild type and *SPPL2a*$^{-/-}$ B cells were determined by flow cytometry. Splenocytes were left unstimulated or stimulated with 10 µg/ml anti-IgG/IgM for 5 min, fixed and permeabilized. Cells were stained for phosphorylated or total forms of ERK1/2 or Akt in combination with CD21, CD24 and B220 to allow gating for the T1 subpopulation. Primary antibodies against phosphorylated and total forms of kinases were detected using an Alexa Fluor 488-coupled secondary antibody. Data are shown as mean of MFI ratios ± SD, MFI ratios were normalized to the unstimulated wild type MFI ratio; n = 5, three independent experiments. ***, $P < 0.001$; *, $P < 0.05$; unpaired, two-tailed Student's *t*-test.

Basal pERK1/2 as well as pERK1/2 levels upon BCR stimulation of *SPPL2a*$^{-/-}$ B220^{+} B cells were found to be similar to the wild type levels. Equivalent results were obtained for the T1 subpopulation of wild type and SPPL2a-deficient mice by flow cytometric analysis (Figure 35 C). Interestingly, analysis of Akt by Western Blotting revealed a significant reduction of its phosphorylated form in *SPPL2a*$^{-/-}$ B220^{+} B cells upon BCR ligation (Figure 35 D and E). The reduction of pAkt levels in SPPL2a-deficient B cells could be confirmed for the T1 subpopulation by flow cytometric analysis (Figure 35 F). In addition, diminished tonic Akt phosphorylation was detectable in T1 B cells of *SPPL2a*$^{-/-}$. Accordingly, deficiency of SPPL2a appears to cause a considerable impairment of tonic as well as ligand-induced Akt activation without affecting the MAPK pathway.

In order to elucidate the reason for the impaired Akt activation in *SPPL2a*$^{-/-}$ B cells, levels of the PI3K product phosphatidylinositol-(3,4,5)-trisphosphate (PIP_3), which is a prerequisite for Akt activation, were determined flow cytometrically. Therefore, PIP_3 was detected with a biotinylated anti-PIP_3 antibody which was visualized using streptavidin coupled to the fluorophor APC. Simultaneous staining for CD21, CD24 and B220 allowed gating for B220^{+} and T1 B cells. In comparison to the wild type, both B cell populations of *SPPL2a*$^{-/-}$ mice showed reduced levels of PIP_3 upon BCR cross-linking (Figure 36). Surprisingly, levels of basal PIP_3 were comparable in wild type and knock-out T1 B cells. Thus, PIP_3 levels are not as significantly reduced as the decreased Akt activation would suggest.

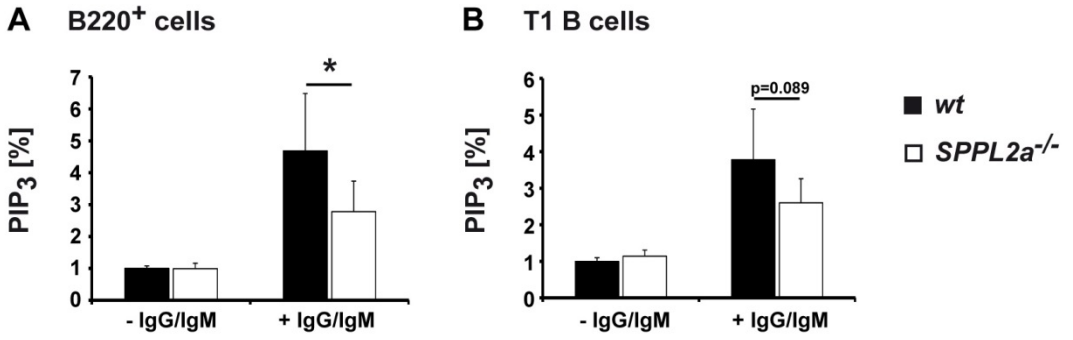

Figure 36. Diminished PIP_3 levels in B220^{+} and T1 *SPPL2a*$^{-/-}$ B cells upon BCR ligation. Wild type (*wt*) and SPPL2a-deficient (*SPPL2a*$^{-/-}$) splenocytes were stimulated with 10 µg/ml anti-IgG/IgM for 5 min or left untreated. After fixation and permeabilization, cells were stained for PIP_3 using a biotin-coupled antibody in combination with CD21, CD24 and B220 to allow gating for B220^{+} and T1 B cells. Finally, PIP_3 was detected with APC-coupled streptavidin. MFI of PIP_3 was determined for the B220^{+} (A) and T1 subpopulation (B220^{+} CD21^{low} CD24^{high}, B) by flow cytometry. Data are shown as mean of normalized MFI ± SD, n = 6, four independent experiments. *, $P < 0.05$; unpaired, two-tailed Student's *t*-test.

According to this, SPPL2a-deficiency in B cells seems to more dramatically affect Akt phosphorylation than PIP_3 levels which could point to a direct inhibitory effect of CD74 NTF accumulation on the activation of Akt.

Both MAPK and PI3K/Akt signaling originate from an exogenous stimulus transmitted by the BCR which is further forwarded by the kinase Syk (Figure 7). Thus, the observation of a reduced activation of the PI3K/Akt pathway without detecting any impairment in the MAPK cascade seems to be unexpected at first glance. Closer inspection shows that activation of PI3K requires, besides the BCR, the presence of the Co-BCR complex composed of CD19, CD21 and CD81. In contrast, activation of RAS and subsequent phosphorylation of ERK1/2 is not dependent on the Co-BCR complex (Figure 7). In order to assess the potential impact of the Co-BCR on downstream signaling, surface levels of CD19 and CD21 were determined flow cytometrically. Both cell surface molecules were considerably reduced in T1 B cells of *SPPL2a*$^{-/-}$ mice (Figure 37) which may explain the divergently affected MAPK and PI3K/Akt downstream signaling.

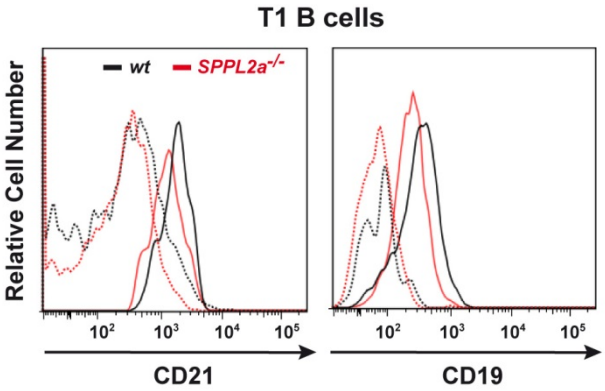

Figure 37. *SPPL2a*$^{-/-}$ have reduced surface expression of the Co-BCR molecules CD21 and CD19. Surface expression of CD21 in and CD19 in T1 B cells (B220^{+} CD21^{low} CD24^{high}) of wild type (*wt*) and *SPPL2a*$^{-/-}$ mice was determined by flow cytometry after surface staining of cells for CD19, CD21, CD24 and B220. Histograms are representatives of two independent experiments. Isotype controls of each genotype are illustrated as dashed lines.

3.2.4 SPPL2a-mediated clearance of CD74 NTF is essential for adequate PI3K/Akt signaling

It could be clearly shown that signaling via the BCR is severely affected in SPPL2a-deficient B cells. In order to elucidate the impact of the accumulating CD74 NTF on the defective signaling cascade, activation of the kinases Syk and Akt was examined in B cells of SPPL2a CD74 double-deficient mice. In *SPPL2a*$^{-/-}$ *CD74*$^{-/-}$ splenic B220^{+} cells, activation of Syk by phosphorylation was comparable to the wild type as revealed by Western Blotting (Figure 38 A and B). In agreement, flow cytometric analysis of T1 B cells showed the same tendency (Figure 38 C) Hence, the impaired Syk activation seen in SPPL2a-deficient B cells was

reversed by additional ablation of CD74. A similar trend was observed for the ligand-induced activation of the kinase Akt. Analysis of $B220^+$ B cells by Western Blotting and T1 B cells by flow cytometry showed a significant recovery of the PI3K/Akt signaling in SPPL2a CD74 double-deficient mice (Figure 38 D-F).

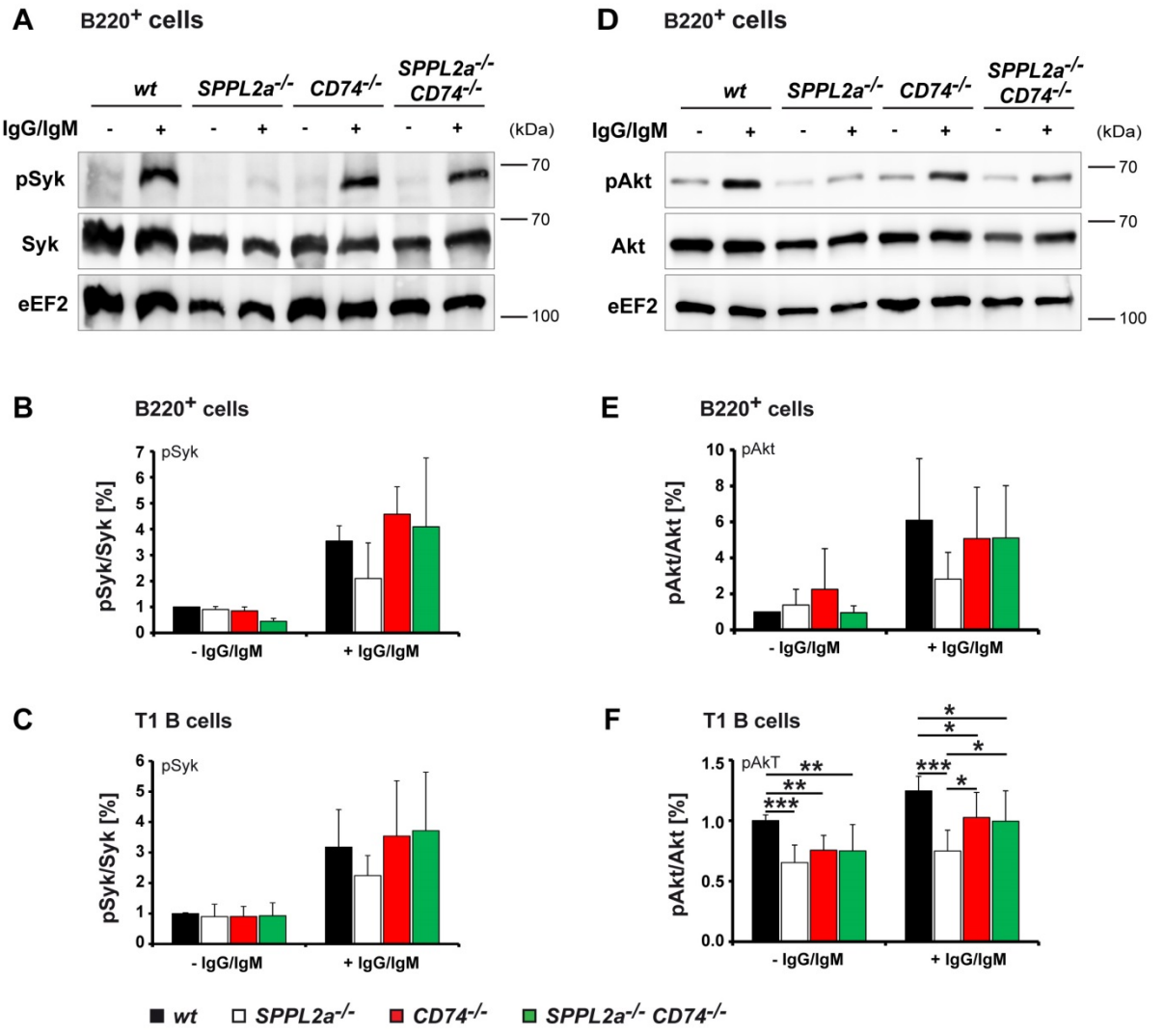

Figure 38. The impaired ligand-induced PI3K/Akt activation in *SPPL2a*$^{-/-}$ B cells can be alleviated by additional ablation of CD74. (A and D) Activation of Syk (pSyk) and Akt (pAkt) was examined by Western Blotting in total cell lysates of wild type (*wt*), *SPPL2a*$^{-/-}$, *CD74*$^{-/-}$ and *SPPL2a*$^{-/-}$ *CD74*$^{-/-}$ $B220^+$ B cells. Prior to cell lysis, BCR stimulation was performed with 10 µg/ml anti-IgG/IgM for 5 min. eEF2 served as loading control. Quantification of the respective immunoblots by densitometry is shown (B and E). Data are depicted as mean ± SD, n = 5, five independent experiments. (C and F) Phosphorylation of Syk and Akt was quantified flow cytometrically after stimulation of splenocytes for 5 min with 10 µg/ml anti-IgG/IgM. Cells were fixed, permeabilized and stained for phosphorylated and total forms of Syk and Akt along with CD21, CD24 and B220. After kinase detection with an Alexa Fluor 488-coupled secondary antibody, MFI was determined for T1 B cells ($B220^+$ $CD21^{low}$ $CD24^{high}$). Data are shown as mean of MFI ratios ± SD after normalization of the ratios to the unstimulated wild type, n = 8, seven independent experiments. ***, $P < 0.001$; **, $P < 0.05$; *, $P < 0.01$; One-way ANOVA with Newman-Keuls post-hoc testing.

However, no entire rescue was achieved. The reduced tonic activation of Akt in *SPPL2a*$^{-/-}$ T1 B cells was only ameliorated to a minor extent by ablation of CD74 (Figure 38 F). This is reflected by an already impaired basal and ligand-induced Akt phosphorylation in CD74 single-deficient T1 B cells. It is apparent that the activation of Syk and Akt in *SPPL2a*$^{-/-}$ *CD74*$^{-/-}$ B cells was always comparable to CD74 single-deficient B cells. This suggests that potential residual disturbances in the BCR-mediated signaling of SPPL2a CD74 double-deficient B cells may be caused by the deficiency of CD74. In conclusion, the described alleviation of the impaired ligand-induced Syk and Akt activation by additional ablation of CD74 provides clear evidence that optimal BCR signaling requires processing of CD74 NTF by SPPL2a.

3.2.5 IgM trafficking is altered in B cells of SPPL2a-deficient mice

As the delayed OVA degradation reveals, CD74 NTF accumulation due to SPPL2a-deficiency is critical for trafficking events within the endocytic system. Thus it is conceivable that potential alterations in BCR trafficking serve as initiator of impaired BCR downstream signaling. To test this hypothesis, BCR levels and its subcellular localization were analyzed by indirect immunofluorescence to detect the complex with an antibody directed against IgM. In splenic B220^{+} B cells isolated from wild type mice, IgM was localized at the plasma membrane as well as in vesicular structures positive for CD74 and MHCIIβ (Figure 39). Similar IgM localization was observed in SPPL2a-deficient B220^{+} B cells. Consequently, no changes regarding the steady state BCR localization were detectable by microscopic imaging. Indirect immunofluorescence can provide information about the subcellular localization of a molecule. However, due to the small size of B cells and the low proportion of cytoplasm in these cells, discrimination between surface localized IgM and IgM residing in intracellular vesicles in close proximity to the membrane is challenging. To evaluate the distribution of IgM more accurately, the amount of surface and total IgM was measured flow cytometrically.

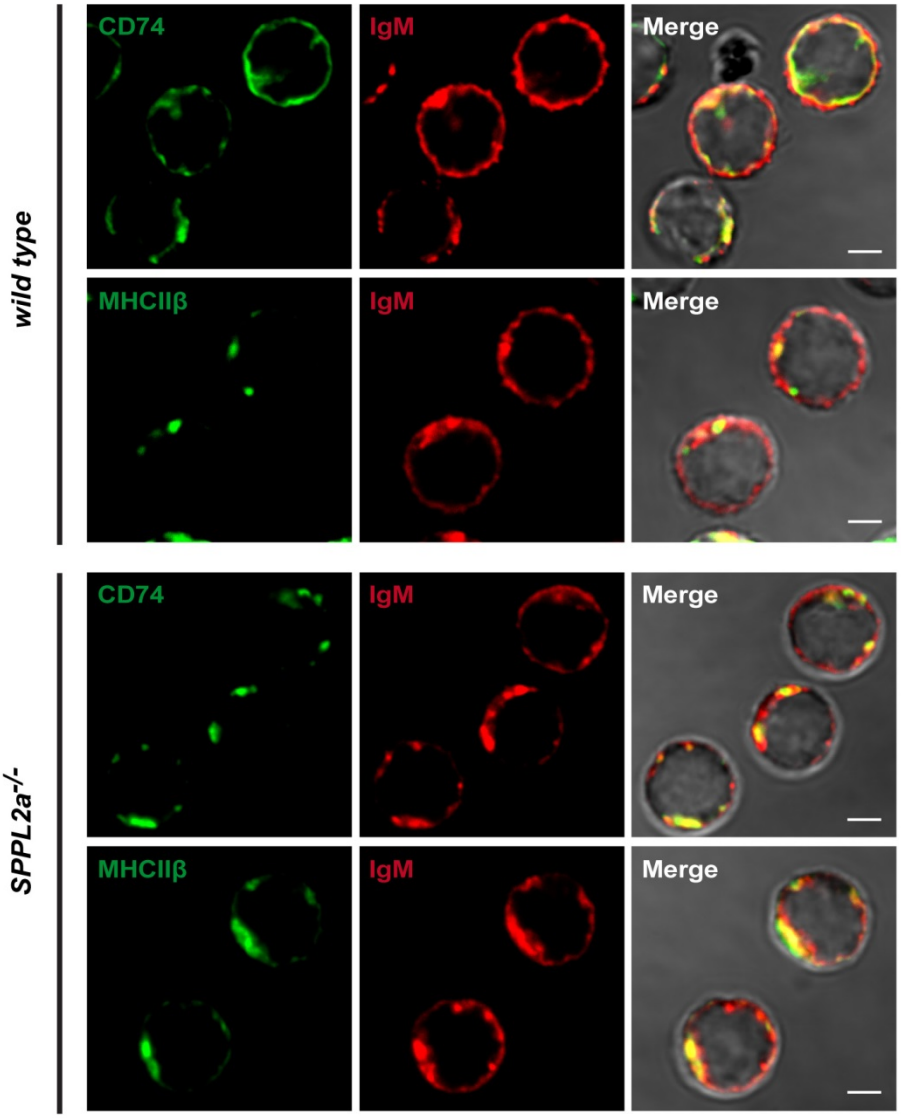

Figure 39. The steady state localization of IgM appears to be unaffected in B cells of *SPPL2a*$^{-/-}$ mice by confocal microscopy. Splenic B220^{+} B cells isolated from *wild type* and *SPPL2a*$^{-/-}$ mice were adhered to poly-L-lysine coated coverslips followed by fixation and permeabilization. CD74 (clone IN-1) and MHCIIβ were visualized by staining with primary antibodies and the corresponding Alexa Fluor 488-conjugated secondary antibody. Detection of IgM was accomplished using an anti-mouse IgM Alexa Fluor 594 antibody. Morphology of the cells was visualized by bright field. Co-localization is indicated by yellow staining (merge). Representative pictures from two independent experiments are shown. Scale bar, 2 µm.

Interestingly, *SPPL2a*$^{-/-}$ mice exhibited a substantial decrease of IgM protein levels at the cell surface detectable in T1, T2 as well as mature B cells by flow cytometry (Figure 40). In contrast, total amounts of IgM in the different B cell subsets of the spleen of *SPPL2a*$^{-/-}$ mice were comparable to the wild type levels. Consequently, reduction of IgM in SPPL2a-deficient B cells is restricted to the cell surface, assuming an accumulation of IgM in intracellular compartments. Subsequently, the reduced level of surface localized IgM in SPPL2a-deficient

B cells decreases the amount of BCR that is capable of transmitting signals upon BCR cross-linking. Therefore, the re-distribution of the BCR might be one reason for the decreased signal response upon BCR-ligation. In order to define whether CD74 NTF accumulation is associated with the diminished IgM surface level, IgM levels were determined in *SPPL2a*$^{-/-}$ *CD74*$^{-/-}$ B cells. As flow cytometric analysis of T1 B cells revealed, IgM levels are fully restored in these double-deficient cells (Figure 40 B). Interestingly, CD74 single-deficient as well as SPPL2a CD74 double-deficient T1 B cells showed increased IgM surface levels when compared to wild type B cells (Figure 40 B).

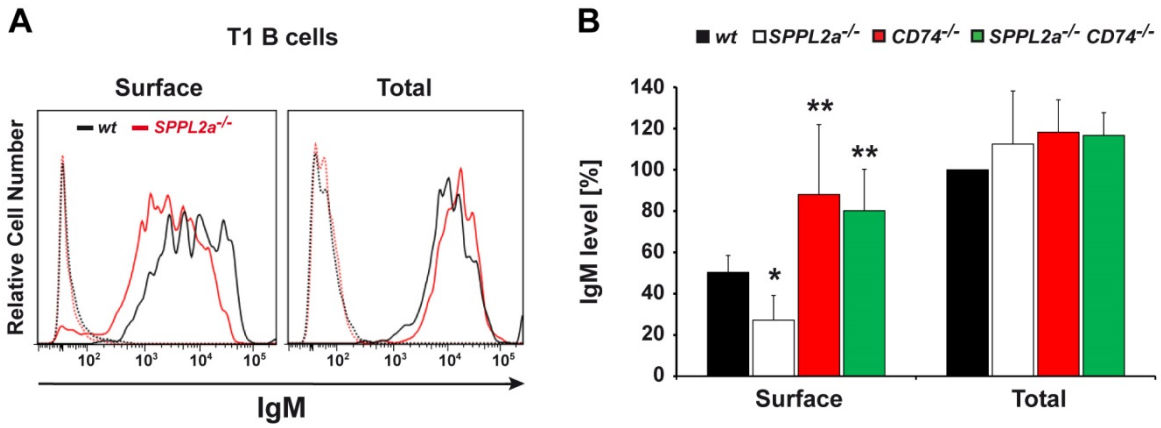

Figure 40. SPPL2a-deficient B cells show reduced IgM surface levels. Splenocytes of wild type (*wt*) and *SPPL2a*$^{-/-}$ mice were stained for IgM, either without or after fixation and permeabilization, along with the surface markers CD21, CD24 and B220. Surface and total IgM levels were determined flow cytometrically for T1 (B220^{+} CD21^{low} CD24^{high}) B cells. Data are shown as histogram of one representative experiment (A) or as mean of normalized MFI ± SD, n = 5-9 per genotype, three-seven independent experiments (B). Respective isotype controls are indicated as dashed lines. **, $P < 0.01$; *, $P < 0.05$; One-way ANOVA with Neuman-Keuls post-hoc testing. Significances are shown only related to the wild type.

In search for the reason of the reduced IgM surface levels, transcription of the gene coding for the membrane form of the constant region of the Ig heavy chain μ (allele b) was analyzed by qRT-PCR. *Ig μ* mRNA levels were found to be unaltered in SPPL2a-deficient splenic B220^{+} B cells (Figure 41). Accordingly, diminished IgM surface levels are not caused by dysregulated transcription of the corresponding gene. Instead, the observed reduction of IgM surface levels in *SPPL2a*$^{-/-}$ B cells in combination with unaffected total protein levels points to an altered trafficking of the BCR complex.

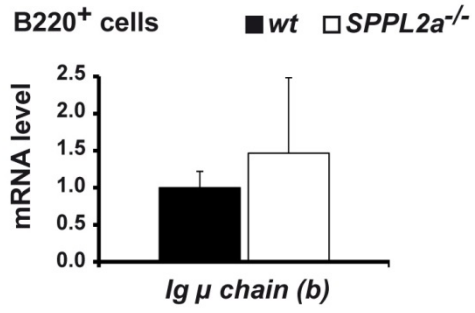

Figure 41. Transcription of the gene coding for the membrane-bound constant region of the Ig heavy chain µ (allele b) is not significantly altered in *SPPL2a*$^{-/-}$ B220^{+} B cells. Total RNA isolated from splenic B220^{+} B cells of wild type (*wt*) and SPPL2a-deficient (*SPPL2a*$^{-/-}$) mice was transcribed into cDNA and *Ig µ chain* mRNA levels were determined by qRT-PCR using the Universal Probe Library Technology and gene specific primers. Data are shown as mean of normalized ΔΔCp ± SD, n = 3, three independent experiments.

To test this hypothesis, the kinetics of BCR-mediated endocytosis were examined by an internalization assay. Therefore, the surface-localized BCRs of splenocytes isolated from wild type and SPPL2a-deficient mice were labeled with a biotinylated anti-IgM antibody at 4 °C (Figure 42). Subsequently, internalization of the antibody-BCR complex was accomplished by incubation at 37 °C for different time points. Finally, endocytosis was terminated by the addition of ice-cold PBS followed by the detection of the remaining surface IgM using APC-conjugated streptavidin. Simultaneous staining for the cell surface markers CD21, CD24 and B220 allowed flow cytometric gating of the T1 B cell population.

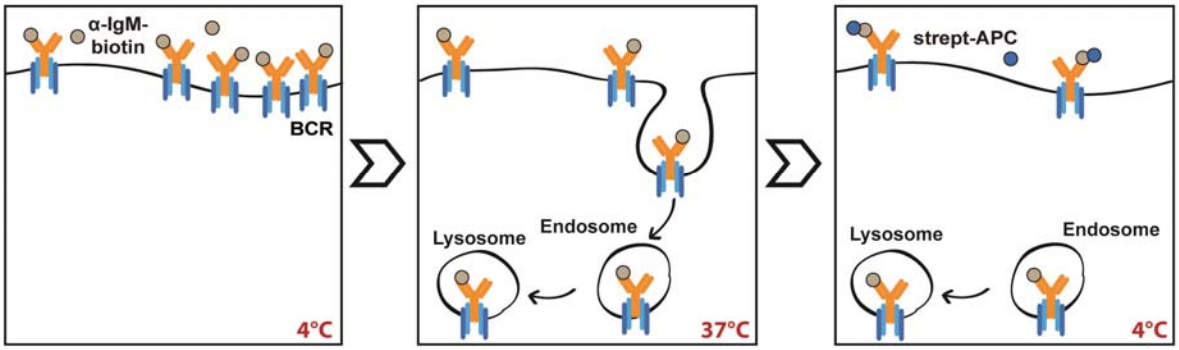

Figure 42. Experimental design of the established BCR-mediated endocytosis assay. Surface BCR of wild type and SPPL2a-deficient splenocytes were labeled with biotin-coupled anti-IgM for 30 min at 4 °C followed by endocytosis of the BCR-antibody complex for 0 - 30 min at 37 °C. After terminating the internalization with ice-cold PBS, IgM was visualized with streptavidin-APC (strept-APC) in combination with the B cell markers CD21, CD24 and B220 at 4 °C. MFI of the APC channel was determined by flow cytometric analysis for the T1 B cell population (B220^{+} CD21^{low} CD24^{high}).

In T1 B cells of wild type mice the signal intensity for surface labeled IgM decreased over time indicating a time-dependent endocytosis of the BCR (Figure 43). After 30 min of internalization, approximately 40 % of the BCR-antibody complex was endocytosed and thus reached intracellular compartments. In contrast, *SPPL2a*$^{-/-}$ T1 B cells endocytosed the complex much faster than wild type cells (Figure 43). Already after 5 min, a considerable

difference in the amount of remaining surface IgM was detectable between wild type and knock out cells. Additionally, endocytosis of the labeled BCR in SPPL2a-deficient T1 B cells reached a plateau after 20 min of internalization, whereas wild type cells still seemed to effectively endocytose at this time point.

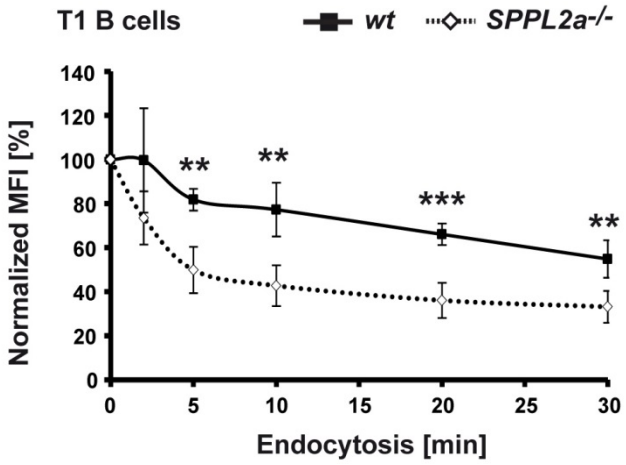

Figure 43. SPPL2a-deficient B cells show accelerated endocytosis of the BCR complex. Surface-localized IgM of wild type (*wt*) and SPPL2a-deficient (*SPPL2a*$^{-/-}$) splenocytes was labeled with biotin-coupled anti-IgM for 30 min at 4 °C. The antibody-BCR complex was allowed to internalize for various time points at 37 °C. The remaining antibody-BCR complexes at the cell surface were labeled with APC-streptavidin for 30 min at 4 °C along with staining for CD21, CD24 and B220. MFI of APC-labeled surface IgM was determined for T1 B cells (B220^{+} CD21^{low} CD24^{high}) by flow cytometry. For each genotype, the resulting MFIs were normalized to the MFI measured at time point 0. Data are shown as mean of normalized MFI ± SD, n = 4, two independent experiments. ***, $P < 0.001$; **, $P < 0.01$; unpaired, two-tailed Student's *t*-test.

Within the PI3K/Akt pathway, the kinase Akt has been shown to be activated only after internalization of the BCR complex and its delivery to endosomal compartments (Chaturvedi *et al.*, 2012). To analyze the fate of the endocytosed BCR complex and to exclude a potential mistrafficking of the BCR as a reason for impaired Akt activation, microscopic imaging methods were applied. Therefore, surface localized IgM of splenic B220^{+} B cells isolated from wild type and SPPL2a-deficient mice was labeled with Alexa Fluor 594-coupled anti-IgM at 4 °C. Subsequently, BCRs were allowed to internalize for 30 min at 37 °C followed by fixation of cells and staining for MHCIIβ by indirect immunofluorescence. In both wild type and *SPPL2a*$^{-/-}$ B220^{+} B cells, the internalized BCR complexes were delivered into intracellular vesicles which partially co-localized with MHCIIβ (Figure 44 A). The ultrastructure of these vesicles was further examined by electron microscopy. After labeling of wild type and *SPPL2a*$^{-/-}$ splenic B cells with IgM MicroBeads of the MACS system at 4 °C, controlled internalization of IgM MicroBeads was allowed for 20 min at 37 °C.

Subsequent electron microscopy was performed by Dr. Michaela Schweizer, ZMNH Hamburg, Germany. In wild type B cells, endocytosed IgM MicroBeads were detected in endocytic compartments with mostly multivesiculated structures (Figure 44 B). The morphology of IgM MicroBead-containing vesicles of SPPL2a-deficient B cells was found to be comparable to the one of wild type cells.

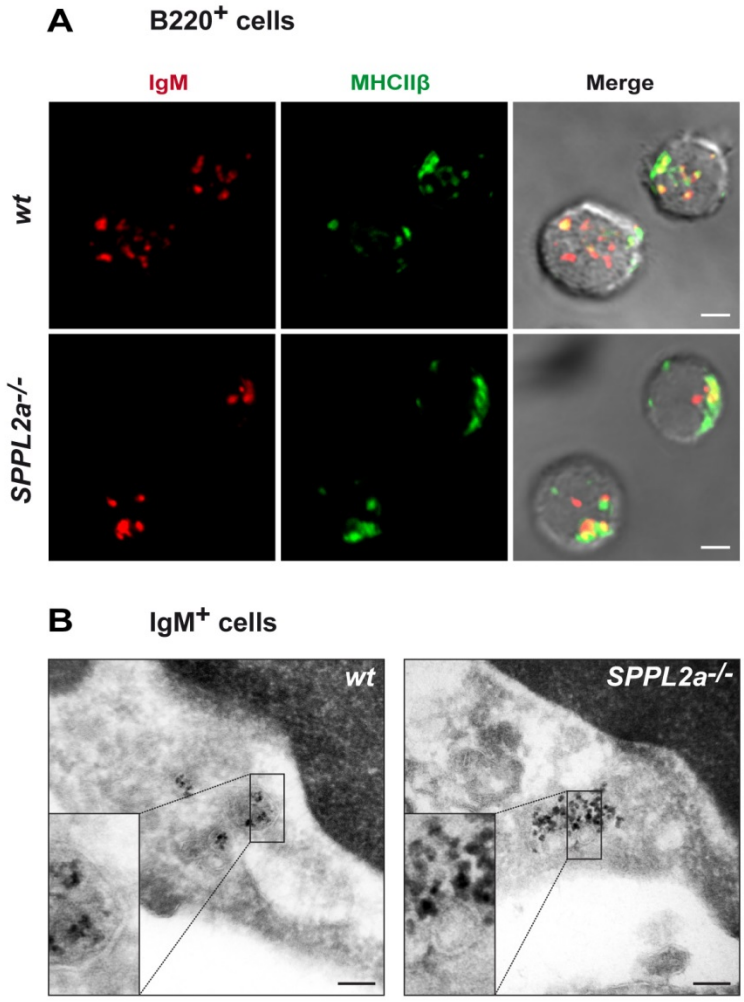

Figure 44. In wild type and SPPL2a-deficient splenic B cells, endocytosed BCR complexes reached endocytic compartments. (A) Internalized BCR was visualized by indirect immunofluorescence in splenic B220^{+} wild type (*wt*) and *SPPL2*$^{-/-}$ B cells. Surface IgM was labeled for 30 min at 4 °C followed by internalization of the BCR complex for 30 min at 37 °C. Cells were fixed and stained for MHCII β-chain (MHCIIβ) in order to label MHCII compartments. Representative pictures of two independent experiments are shown. Scale bar, 2 µm. (B) Electron microscopy of splenic IgM^{+} B cells isolated from wild type and SPPL2a-deficient mice was performed after 20 min internalization of bound IgM MicroBeads. Scale bar, 0.25 µm. Electron microscopy was performed by Dr. Michaela Schweizer, ZMNH Hamburg, Germany.

In summary, endocytosis of the BCR is significantly accelerated in *SPPL2a*$^{-/-}$ B cells leading to a reduction of IgM surface levels presumably accounting for the increase of intracellular IgM. Consequently, a considerable impairment of BCR trafficking has been allocated for

SPPL2a-deficient B cells. However, trafficking of the BCR to endocytic compartments is still functional in *SPPL2a*$^{-/-}$ B cells precluding a delivery defect as a cause for the impaired Akt activation.

3.2.6 Impaired BCR signaling is not exclusively caused by reduced IgM surface levels

The previously shown experiments focused on the analysis of splenic B cell subpopulations, mainly T1 B cells as the last preserved population in SPPL2a-deficient mice. Due to the fact that the B cell maturation defect manifests at the transition from the T1 to the T2 B cell stage, B cell function is expected to be most compromised at the T1 developmental stage representing an endpoint of the B cell phenotype. In order to study the functionality of BCR-mediated signaling in earlier B cell stages, immature B cells which precede the T1 B cell stage were analyzed. The amount of primary immature B cells which can be isolated from the bone marrow is very low. Thus, immature B220^{+} IgM^{+} B cells were enriched by culturing red bone marrow cells isolated from the tibia, femur and humerus of a mouse for 4 days in medium supplemented with 4 ng/ml IL-7 (Rowland *et al*., 2010). Prior to analysis, cells were cultured for one additional night in medium without IL-7. By flow cytometric analysis, an enrichment of 17-25 % of B220^{+} IgM^{+} could be proven for both wild type and *SPPL2a*$^{-/-}$ in each individual experiment (Figure 45).

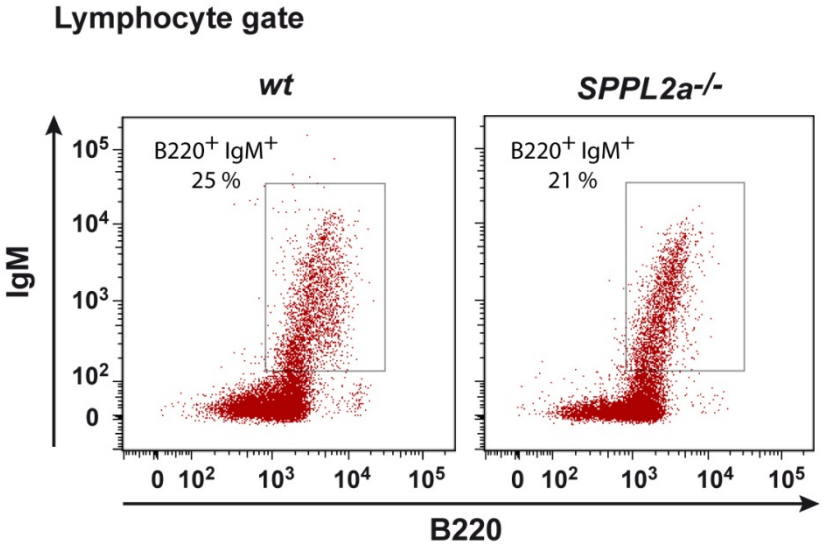

Figure 45. Analysis of immature B220^{+} IgM^{+} enriched cells by flow cytometry. Red bone marrow cells of tibia, femur and humerus of wild type (*wt*) and SPPL2a-deficient (*SPPL2a*$^{-/-}$) mice were isolated and cultured for 4 days in the presence of 5 ng/ml IL-7 and one day in the absence of the cytokine. Purity of the obtained cells was examined flow cytometrically after staining the cells with IgM and B220. One representative dot plot for each genotype is shown.

In order to detect the levels of CD74 NTF accumulation in immature B cells and B cells beyond the T1 developmental stage, CD74 protein levels were analyzed flow cytometrically by intracellular staining. Therefore, the antibody IN-1 directed against the N-terminus of CD74 was used which allows the detection of full-length CD74 as well as the NTF. Flow cytometric analysis revealed a considerable increase of CD74 in SPPL2a-deficient B cells of the immature, T1, T2 and mature stage when compared to the corresponding wild type control (Figure 46). Since deficiency of SPPL2a has no impact on the abundance of full-length CD74 (Schneppenheim, Dressel, Hüttl *et al.*, 2013; Schneppenheim, Hüttl *et al.*, 2014), the increase of the CD74 signal can be attributed to the accumulation of the CD74 NTF. Compared to wild type cells, *SPPL2a*$^{-/-}$ immature B cells showed a 3-fold increase of the CD74 signal which was found to be comparable in splenic T1 B cells (Figure 46). Thus, CD74 NTF significantly accumulates in immature B cells of SPPL2a-deficient mice.

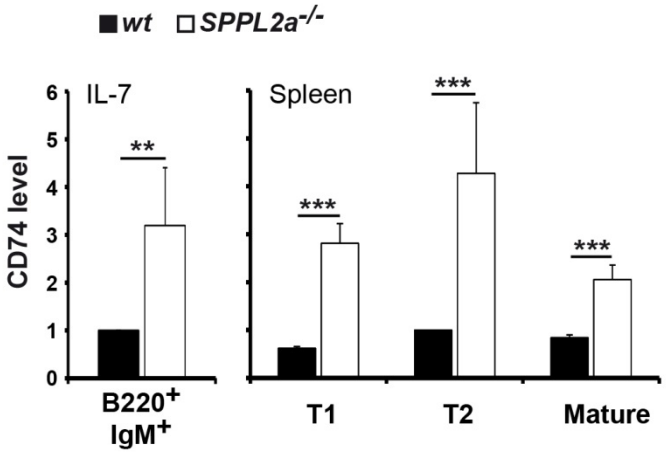

Figure 46. Increased CD74 NTF levels in immature B220$^+$ IgM$^+$ B cells as well as splenic B cells of *SPPL2a*$^{-/-}$ mice. Total CD74 levels were determined flow cytometrically in B cells of wild type (*wt*) and SPPL2a-deficient (*SPPL2a*$^{-/-}$) mice after intracellular staining. Immature B220$^+$ IgM$^+$ B cells were obtained from isolated red bone marrow cells cultured for 5 d with IL-7 and stained for IgM and B220 prior to flow cytometric analysis. Splenocytes were co-stained with CD21, CD24 and B220 and gated for T1 (B220$^+$ CD21^{low} CD24^{high}), T2 (B220$^+$ CD21^{high} CD24^{high}) and mature (B220$^+$ CD21^{low} CD24^{low}) B cells. Data are shown as normalized mean ± SD, n = 5, three independent experiments. ***, $P < 0.001$; **, $P < 0.01$; unpaired, two-tailed Student's *t*-test.

In addition to CD74 amounts, BCR-mediated signaling was analyzed in immature B220$^+$ IgM$^+$ B cells. As shown in Figure 47 A, activation of the tyrosine kinase Syk was significantly compromised in immature *SPPL2a*$^{-/-}$ B cells upon BCR stimulation which was comparable to T1 B cells of the same genotype (compare Figure 34). Interestingly, tonic and ligand-induced phosphorylation of the kinase Akt was only marginally reduced in immature *SPPL2a*$^{-/-}$ B cells (Figure 47 A). Additionally, IgM surface levels were analyzed flow

cytometrically and were found to be considerably decreased in *SPPL2a*$^{-/-}$ immature B cells when compared to wild type cells (Figure 47 B).

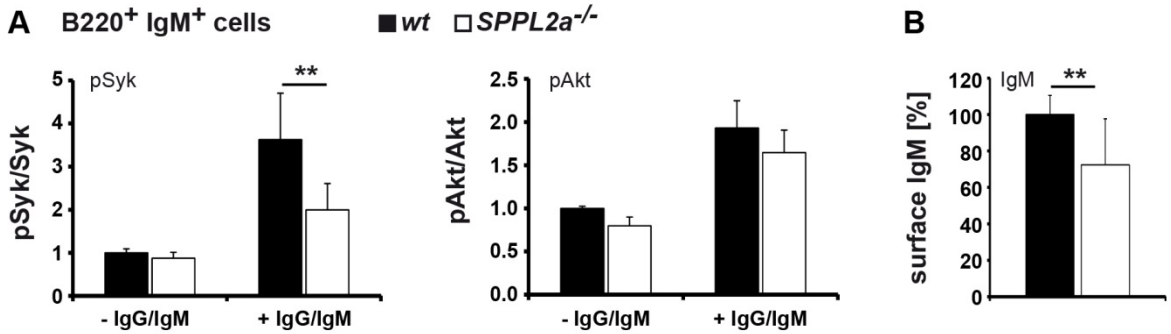

Figure 47. Immature B220$^+$ IgM$^+$ *SPPL2a*$^{-/-}$ B cells show significant impairments of Syk activation while Akt phosphorylation is only marginally affected. (A) Activation of the kinases Syk and Akt were measured flow cytometrically in B220$^+$ IgM$^+$ immature B cells isolated from wild type (*wt*) and *SPPL2a*$^{-/-}$ mice. Therefore, IL-7 cultured cells were stimulated with 10 µg/ml anti-IgG/IgM for 5 min at 37 °C or left unstimulated. Staining for phosphorylated and total Syk and Akt was performed as described previously along with staining for IgM and B220. MFIs were determined for B220$^+$ IgM$^+$ B cells. Data are shown as mean of MFI ratios ± SD after normalization of the ratios to the ratios of the unstimulated wild type samples, n = 8, four independent experiments. (B) IgM surface level of immature IL-7 cultured cells was determined by flow cytometry after staining of cells for IgM and B220. MFIs for the IgM-derived signal of B220$^+$ IgM$^+$ cells were determined. Data show MFIs normalized to the wild type ± SD, n = 6, three independent experiments. **, $P < 0.01$; unpaired, two-tailed Student's *t*-test.

To validate the observation of the differentially affected Syk and Akt activation, BCR signaling was examined in primary wild type B cells after short-term inhibition of SPPL2a. Therefore, freshly isolated splenocytes of wild type mice were cultivated overnight with the established SPP/SPPL inhibitors $(Z\text{-}LL)_2$ ketone and inhibitor X. As shown by flow cytometry, overnight application of the inhibitors induced a significant accumulation of CD74 NTF in wild type T1 B cells when compared to DMSO-treated control cells (Figure 48 A). Additionally, IgM surface levels were found to be considerably decreased (Figure 48 A). Analysis of the phosphorylation status of the kinase Syk demonstrated a tendency towards a reduction of ligand-induced pSyk levels in inhibitor-treated wild type T1 B cells compared to control cells (Figure 48 B). In line with the results obtained for immature B cells, the inhibitor-treatment did not affect the activation of Akt (Figure 48 B).

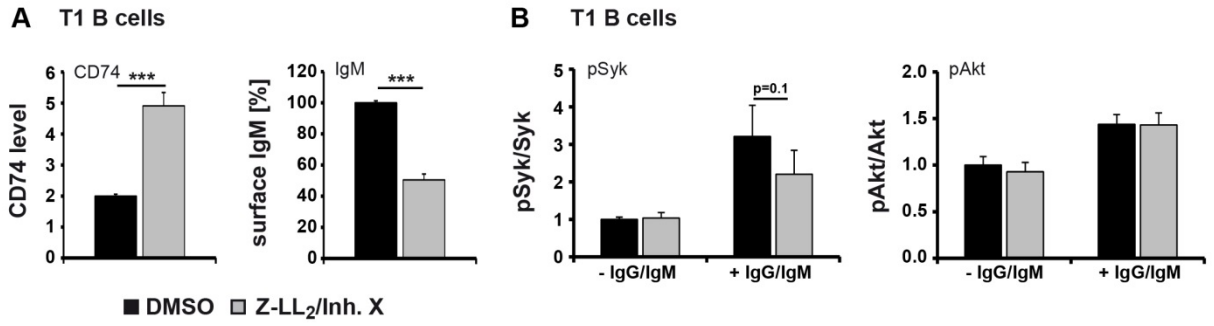

Figure 48. Inhibition of SPP/SPPLs by (Z-LL)$_2$ ketone and inhibitor X negatively affects the activation of the kinase Syk. Freshly isolated splenocytes from wild type mice were cultivated overnight in the presence of 10 µM (Z-LL)$_2$ ketone and 1 µM inhibitor X (Inh. X) or DMSO as control. (A) CD74 and IgM surface level were determined flow cytometrically. CD74 labeling was performed after permeabilization of cells, for detection of IgM non-permeabilized cells were used. Cells were co-stained for CD21, CD24 and B220 to allow gating for T1 B cells (B220$^+$ CD21^{low} CD24^{high}). Data represent MFIs normalized to the wild type ± SD. (B) BCR cross-linking of inhibitor- and DMSO-treated splenocytes was induced by incubation in 10 µg/ml anti-IgG/IgM for 5 min at 37 °C. Cells were fixed, permeabilzed and stained for the phosphorylated and total forms of Syk and Akt with primary antibodies which were finally detected with an Alexa Fluor 488-conjugated secondary antibody. MFIs of the FITC-channel were determined for T1 B cells and normalized to the unstimulated DMSO-treated wild type control. Mean of MFI ± SD, n = 4, three independent experiments. ***, $P < 0.001$; unpaired, two-tailed Student's t test.

Based on these observations it can be concluded that the reduced IgM surface levels and the compromised activation of Syk are two interconnected processes but do not necessarily involve impairments of the PI3K/Akt pathway.

The lowered activation of the protein tyrosine kinase Syk most likely reflects the diminished IgM surface levels. However, activation of Syk has been shown to be dependent on Src kinases which mediate the phosphorylated of Syk (Tsang *et al.*, 2008). In general, Src kinases are considered to be critical regulators of a variety of intracellular signaling pathways (Korade-Mirnics & Corey, 2000). They are found in association with the lipid membrane and their activation leads to the phosphorylation of downstream PTKs. To evaluate the expression profile of Src kinases in *SPPL2a*$^{-/-}$ B cells, the transcription of selected Src kinase family members were examined by qRT-PCR. In B cells, the Src kinases Fyn (Fyn proto-oncogene), Blk (B lymphoid kinase), Fgr (Gardner-Rasheed feline sarcoma viral (Fgr) oncogen), Hck (hemopoietic cell kinase) and Lyn (Yamaguchi sarcoma viral (v-yes-1) oncogene homolog) are predominantly expressed (based on BioGPS data). Splenic B220$^+$ B cells isolated from SPPL2a-deficient mice possessed only about half as much mRNA of *Fyn* compared to wild type B cells (Figure 49), In contrast to this, *Blk* and *Fgr* mRNA amounts were considerably up-regulated. The genes coding for Hck and Lyn were not differentially expressed.

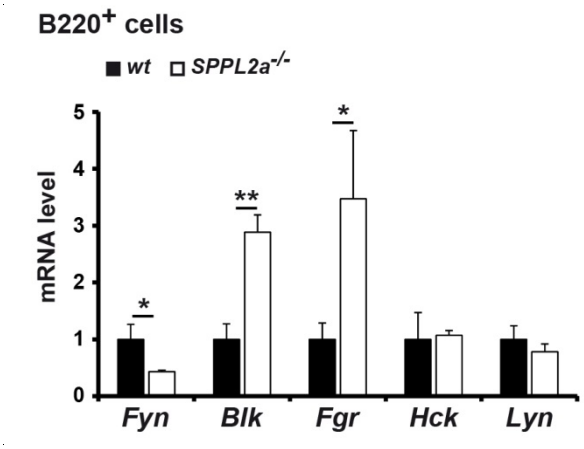

Figure 49. Src kinase gene expression is partially dysregulated in SPPL2a-deficient B cells. mRNA levels of the genes coding for the Src kinases Fyn, Blk, Fgr, Hck and Lyn were determined in wild type (*wt*) and *SPPL2a*$^{-/-}$ splenic B220^{+} B cells by qRT-PCR using the Universal Probe Library Technology and gene-specific primers. Data are shown as mean of normalized $\Delta\Delta Cp \pm SD$, $n = 3$, three independent experiments. **, $P < 0.01$; *, $P < 0.05$; unpaired, two-tailed Student's *t*-test.

In summary, *Fyn* mRNA levels were shown to be down-regulated in *SPPL2a*$^{-/-}$ B cells whereas *Blk* and *Fgr* were found to be transcriptionally up-regulated.

3.2.7 Disturbed PI3K/Akt signaling in *SPPL2a*$^{-/-}$ B cells promotes expression of pro-apoptotic genes and fails to down-regulate *RAG* gene expression

The previously described experiments clearly show that PI3K/Akt signaling is compromised in SPPL2a-deficient B cells resulting from accumulating CD74 NTF. In order to define whether the B cell phenotype of *SPPL2a*$^{-/-}$ mice can be directly linked to the defective BCR-mediated signaling, PI3K/Akt downstream signaling was analyzed in more detail. In B cells, the transcription factor FoxO1 is one prominent target of the kinase Akt and has been implicated in B cell differentiation with unique roles at the different maturation stages (Dengler *et al.*, 2008). To evaluate the impact of reduced Akt signaling on FoxO1 phosphorylation that leads to the inactivation of the protein, pFoxO1 was analyzed upon initiation of BCR signaling by Western Blotting. In wild type splenic B220^{+} cells, the level of phosphorylated FoxO1 increased by stimulation with anti-IgG/IgM (Figure 50). In comparison, basal as well as induced phosphorylation of FoxO1 was significantly diminished in *SPPL2a*$^{-/-}$ B220^{+} cells indicating a reduced inactivation of FoxO1 at the basal as well as ligand-induced levels.

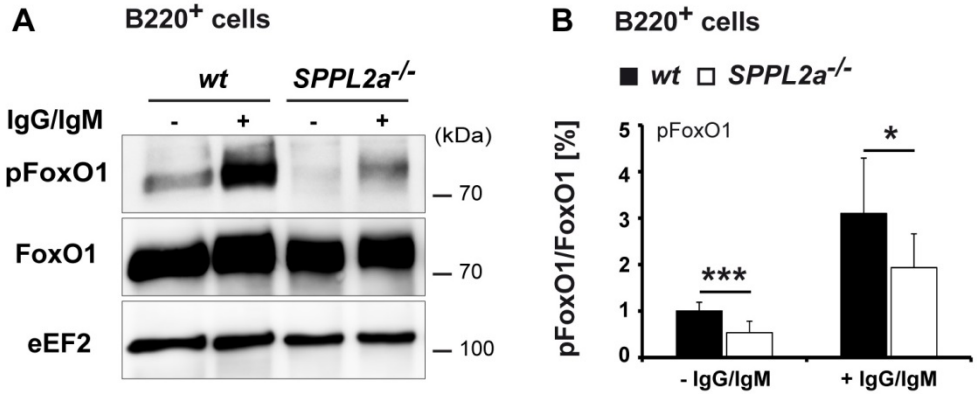

Figure 50. Impaired PI3K/Akt signaling in SPPL2a-deficient B cells causes reduced inactivation of FoxO1. BCRs of B220$^+$ B cells isolated from wild type (*wt*) and *SPPL2a*$^{-/-}$ mice cross-linked for 5 min with 10 µg/ml anti-IgG/IgM. Phosphorylation of FoxO1 was analyzed in total cell lysates by Western Blotting using a phosphorylation-specific antibody as well as an antibody recognizing total FoxO1. Equal protein loading was confirmed by staining for eEF2. Data are shown as one representative Western Blot (A) or were quantified by densitometric analysis (B), mean ± SD after normalization to the unstimulated wild type, n = 8, six independent experiments. ***, P < 0.001; *, P < 0.05; unpaired, two-tailed Student's *t*-test.

FoxO1 mRNA levels have been shown to be regulated by BCR signaling (Hinman et al., 2014). In detail, an increase of BCR-induced signaling via the PI3K leads to a down-regulation of FoxO1 mRNA expression minimizing the expression of pro-apoptotic genes and thus promoting cell survival and differentiation of the B cell. To examine BCR signaling-mediated down-regulation of FoxO1 mRNA in SPPL2a-deficient B cells, mRNA levels were quantified by qRT-PCR. In general, FoxO1 mRNA levels decreased in a time-dependent manner upon initiation of BCR signaling in wild type and *SPPL2a*$^{-/-}$ B cells with similar kinetics as described by Hinman and co-workers (Figure 51) (Hinman *et al.*, 2014).

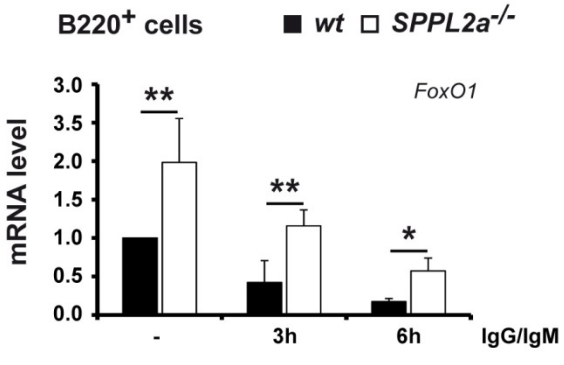

Figure 51. Upregulated *FoxO1* expression in *SPPL2a*$^{-/-}$ B220$^+$ B cells. *FoxO1* mRNA levels of wild type (*wt*) and SPPL2a-deficient (*SPPL2a*$^{-/-}$) splenic B220$^+$ B cells were determined by qRT-PCR using the Universal Probe Library Technology and gene-specific primers. Prior to total RNA isolation and first strand cDNA synthesis, B220$^+$ cells were stimulated with 10 µg/ml anti-IgG/IgM for 3 or 6 h or left unstimulated. Data are shown as mean normalized to the unstimulated wt ± SD, n = 3, three independent experiments. **, P < 0.01; *, P < 0.05; unpaired, two-tailed Student's *t*-test.

However, SPPL2a-deficient B220$^+$ B cells showed approximately 2-fold increased FoxO1 mRNA amounts after both tonic and initiated BCR signaling. Total FoxO1 protein levels analyzed by Western Blotting (Figure 50) did not reflect the elevated FoxO1 mRNA levels of *SPPL2a*$^{-/-}$ B cells which might be explained by rapid degradation of FoxO1 proteins.

To determine whether the impaired PI3K/Akt signaling and the dysregulated FoxO1 activity has an impact on the transcription of cell cycle regulating genes, the expression level of two representative FoxO1 targets was determined by qRT-PCR: *CDKN1B B*, the gene encoding the cyclin-dependent kinase inhibitor 1B (p27, Kip1) (Medema *et al*., 2000); and *CL2L11,* encoding the Bcl-2-interacting mediator of cell death (Bim) (Dijkers *et al.,* 2000). Both proteins have pro-apoptotic functions and are associated with B cell proliferation and survival (Su *et al.*, 2011). In B220$^+$ wild type B cells, *Bim* mRNA levels diminished after 6 h of anti-IgG/IgM stimulation as a response to BCR signaling and an increased amount of phosphorylated FoxO1 (Figure 52 A). In contrast, *SPPL2a*$^{-/-}$ B220$^+$ B cells showed an extensively upregulated transcription of *CL2L11* upon initiation of BCR signaling. Similarly, transcription of p27 was found to be considerably upregulated in SPPL2a-deficient B220$^+$ B cells upon BCR stimulation even without BCR ligation (Figure 52 B). In summary, reduced PI3K/Akt signaling in *SPPL2a*$^{-/-}$ B cells leads to restricted phosphorylation and potentially lowered cytoplasmic sequestration of FoxO1. Consequently, transcription of the pro-apoptotic genes *p27* and *Bim* is significantly upregulated in B cells of SPPL2a-deficient mice.

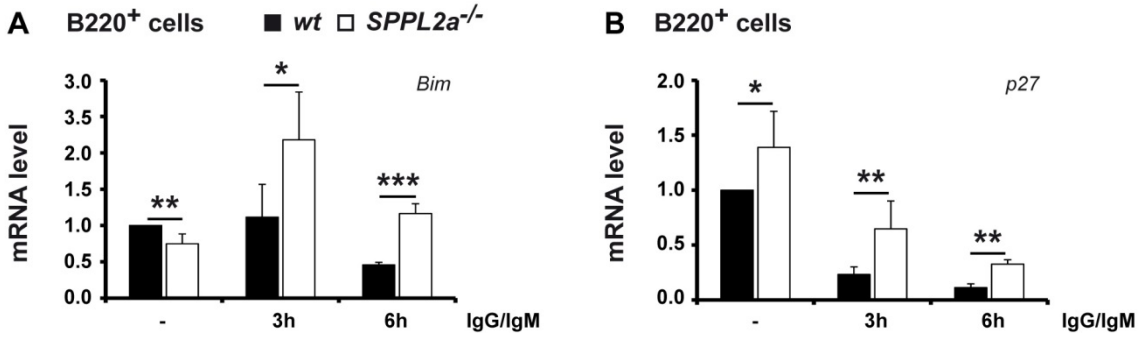

Figure 52. Reduced FoxO1 inactivation results in increased transcription of the genes coding for the pro-apoptotic proteins Bim and p27. Wild type (*wt*) and *SPPL2a*$^{-/-}$ B220$^+$ B cells were stimulated for 3 or 6 h with 10 µg/ml anti-IgG/IgM. Total RNA was extracted and transcribed into cDNA. Finally, mRNA levels were determined by qRT-PCR using the Uiniversal Probe Library Technology and gene-specific primers. Data are shown as mean normalized to the unstimulated wild type ± SD, n = 3, three independent experiments. ***, $P < 0.001$; **, $P < 0.01$; *, $P < 0.05$; unpaired, two-tailed Student's *t*-test.

According to previous studies, expression of the recombination-activating genes 1 and 2 (*RAG1*, *RAG2*) is regulated by the PI3K/Akt pathway and involves the action of FoxO1 (Amin & Schlissel, 2008; Novak *et al*., 2010; Verkoczy *et al.*, 2007; Grawunder *et al*., 1995; Keren *et al.*, 2004). *RAG1* and *RAG2* are predominantly expressed in the pro-B cell and small pre-B cell stage and drive the V(D)J recombination (Figure 6) (Sadofsky, 2001). After successful immunoglobulin rearrangement, the expression of *RAG1* and *RAG2* is turned off by increased signaling via the pre-BCR and BCR in order to prevent further rearrangements. By determination of the *RAG*s mRNA levels in splenic B220$^+$ B cells via qRT-PCR, the efficiency of down-regulated *RAG* expression was analyzed. Interestingly, splenic *SPPL2a*$^{-/-}$ B220$^+$ B cells showed 5- to 6-fold up-regulated steady state mRNA levels for both *RAG1* and *RAG2* compared to wild type B cells (Figure 53).

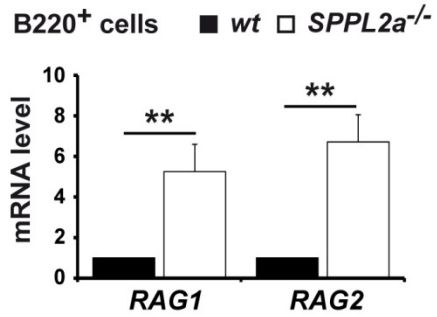

Figure 53. SPPL2a-deficient B220$^+$ B cells show up-regulated *RAG1* and *RAG2* mRNA levels. Total RNA was isolated from splenic B220$^+$ B cells from wild type (*wt*) and *SPPL2a*$^{-/-}$ mice and transcribed into cDNA. mRNA levels were determined by qRT-PCR using gene-specific primers and the Universal Probe Library Technology. Data are shown as normalized ΔΔCp ± SD, n = 3, three independent experiments. **, P < 0.01; unpaired, two-tailed Student's *t*-test.

In conclusion, it can be assumed that the intensity of tonic PI3K/Akt signaling in immature SPPL2a-deficient B cells is not sufficient to efficiently down-regulate *RAG* expression finally causing constitutively high levels of *RAG* mRNA.

4 Discussion

4.1 The CD74 NTF regulates the integrity of the endocytic system

4.1.1 CD74 NTF accumulation disturbs membrane trafficking

In the course of this work, the effects of CD74 NTF accumulation on the endocytic system were examined. Microscopic analysis showed that overexpression of CD74 in HeLa cells induces the formation of enlarged endocytic vesicles and that this effect is highly dependent on the net charge of the cytosolic domain of CD74. These observations are in line with studies from Bakke and co-workers who identified CD74 as regulator for endosome morphology and fusion (Nordeng *et al.*, 2002; Stang & Bakke, 1997). They propose that the negative net charge of the N-terminus of CD74 causes an imbalance of endosome fusion and fission upon overexpression of full-length CD74. In this context, the uncoating ATPase Hsc70 which is involved in the dissociation of clathrin coated vesicles was identified as an interaction partner of CD74. Overexpression studies revealed that trimerization of CD74 leads to the recruitment of Hsc70. The ATPase activity is suspected to cause premature uncoating of CD74-containing vesicles thereby shifting the balance towards endosome fusion which increases the size of these endosomes (Lagaudrière-Gesbert *et al.*, 2002).
In primary splenic B cells of *SPPL2a*$^{-/-}$ mice, CD74 NTF accumulation did not cause an obvious increase in vesicle size as shown for CD74 overexpression, but rather an increase in vesicle number. These divergent effects might be explained by the different cell systems (HeLa cells versus primary B cells) and the length of the accumulating CD74 fragment (full-length versus NTF). However, the mechanism underlying the process of vesicle enlargement and vesicle accumulation might be similar and both related to the high abundance of CD74 N-termini and their interaction with Hsc70 (Figure 55).

Studies in cell culture-based systems demonstrated that overexpression of CD74 delays endosome-to-lysosome transport (Gorvel *et al.*, 1995; Gregers *et al.*, 2003; Landsverk *et al.*, 2011). Consistently, the degradation of the fluid-phase cargo OVA-FITC is retarded in SPPL2a-deficient T1 B cells which is associated with the accumulating CD74 NTF. Since the maturation of several cathepsins as representative lysosomal proteases is unaffected in *SPPL2a*$^{-/-}$ B cells (data not shown) and no alterations in the lysosomal pH were detectable, impairments in lysosome function are unlikely. Instead, a delayed endosomal maturation is conceivable, similar to what has been published for the overexpression of CD74. The recycling kinetics of Tfn-488 after receptor-mediated endocytosis are largely comparable in

wild type and SPPL2a-deficient T1 B cells. However, *SPPL2a*$^{-/-}$ B cells retained an increased amount of Tfn in intracellular compartments as compared to wild type cells. This observation also argues for an impaired endocytic trafficking caused by CD74 NTF accumulation. Transport processes and fusion events within the endocytic system of a cell depend on a complex machinery consisting of different functional molecules. In particular, soluble N-ethylmaleimide-sensitive-factor attachment receptor (SNARE) complexes mediate the fusion of membranes together with Rab GTPases and the tethering factors CORVET and HOPS (Huotari & Helenius, 2011; Kümmel & Ungermann, 2014). Hypothetically, the high abundance of CD74 NTF in the late endosomal/lysosomal membrane of *SPPL2a*$^{-/-}$ B cells might disturb the interaction of membrane tethering factors such as Rabs, SNARES and the CORVET/HOPS complex. Since the accumulated CD74 NTF is primarily located in late endosomes and lysosomes, it can be speculated that this fragment might preferentially prevent the tethering of late endosomes and lysosomes thereby decelerating the lysosomal delivery of cargo molecules.

4.1.2 CD74 NTF accumulation affects the localization of certain receptors

Besides the discussed impairments in endosome trafficking, the distribution of certain receptors was found to be affected in splenic *SPPL2a*$^{-/-}$ B cells. The expression of the BAFFR is reduced concomitantly at the cell surface and in intracellular compartments (Figure 54). Analysis of the mRNA level of *BAFFR* did not reveal a reduced synthesis of the protein. Thus, the decreased BAFFR levels in SPPL2a-deficient B cells are likely to be caused by deregulated turnover of the protein. The most conceivable reason for this observation is the diminished tonic BCR signaling that is capable of regulating the BAFFR surface levels and will be discussed in the following course of this discussion. In contrast to the BAFFR which is equally reduced at the cells surface and intracellularly, the surface expression of the BCR is diminished whereas the total protein amount is comparable in *SPPL2a*$^{-/-}$ and wild type B cells (Figure 54). An accumulation of the BCR in intracellular vesicles of B cells deficient for SPPL2a can be assumed which would be in line with the observed enhanced endocytosis of the receptor in these cells. The synthesis of IgM is not significantly altered and the degradation of the BCR complex does not seem to be affected as well due to the comparable amount of total BCRs in wild type and *SPPL2a*$^{-/-}$ B cells. Thus, the reduced BCR surface levels are most likely caused by a redistribution of the receptor and an intracellular sequestration without affecting the overall amount of the protein.

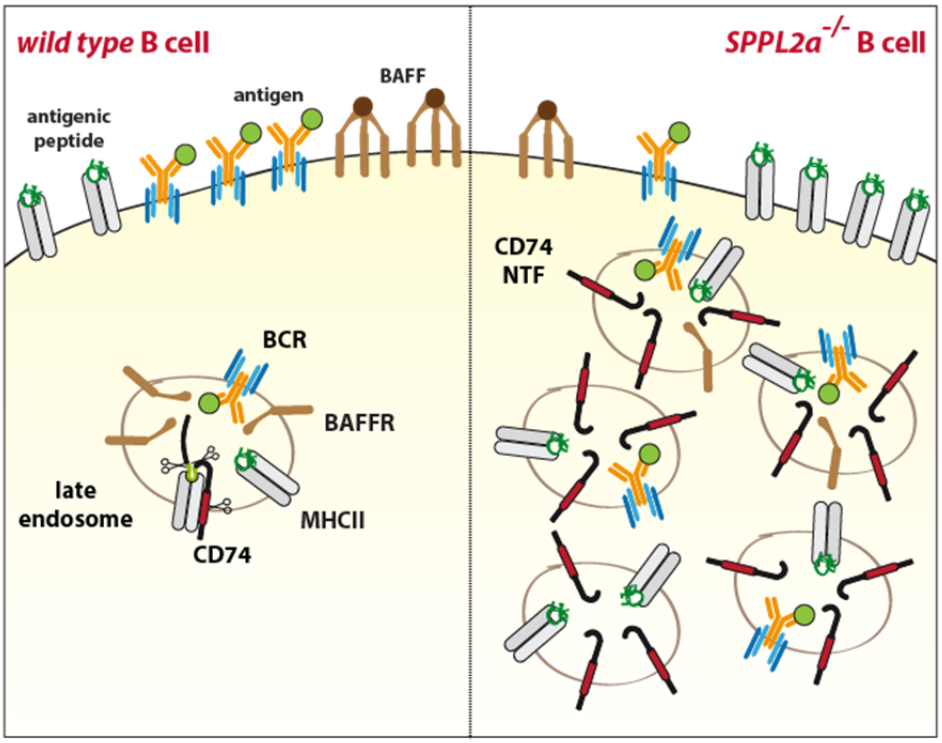

Figure 54. Scheme presenting the distribution of BAFFR, BCR and MHCII in wild type versus *SPPL2a*$^{-/-}$ B cells. In comparison to wild type B cells, B cells isolated from SPPL2a-deficient mice show a reduction of surface and intracellular BAFFR. Total BCR levels are comparable in B cells of both genotypes, however, localization of the BCR in *SPPL2a*$^{-/-}$ B cells seems to be shifted towards intracellular vesicles. SPPL2a-deficient B cells show elevated MHCII levels at the cell surface and in intracellular compartments.

Several reasons might be possible in order to explain this phenomenon. First, high levels of membrane cholesterol are associated with an enhanced IgD endocytosis in anergic B cells (Bléry *et al.*, 2006). A similar mechanism is conceivable for *SPPL2a*$^{-/-}$ B cells. The membrane composition of SPPL2a-deficient B cells could be analyzed to evaluate this hypothesis. Second, the reported interaction between CD74 and the actin-associated motor protein myosin II could be deregulated by the highly abundant CD74 NTF causing an accelerated endocytosis of the BCR. An interaction of CD74 and myosin II was demonstrated in B cells as well as dendritic cells (Faure-André *et al.*, 2008; Vascotto *et al.*, 2007). In murine BMDCs, the migration of these cells is suggested to be faster in the absence of CD74 identifying CD74 as regulator of dendritic cell motility (Faure-André *et al.*, 2008). Moreover, CD74 was implicated in the intracellular trafficking of MHCII and the BCR (Vascotto *et al.*, 2007). Upon BCR-ligation, the light chain of myosin II is phosphorylated and associates with MHCII-CD74 complexes. A polarized trafficking of MHCII-CD74-containing vesicles to the cell center is initiated. Inhibition of myosin II and deletion of CD74 impairs the clustering of these vesicles resulting in a compromised maturation of MIICs. An increase of CD74 cytosolic tails in *SPPL2a*$^{-/-}$ B cells could augment the amount of interactions between myosin

II and CD74 (Figure 55). Thereby, the uptake of BCR complexes and their transport through the endocytic system might be enhanced and could explain the accelerated endocytosis of the BCR in SPPL2a-deficient B cells. An additional interaction of the uncoating ATPase Hsc70 in this process is possible (Figure 55). Whether the turnover of the internalized BCR is delayed comparable to what has been observed for the endocytosed fluid-phase cargo OVA-FITC remains to be analyzed.

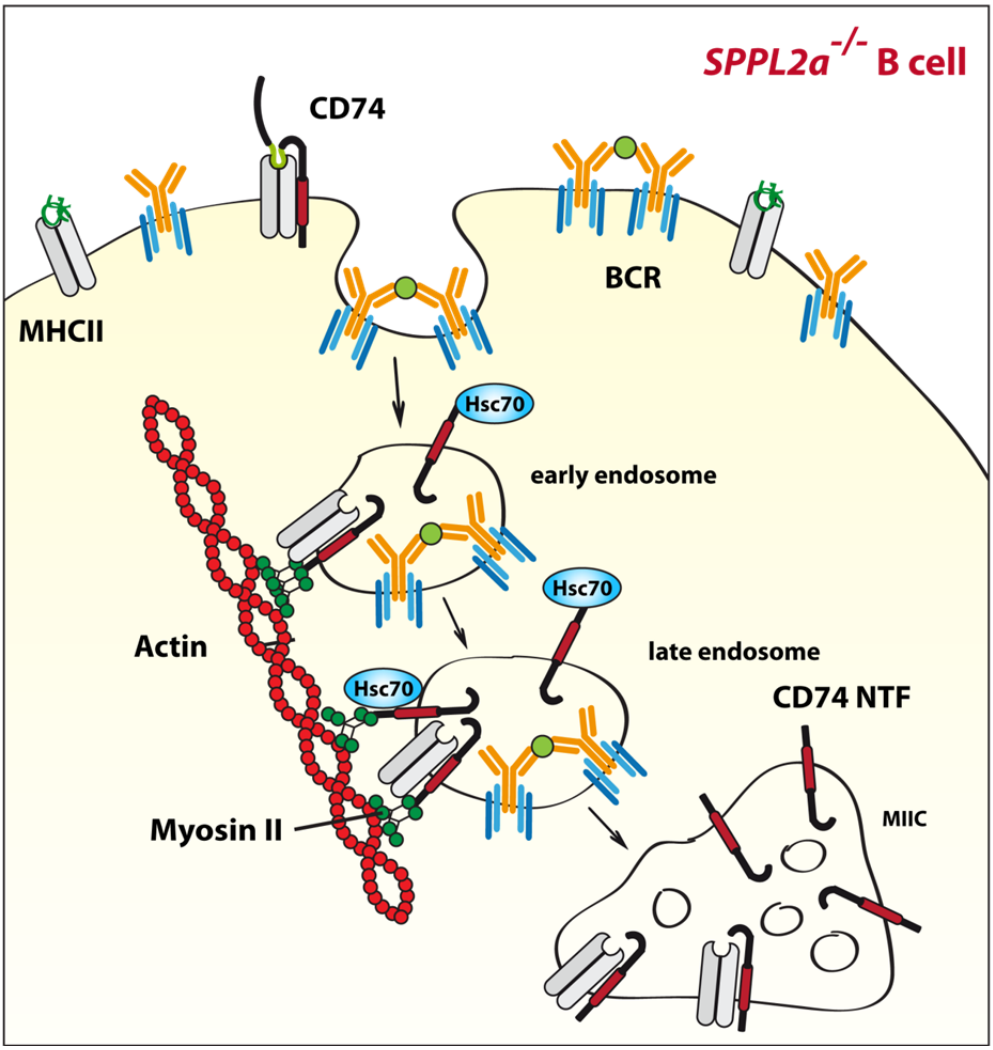

Figure 55. Model showing the interaction between CD74 and myosin II. The cytosolic tail of CD74 NTF is suggested to interact with the actin-associated motor protein myosin II. In comparison to wild type cells, high levels of CD74 NTF in SPPL2a-deficient B cells increase the amount of interacting CD74 and myosin II molecules. This is expected to accelerate the endocytosis of BCRs and their transport through the endocytic system. The recruitment of the uncoating ATPase Hsc70 by the CD74 NTF might play a role in this process as well.

Additionally, MHCII levels are considerably increased both at the surface and in intracellular compartments of splenic SPPL2a-deficient B cells (Figure 54) and will be discussed in detail in the following chapter.

4.2 CD74 and MHCII – two interdependent proteins

CD74 and MHCII are known to interact with each other via the CLIP domain of CD74 (Bijlmakers *et al.*, 1994; Freisewinkel *et al.*, 1993; Romagnoli & Germain, 1994). This is supported by the fact that CTSS, which mediates the liberation of the CLIP domain and subsequently enables the loading of MHCII, is required for the trafficking of MHCII complexes. In B cells and dendritic cells derived from CTSS-deficient mice, remarkable amounts of MHCII molecules are retained in endocytic compartments whereas MHCII surface expression is largely unaffected (Driessen *et al.*, 1999; Shi *et al.*, 1999). Accordingly, the release of the CLIP domain of CD74 is required to promote trafficking of MHCII through the endocytic system. The accumulating CD74 NTF in *SPPL2a*$^{-/-}$ B cells does not contain the CLIP domain. Hence, no significant direct effects of CD74 NTF accumulation on MHCII in the absence of SPPL2a are expected.

Surprisingly, the accumulation of CD74 NTF in *SPPL2a*$^{-/-}$ B cells causes an elevation of MHCII complexes at the cell surface and in intracellular vesicles. The transmembrane domain of CD74 was also shown to mediate the binding to MHCII in a CLIP-independent manner (Castellino *et al.*, 2001). Thus, an interaction between CD74 NTFs and MHCII complexes is reasonable and could be involved in a CD74 NTF-mediated increase of MHCII. mRNA levels of a representative MHCII α and β chain-encoding gene were found to be slightly down-regulated excluding an increased transcription of MHCII-encoding genes as cause for elevated MHCII protein levels. The decrease of MHCII gene transcription might be due to a feedback loop that reduces the gene transcription because of high MHCII protein levels.

The cellular distribution and half-life of MHCII complexes is determined by its ubiquitination and subsequent lysosomal degradation. In dendritic cells and B cells it has been shown that the ubiquitin E3 ligase MARCH I controls the ubiquitin chain length of MHCII and thus designates MHCII for degradation (Gassart *et al.*, 2008; Ma *et al.*, 2012). Additionally, processing of CD74 in dendritic cells is considered to be prerequisite for endocytosis and sorting of surface localized MHCII complexes (van Niel *et al.*, 2006) allowing subsequent degradation. Therefore it can be hypothesized that the accumulation of CD74 NTF in *SPPL2a*$^{-/-}$ B cells interferes with the ubiquitination of MHCII due to a masking of its ubiquitination site thereby decreasing MHCII turnover and resulting in elevated MHCII protein levels. Moreover, the lysosomal delivery of MHCII might be disturbed in SPPL2a-deficient B cells in a way comparable to the effect observed for endocytosed OVA-FITC. An impaired maturation of endosomes or a delayed fusion of late endosomes and lysosomes due

to high abundance of CD74 NTF could decelerate the degradation of MHCII molecules causing their accumulation.

The important role of CD74 and MHCII in B cell development is discussed in several publications. A single knock-out of CD74 has major effects for the development of B cells (Bikoff *et al.*, 1993). Compared to *SPPL2a*$^{-/-}$ mice in which the B cell maturation defect starts beyond the splenic T1 stage, *CD74*$^{-/-}$ mice show a reduction of mature B cells. Additionally, absence of CD74 causes a decrease of MHCII surface levels leading to a disturbed antigen presentation and a reduction of CD4^{+} T helper cells (Bikoff *et al.*, 1993). The B cell phenotype was completely restored by additional ablation of MHCII in *CD74*$^{-/-}$ mice (Maehr *et al.*, 2004). Mice with a complete knock-out of MHCII show normal B cell maturation as well (Madsen *et al.*, 1999). This indicates that neither CD74 nor MHCII are absolutely essential for the B cell development in mice. However, a B cell maturation defect is induced by a knock-out of the MHCII α chains (Labrecque *et al.*, 1999). Taking these findings into consideration, a dysregulation of MHCII homeostasis caused by either absence of CD74 or individual free MHCII chains is likely to be the major cause of a compromised B cell differentiation. As shown, deficiency of SPPL2a also leads to a disturbed MHCII homeostasis in B cells, most likely caused by the accumulation of the CD74 NTF. Thus, a link between the increase of MHCII protein levels and the B cell maturation block of SPPL2a-deficient mice can be assumed. To test this hypothesis, SPPL2a-deficient mice were bred into an MHCII-deficient background. If the compromised MHCII homeostasis is considered to be the main reason for the developmental defects of *SPPL2a*$^{-/-}$ B cells, the B cell phenotype should be restored by additional ablation of MHCII. Surprisingly, first experiments showed that SPPL2a MHCII double-deficient mice have an even stronger B cell maturation defect than SPPL2a single-deficient mice. In detail, flow cytometric analysis of the splenic B cells of *SPPL2a*$^{-/-}$ *MHCII*$^{-/-}$ mice revealed a further reduction of B220^{+} cells in different lymphatic tissues compared to *SPPL2a*$^{-/-}$ mice (data not shown). Moreover, the amount of splenic T1 B cells was decreased in these mice (data not shown). If the B cell maturation defect of SPPL2a-MHCII double-deficient mice manifests at an earlier stage, e.g. in the bone marrow at the immature B cell stage, needs to be analyzed in further experiments. In addition to the aggravated B cell maturation block, the PI3K/Akt signaling in T1 B cells deficient for both SPPL2a and MHCII seems to be even more compromised than in the corresponding B cells of SPPL2a single-deficient mice (data not shown). Accordingly, additional ablation of MHCII does not reverse the phenotype of *SPPL2a*$^{-/-}$ mice. In contrast to the initial hypothesis, splenic B cell numbers and PI3K/Akt signaling in these B cells seems to be even more affected.

Therefore it is likely that an interaction of CD74 with MHCII is able to mitigate the effects of the accumulating CD74 NTF. This theory is supported by data gained by analyzing CTSS-deficient mice. In these mice, a CD74 fragment accumulates which still includes the CLiP domain and has therefore a larger interaction site with MHCII than the CD74 NTF (Figure 56). *CTSS*$^{-/-}$ B cells showed an accumulation of endocytic vesicles, however, less severe than observed for *SPPL2a*$^{-/-}$ B cells (data not shown). Additionally, first analysis of the PI3K/Akt signaling pathway revealed a reduced basal and BCR-induced activation of Akt in CTSS-deficient splenic B cells (data not shown). Again, this effect was not as pronounced as in B cells isolated from *SPPL2a*$^{-/-}$ mice.

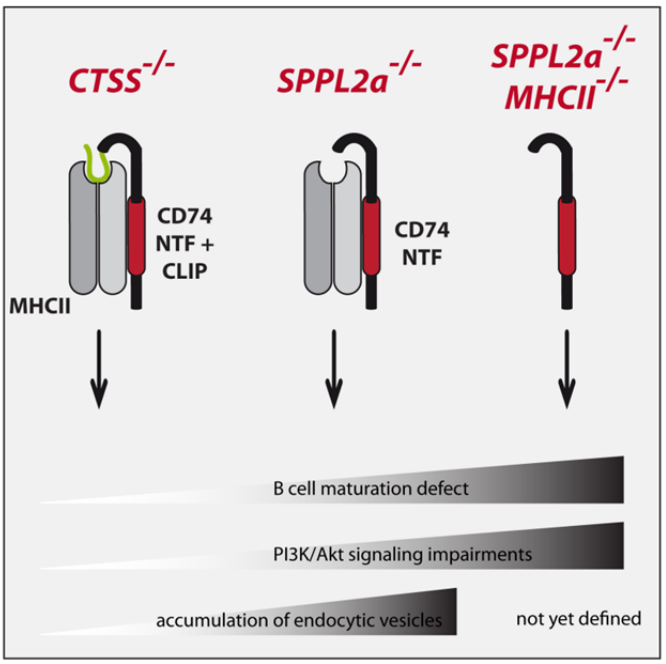

Figure 56. Comparison of the phenotype of *CTSS*$^{-/-}$, SPPL2a$^{-/-}$ and SPPL2a$^{-/-}$ MHCII$^{-/-}$ mice. The intensity of MHCII-CD74 interaction seems to determine the magnitude of the B cell maturation defect and impairments in PI3K/Akt signaling. In *CTSS*$^{-/-}$ B cells, MHCII and CD74 interact via their transmembrane domains and the CLIP domain of CD74. These mice show no severe B cell maturation defect, minor impairments in PI3K/Akt signaling and a moderate accumulation of endocytic vesicles. In *SPPL2a*$^{-/-}$ B cells, the accumulating CD74 NTF only interacts via the transmembrane domain with MHCII molecules, most likely leading to an aggravation of the described phenotypic alterations. Additional ablation of MHCII in *SPPL2a*$^{-/-}$ mice further impairs B cell maturation and PI3K/Akt signaling.

Based on these observations, it can be concluded that the interaction between CD74 and MHCII has the potential to alleviate effects on the endosomal system and PI3K/Akt signaling (Figure 56). Moreover, the strength of the interaction of both proteins seems to be decisive. A larger interaction site between both proteins in *CTSS*$^{-/-}$ B cells causes a milder phenotype whereas a more loose interaction between MHCII and the NTF of CD74 in *SPPL2a*$^{-/-}$ B cells aggravates the B cell phenotype. Complete lack of interaction in SPPL2a MHCII double-deficient mice exacerbates the signaling impairments and B cell maturation defect further. It can be hypothesized that a direct interaction of the CD74 NTF with MHCII reduces the interaction between the NTF of CD74 with molecules such as Hsc70 and myosin II. Thereby, direct negative effects of the NTF on these interaction partners are decreased finally

mitigating phenotypical alterations such as the impaired PI3K/Akt signaling and vesicle accumulation.

4.3 *SPPL2a*$^{-/-}$ T1 B cells exhibit characteristics of anergic B cells

At the immature as well as mature developmental stage, B cells are tested for their reactivity towards self-antigens (1.2.1). If an autoreactive B cell is not able to induce immediate apoptosis or clonal deletion, the cell is arrested in an anergic non-responsive state. Interestingly, B cells of *SPPL2a*$^{-/-}$ mice seem to share common characteristics with this class of B cells (Cambier *et al.*, 2007; Merrell *et al.*, 2006). The best studied transgenic model of B cell anergy is the hen-egg lysozyme (HEL) model (Cambier *et al.*, 2007). This model was constructed by engineering so called MD4 mice which co-express transgenes encoding the Ig heavy chains μ and δ and light chains that create a BCR with a high affinity for HEL. These MD4 mice were crossed with a mouse strain that express soluble HEL (ML5 mice) finally leading to MD4 x ML5 mice. These mice are characterized by a large pool of anergic B cells due to chronic exposure to HEL. In general, anergic B cells typically have a low proliferation capacity, are not able to upregulate activation markers and do not secrete antibodies upon B cell activation (Eris *et al.*, 1994; Goodnow *et al.*, 1988).

In agreement, SPPL2a-deficient mice show significantly reduced plasma immunoglobulin levels after T cell-dependent and -independent immunization as compared to wild type mice (Schneppenheim, Dressel, Hüttl *et al.*, 2013). Furthermore, B cell specific cell surface markers (e.g. B220^{+}, CD21, CD19) which are hallmarks of their maturation stage are diminished on *SPPL2a*$^{-/-}$ B cells. The reported reduction of surface IgM levels in anergic cells (Goodnow *et al.*, 1988) was also seen in splenic B cells of SPPL2a-deficient mice. Another important key feature of anergic B cells is the accelerated BCR internalization which was studied in MD4 x ML5 mice (Bléry *et al.*, 2006). B cells isolated from these mice showed an enhanced endocytosis of IgD leading to a large pool of intracellular sequestered BCR. This effect could be identified as a mechanism which depends on plasma membrane cholesterol levels (Bléry *et al.*, 2006b). Interestingly, *SPPL2a*$^{-/-}$ B cells show an accelerated BCR internalization which is highly comparable to the described phenotypic feature of anergic B cells of MD4 x ML5 mice. The reduction of surface BCR was described to be responsible for the reduced phosphorylation of Syk (Cambier *et al.*, 2007) what is in line with the observed decrease of phosphorylated Syk in SPPL2a-deficient B cells upon BCR ligation. An additional similarity between B cells of *SPPL2a*$^{-/-}$ and MD4 x ML5 mice is related to the

generation of PIP_3 as inducer of Akt phosphorylation which is reduced in B cells of both *SPPL2a*$^{-/-}$ and MD4 x ML5 mice after anti-IgM stimulation (Browne *et al.*, 2009). In anergic B cells of MD4 x ML5 mice, the decrease of PIP_3 levels could be ascribed to an increased expression of PTEN as antagonist of PI3K and could be reversed by ablation of PTEN (Browne *et al.*, 2009). One publication also suggests that autoreactive B cells can induce both anergy and receptor editing as two connected processes (Tze *et al.*, 2000).

Besides the typical characteristics of anergic cells, immature bone marrow-derived B cells of MD4 x ML5 mice express elevated levels of the RAG2-encoding gene and rearrange new endogenous V-J light chains of the BCR. As shown within this work, also *SPPL2a*$^{-/-}$ B cells isolated from the spleen show increased transcription of *RAG1* and *RAG2* that could point to a potential rearrangement of the surface Ig. Based on these described similarities between anergic cells and the splenic B cells of *SPPL2*$^{-/-}$ mice, it can be speculated that SPPL2a deficiency and chronic exposure to antigens involve comparable pathways in B cells. Nonetheless, the identification of B cells in the anergic state is challenging and makes it therefore difficult to define the remaining splenic *SPPL2a*$^{-/-}$ B cells as anergic cells. Anergic B cells which are also described as T3 cells express CD93 at their cell surface but also show characteristic markers of mature follicular B cells, e.g. $CD23^+$ and IgM^{low}. To unequivocally show that *SPPL2a*$^{-/-}$ T1 B cells exhibit features of anergic cells, experiments in which SPPL2a-deficient splenic B cells and B cells from MD4 x ML5 mice are directly compared would be of help. The anergic B cell population ($CD93^+$ $CD23^+$ IgM^{low}) of both genotypes could be compared as well as major characteristics of anergic cells, such as surface IgM levels, BCR internalization and *RAG1/2* gene expression.

How *SPPL2a*$^{-/-}$ B cells might enter the anergic state can only be speculated. A continuous signaling via the BCR has to take place at the immature B cell stage just before the tesing for auto-reactivity. Theoretically, high BCR surface levels could lead to a permanent activation of BCR-mediated signaling pathways. Alternatively, the decreased lysosomal delivery shown for the cargo OVA-FITC might lead to a delayed lysosomal delivery of internalized BCRs and a decreased turnover leading to a sustained signaling from intracellular compartments. Failures within the PI3K/Akt pathway might also account for a prolonged BCR signaling, for instance due to a decreased activity of the Akt antagonist PTEN resulting in a sustained activation of the Akt signaling cascade.

4.4 Relevance of BCR-mediated signaling for B cell survival

4.4.1 SPPL2a deficiency primarily affects the PI3K/Akt pathway

Within this project, the molecular mechanism of the B cell maturation defect of *SPPL2a*$^{-/-}$ mice was analyzed. It could be shown that signaling mediated by the BCR is compromised in SPPL2a-deficient splenic B cells at different downstream levels. The main findings regarding the signaling impairments are summarized in Figure 57. Activation of the kinase Syk upon BCR cross-linking is reduced in B cells deficient for SPPL2a. Furthermore, activation of the kinase Akt is significantly diminished at the basal level as well as upon BCR cross-linking. Although activation of ERK1/2 and Akt are both dependent on Syk as the upstream kinase, phosphorylation of ERK1/2 is not altered in *SPPL2a*$^{-/-}$ B cells.

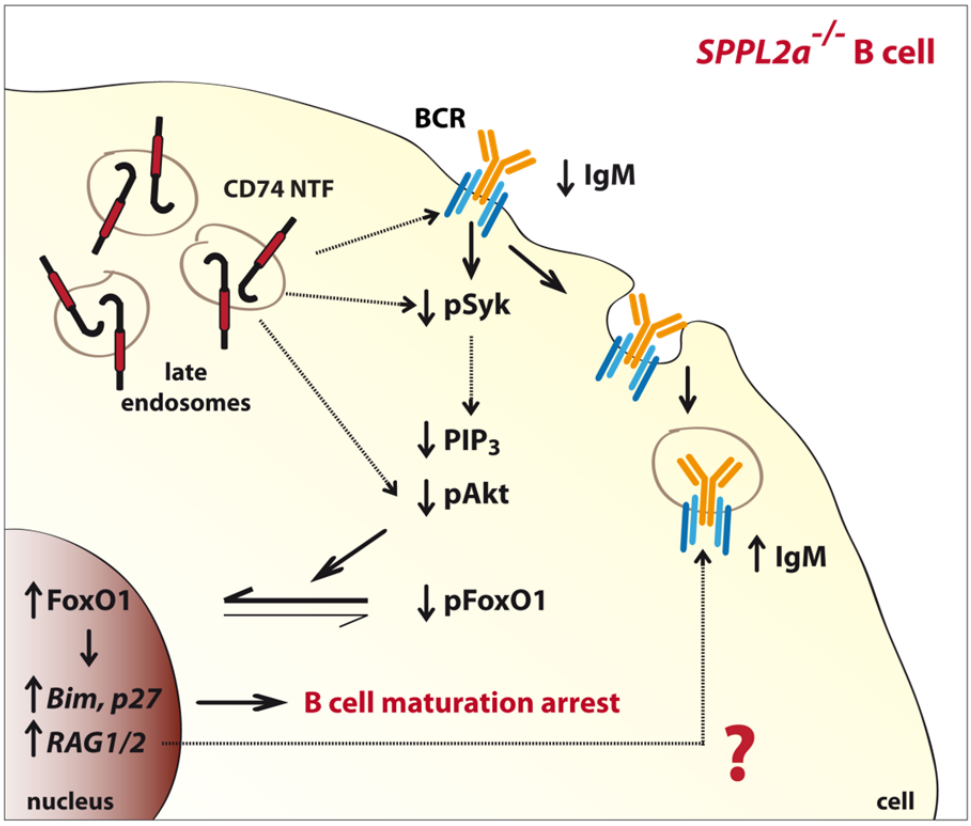

Figure 57. Scheme of impaired BCR-mediated signaling in *SPPL2a*$^{-/-}$ B cells. Splenic B cells of SPPL2a-deficient mice accumulate CD74 NTF in highly abundant late endosomes what disturbs BCR-mediated downstream signaling. Decreased surface IgM levels, probably caused by an accelerated endocytosis of the BCR, causes a reduced activation of the kinase Syk and decreased generation of PIP_3. Additionally, phosphorylation of Akt is compromised leading to a diminished deactivation of the transcription factor FoxO1. Subsequently, FoxO1-mediated transcription of the pro-apoptotic genes *Bim* and *p27* is enhanced probably contributing to the B cell maturation arrest of *SPPL2a*$^{-/-}$ mice. Furthermore, decreased inactivation of FoxO1 fails to down-regulate the transcription of *RAG1/2*. The detailed mechanism how CD74 NTF accumulation impairs kinase activation and BCR trafficking needs to be explored.

Signaling by the kinases ERK1/2 was thought to be primarily important for the development of B cells in earlier maturation stages (Gold, 2008). By deleting both ERK1 and ERK2 in mice it was demonstrated that the kinases control the cell expansion mediated by the pre-BCR and the transition of pro-B to pre-B cells (Yasuda *et al.*, 2008). It was proposed that activated ERK1/2 translocate to the nucleus and activate the transcription factors c-Myc, Mef2c, Mef2d and Ilf2 which in turn promote B cell expansion (Yasuda *et al.*, 2008). However, a recent study also implicates ERK in the development of transitional and mature B cells (Rowland, DePersis *et al.*, 2010). B cells expressing low BCR surface levels show a reduced tonic BCR signaling which can be rescued by activation of the RAS pathway. Thus, a contribution of ERK1/2 to the B cell maturation block of SPPL2a-deficient mice would be expected. Interestingly, activation of the PI3K/Akt pathway can be accomplished by a process that is independent of Syk and would therefore allow a divergent activation of Akt and ERK1/2 (Yokozeki *et al.*, 2003).

It has been reported that activation of the PI3K/Akt signaling cascade highly depends on the contribution of the BCR co-complex composed of CD19, CD21 and CD81 (Aiba *et al.*, 2008). Kurosaki and co-workers showed that deletion of CD19 and BCAP, an adaptor molecule which recruits the PI3K to the co-BCR complex, causes an almost complete block of BCR-mediated Akt phosphorylation in mice resulting in developmental defects of B cells. By introducing constitutively active PI3K, the B cell development could be partially restored (Aiba *et al.*, 2008). Interestingly, B cells of SPPL2a-deficient mice have reduced levels of cell surface CD19 and CD21. Thus, a reduction of PI3K/Akt signaling could be caused by a concomitant decrease of pSyk and BCR co-complex levels in these mice. ERK1/2 activation does not depend on the co-BCR complex and might therefore not be affected.

4.4.2 Diverse functions of BCR-signaling components in B cell survival

In the past, multiple mouse models were generated in order to characterize the *in vivo* function of components involved in BCR-mediated signaling. The phenotypic alterations of mice with deletions or mutations in proteins involved in pathways found to be deregulated in SPPL2a-deficient mice are summarized in Table 15. According to several studies, deletion of Syk is critical for B cell development in the early maturation stages due to its requirement for signaling mediated by the pre-BCR (Cheng *et al.*, 1995; Cornall *et al.*, 2000; Turner *et al.*, 1995; Turner *et al.*, 1997). Absence of Syk causes an arrest at the pro- and immature B cell stage (Table 15). In *SPPL2a*$^{-/-}$ mice, the B cell stages in the bone marrow are still preserved.

This would indicate that the impairments of Syk activation in SPPL2a-deficient B cells are not as severe to induce a B cell maturation defect beyond the T1 stage. Alternatively, CD74 NTF accumulation might not be strong enough in pro-B cells in order to induce a maturation arrest at this stage. It can be hypothesized that CD74 NTF accumulation in *SPPL2a*$^{-/-}$ B cells manifests not before the immature B cell stage. Thus, impairments in BCR signaling are expected to correlate with the onset of CD74 NTF accumulation and might therefore emerge the earliest at the immature B cells stage as shown for Syk.

Deletion of regulatory and catalytic subunits of the PI3K, especially p85α and p110δ, disturb B cell maturation and function as well (Table 15) (Al-Alwan *et al.*, 2007; Clayton *et al.*, 2002; Fruman *et al.*, 1999; Jou *et al.*, 2002; Okkenhaug *et al.*, 2002; Suzuki *et al.*, 1999). Common phenotypic alterations include a B cell maturation arrest at the pro-B cell stage as well as reduced numbers of mature B cells. Furthermore, these mice show a disturbed germinal center formation and massively reduced antibody secretion upon immunization with T cell-dependent and -independent antigens.

Phenotypic alterations that resemble the one of *SPPL2a*$^{-/-}$ mice were also shown for mice with a deletion of the genes coding for Akt1 and Akt2 (Calamito *et al.*, 2010) (Table 15). Akt1/2-deficient mice are characterized by reduced amounts of MZ and B-1 B cells what was also found in SPPL2a-deficient mice (Schneppenheim, Dressel, Hüttl *et al.*, 2013). Thus, it seems likely that impairments in the PI3K/Akt signaling significantly contribute to the B cell maturation defect of *SPPL2a*$^{-/-}$ mice at the T1 stage.

FoxO transcription factors as major downstream target of the PI3K/Akt pathway are also implicated in the maturation of B cells (Table 15) (Szydłowski *et al.*, 2014). Overexpression of wild type FoxO1 in a murine B cell line causes a delay in cell-cycle progression and an increased apoptosis (Yusuf *et al.*, 2004). In agreement, elevated FoxO1 activity *in vivo* increases the apoptosis of peripheral B cells (Su *et al.*, 2011). In detail, ablation of the scaffolding protein 14-3-3δ that is involved in the nuclear export of pFoxO1 results in increased nuclear FoxO1 levels thereby enhancing the transcription rate of pro-apoptotic genes such as *Bim* and *p27*. As a consequence, mice deficient in 14-3-3δ show reduced amounts of MZ, FO and B-1 B cells whereas immature B cell numbers are comparable to wild type controls (Su *et al.*, 2011). These phenotypic features show high similarities to the one of *SPPL2a*$^{-/-}$ mice that also exhibit a considerable depletion of B cells beyond the T1 developmental stage including MZ, FO and B-1 B cells (Schneppenheim, Dressel, Hüttl *et al.*, 2013).

Table 15. Summary of different mouse models with immunological phenotypes with similarities to *SPPL2a*$^{-/-}$ mice.

Mutated/deleted protein	Major phenotypic alterations
RAG1/2 (Mombaerts *et al.*, 1992; Shinkai *et al.*, 1992)	- Lack of mature B and T cells - B cell development arrested prior to immature B cell stage - No V(D)J rearrangement
Syk (Cheng *et al.*, 1995; Cornall *et al.*, 2000; Turner *et al.*, 1995; Turner *et al.*, 1997)	- Disrupted pre-BCR signaling - B cell developmental arrest at pro-B cell stage - Reduction of immature B cells - Immature B cells reach spleen, but fail to enter follicles - No positive B cell selection
PI3K (p85α, p110δ) (Al-Alwan *et al.*, 2007; Clayton *et al.*, 2002; Fruman *et al.*, 1999; Jou *et al.*, 2002; Okkenhaug *et al.*, 2002; Suzuki *et al.*, 1999)	**Regulatory p85α subunit:** - B cell development arrested at pro-B cell stage - Reduced numbers of mature B cells - No T cell-independent antibody secretion - Reduced proliferation upon BCR ligation **Catalytical p110δ subunit:** - Low proliferation upon BCR ligation - Attenuated BCR-mediated Ca^{2+} flux - Decreased Ig levels - Lowered/eliminated response to T cell-independent/-dependent antigens - Disrupted germinal center formation - B cells are prone to apoptosis
Akt1/2 (Calamito *et al.*, 2010)	- Reduced number of MZ B cells - Defective B-1 B cell development - Reduced proliferation in response to BCR stimulation
14-3-3δ (Su *et al.*, 2011)	- Elevated FoxO1 transcription and degradation - Enhanced apoptosis of peripheral B cells - Impaired BCR-mediated signaling via Akt and ERK - Reduced numbers of MZ, FO and B-1 B cells - B cell maturation block beyond the immature stage - Reduced response to T cell-independent antigens

Based on these studies it can be concluded that the PI3K/Akt signaling pathway is critical for the survival of developing B cells. This was additionally validated by different attempts to rescue the reduced B cell survival of BCR-negative mice (Srinivasan *et al.*, 2009). Targeted deletion of the BCR in mature B cells of mice results in their rapid cell death (Lam *et al.*, 1997). Breeding of this mouse strain with mice expressing a constitutively active PI3K or mice deficient for the PI3K antagonist PTEN or FoxO1 was able to rescue the phenotype and restored the survival of B cells (Srinivasan *et al.*, 2009). In contrast, increased NF-κB or MAPK signaling was not able to achieve a comparable alleviation.
In summary, these studies describe the PI3K/Akt/FoxO1 pathway as a main signaling route to maintain the survival of B cells. Therefore it is very likely that the compromised tonic and BCR-induced signaling via the PI3K/Akt/FoxO1 axis represents a major cause of the impaired survival and maturation of SPPL2a-deficient B cells.

4.4.3 Impaired Syk and Akt activation in *SPPL2a*$^{-/-}$ B cells – two independent mechanisms?

As shown within this study, T1 B cells of *SPPL2a*$^{-/-}$ mice exhibit a reduced activation of the kinases Syk and Akt. Since IgM surface levels are decreased as well in these cells, it is evident that impaired kinase activation is the result of a diminished signal transmission via the BCR. It can be concluded that the reduced IgM surface levels and the compromised activation of Syk are two interconnected processes. Experiments accomplished in immature B cells of wild type and SPPL2a-deficient mice as well as wild type T1 B cells treated with the SPPL inhibitors $(Z\text{-}LL)_2$ ketone and inhibitor X revealed that reduced BCR levels are associated with a reduction of Syk phosphorylation upon BCR stimulation. This theory is supported by the fact that the expression of Src kinases as regulators of Syk activation does not seem to be consistently deregulated. Inhibition of Src family kinases in splenic B cells by the inhibitor PP2 causes a delayed phosphorylation of Syk upon BCR ligation (Stepanek *et al.*, 2013). Additionally it has been shown that at least the kinases Blk, Fyn and Lyn have redundant functions and that ablation of all three proteins is required in order to affect downstream pathways such as NF-κB (Saijo *et al.*, 2003). Out of five tested Src kinases which are primarily expressed in B cells, three showed an altered transcription rate in *SPPL2a*$^{-/-}$ B cells as compared to wild type controls: *Fyn* mRNA levels are down-regulated whereas the mRNA levels of *Fgr* and *Blk* are up-regulated. However, due to the described redundant functions of the Src kinases, reduced protein amounts of only one Src kinase member is unlikely to

negatively affect Syk activation. Thus it is likely that the reduced surface IgM levels and the subsequently lower amount of antigens that can bind to the BCR is a main cause why the activation of Syk is impaired in *SPPL2a*$^{-/-}$ B cells.

Although activation of both Syk and Akt is impaired in *SPPL2a*$^{-/-}$ B cells, these two processes are not necessarily connected with each other. Immature SPPL2a-deficient B cells and wild type T1 B cells in which SPPL2a activity has been inhibited do not show a significantly affected Akt activation although Syk phosphorylation is considerably decreased. This could mean that a defect in Syk activation precedes defective Akt phosphorylation and that impairments in the PI3K/Akt pathway require a longer latency period to emerge. This latency period is given in T1 B cells of *SPPL2a*$^{-/-}$ mice due to a constitutive knock-out of the protease, but apparently not in earlier B cells stages like immature B cells as well as in T1 B cells treated over night with SPPL inhibitors. On the other hand, a Syk-independent activation of the PI3K/Akt pathway has been reported which supports the idea of an autonomous Akt activation (Yokozeki *et al.*, 2003). In a Syk-deficient murine A20 B cell line, signaling via the PI3K is partially preserved. Hence, an activation of Akt independent of Syk and its reduced phosphorylation level is conceivable. Due to the high abundance of CD74 NTF as well as endocytic vesicles in *SPPL2a*$^{-/-}$ B cells, a direct inhibitory effect on Akt activation which is independent of the reduced IgM surface exposure and Syk phosphorylation can be proposed. One argument which favors this theory is the divergent impairment of PIP_3 and Akt. Although activation of the kinase Akt depends on PIP_3, the levels of PIP_3 are not as dramatically affected as the pAkt levels. Furthermore, tonic phosphorylation of Akt is reduced whereas tonic PIP_3 levels are not altered. This indicates that Akt phosphorylation could be additionally influenced by a pathway that is independent of the BCR surface levels, pSyk and PIP_3 levels.

4.4.4 Disturbed Akt activation from intracellular compartments

Recent studies demonstrated that signals are not only transmitted via receptors at the plasma membrane. Instead, the endosomal system is also capable of acting as a site of signal transduction for many receptors (Murphy *et al.*, 2009; Sadowski *et al.*, 2009). The prerequisites for signal transmission via the BCR with regard to its cellular localization, however, are controversial. One theory describes BCR-mediated signaling and BCR internalization as processes which are independent of each other (Hou *et al.*, 2006). It was shown that phosphorylation of ITAM and non-ITAM tyrosine residues within the cytosolic

tail of Igα determine the fate of the BCR. According to this study it is suggested that phosphorylated BCRs are preferentially retained at the cell surface and mediate signal transmission. Instead, non-phosphorylated receptors were shown to internalize in an actin-dependent manner (Hou *et al.*, 2006). In contrast to this, another study claims that endocytosis of the BCR is required to guarantee optimal signaling levels via Akt and the MAPK pathway (Figure 58) (Chaturvedi *et al.*, 2012). BCR signaling was reported to be initiated at the plasma membrane. While the BCR internalizes, signaling is continued by sequential phosphorylation of kinases. Blocking the endocytosis of the BCR by the dynamin inhibitor Dynasore in splenic B cells leads to a dysregulated kinase activation, including a hyper-phosphorylation of Syk and MAPKs. In contrast, an opposite pattern was seen for the activation of Akt which was hypo-phosphorylated (Chaturvedi *et al.*, 2012). This is in agreement with own experiments showing that Akt phosphorylation can be blocked in wild type primary splenic B cells by Dynasore treatment (data not shown). In conclusion, phosphorylation of the kinase Akt seems to be dependent on BCR internalization. Although *SPPL2a*$^{-/-}$ B cells accumulate endocytic vesicles and show slowed degradation of endocytosed fluid-phase cargo, internalization of the BCR was shown by microscopy to be well preserved in these cells apart from the described acceleration. Hence, impairments in BCR endocytosis can be excluded as reason for the compromised Akt activation. However, the high amount of intracellular CD74-containing vesicles present in SPPL2a-deficient B cells might have a negative effect on phosphorylation on Akt.

Full activation of this kinase is achieved in intracellular compartments (Chaturvedi *et al.*, 2012). This theory is supported by a study showing that Akt is recruited to the plasma membrane after BCR ligation, stays there to phosphorylate plasma membrane localized targets, but subsequently acts in the cytosol and even in the nucleus (Astoul *et al.*, 1999). In order to be fully activated, Akt needs to be phosphorylated at threonine 308 and serine 473. Phosphorylation at site 308 is achieved by the phosphoinositide-dependent kinase 1 (PDK1) after recruitment of Akt to the plasma membrane by PIP_3 via the Pleckstrin homology domain of Akt (Alessi *et al.*, 1997). Full activation due to phosphorylation of serine 473 can be accomplished by several kinases including the DNA-dependent protein kinase (DNA-PK) and the mammalian target of rapamycin complex 2 (mTORC2) (Feng *et al.*, 2004; Sarbassov *et al.*, 2005). mTORC2 induces Akt phosphorylation at the plasma membrane whereas DNA-PK acts in the nucleus (Feng *et al.*, 2004; Sarbassov *et al.*, 2005). Thus, activation of Akt is accomplished at different locations in the cell and requires transport processes and recruitments to its site of activation.

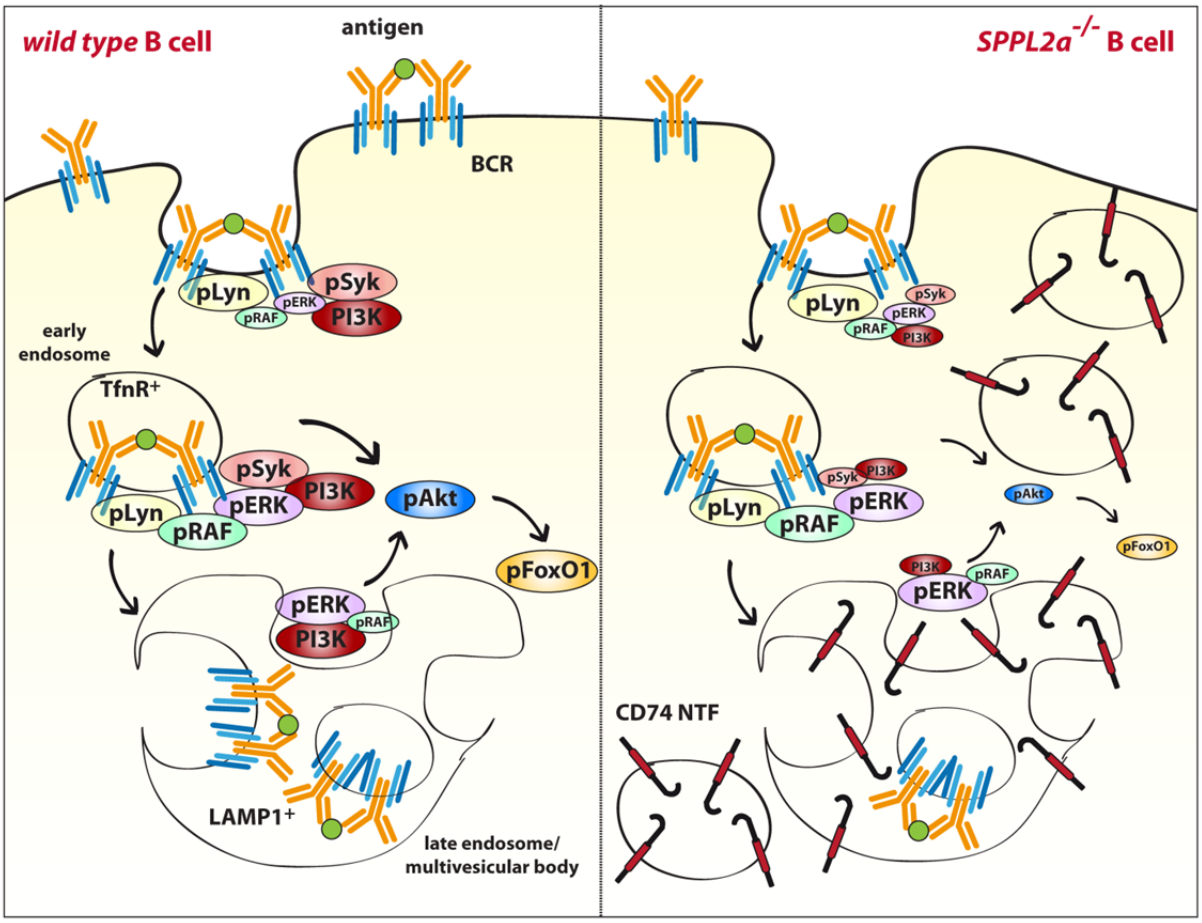

Figure 58. Hypothetical model of the differential activation of the kinase Akt in *wild type* and *SPPL2a*$^{-/-}$ B cells. Upon cross-linking of the BCR at the cell surface, the kinases Syk, Lyn, Raf and ERK are recruited to the plasma membrane and become phosphorylated. The complex is delivered to TfnR-containing early endosomes (EE) and LAMP1-positive late endosomes with multivesiculated characteristics (LE/MVB) in which pLyn and pSyk are not present anymore. Phosphorylation of Akt and its downstream target FoxO1 is suggested to occur from these internalized BCRs. In *SPPL2a*$^{-/-}$ B cells, the accumulating CD74 NTFs and high abundance of endocytic vesicles is suspected to interfere with Akt activation thereby decreasing the phosphorylation of Akt and FoxO1. Low abundance of phosphorylated kinases is depicted as small ovals, high abundance as larger ovals. Modified from (Chaturvedi *et al.*, 2012)**.**

The overload of intracellular vesicles might impair the translocation of Akt to the plasma membrane and back towards the cytosol and nucleus thereby causing a decrease of activatable Akt (Figure 58). Moreover, domains like the Pleckstrin homology domain might be masked due to a high degree of endocytic vesicles and CD74 NTFs that would lead to a decreased recruitment of Akt to its site of activation. In this study, Akt phosphorylation was analyzed in *SPPL2a*$^{-/-}$ B cells by determining the serine 473. In order to evaluate whether Akt is recruited to the plasma membrane in SPPL2a-deficient B cells, phosphorylation of tyrosine 308 can be examined in further experiments. As schematically shown in Figure 58, decreased phosphorylation of Akt by a mechanism hypothesized above would lead to a reduced phosphorylation and thus inactivation of FoxO1. Thus, CD74 NTF accumulation might

directly interfere with Akt phosphorylation and augments the impaired Akt activation caused by a decreased signal transmission via the BCR and Syk.

4.4.5 BAFFR and BCR collectively regulate the survival of B cells

As visualized in Figure 7, the signaling network mediated by the BCR and BAFFR is complex and transmitted signals do not necessarily follow only one straight downstream route. Instead, signaling events via the two receptors are interconnected and can influence each other. For instance, the level of the NF-κB precursor p100 which is needed for BAFFR signal transduction highly depends on tonic signaling mediated by the BCR (Stadanlick *et al.*, 2008). As could be shown within this project, p100 levels are diminished in B cells from *SPPL2a*$^{-/-}$ mice which agree well with the observed impaired tonic BCR signaling including a lowered activation of the kinase Akt. Apart from this described connection between BAFFR- and BCR-mediated signaling, other studies emphasize the cooperation of both receptors which is depicted schematically in Figure 59.

Pelanda and co-workers illustrated that BAFFR expression correlates with that of surface IgM. Hence, the level of tonic BCR signaling determines BAFFR levels (Rowland, Leahy *et al.*, 2010). Moreover, signals via the BAFFR cooperate with components of the BCR signaling pathway. Studies in cultured B cells deficient in the PI3K subunit p110δ revealed a reduced BAFF-mediated survival of these cells demonstrating that regulation of B cell survival by the BAFFR can utilize the PI3K pathway (Henley *et al.*, 2008). This finding was strengthened by applying *in vivo* models. Impaired survival of B cells in mice with an ablation of the BAFF-encoding gene can be partially rescued by inactivation of PTEN what causes constitutively active PI3K signaling (Jellusova *et al.*, 2013). Furthermore, studies in mice with an inducible deletion of the kinase Syk support the theory of BAFFR and BCR cross-signaling (Schweighoffer *et al.*, 2013). Deletion of Syk reduces the signaling response initiated by the cytokine BAFF finally resulting in a loss of most mature B cells. In detail, the study illustrates that the BAFFR transduces B cell survival signals by co-opting the BCR pathway and signaling via ERK and the PI3K. This was identified by the ability of BAFF-mediated signals to phosphorylate Syk and the BCR-associated Igα chain.

In conclusion, the BAFFR and BCR synergistically regulate the survival of B cells. Therefore, reduced BAFFR surface levels observed in *SPPL2a*$^{-/-}$ splenic B cells might also contribute to the arrested B cell maturation by diminished signal propagation via the PI3K/Akt pathway.

Additionally, the impaired tonic signaling via PI3K and Akt results in a reduction of BAFFR surface levels finally creating a vicious circle.

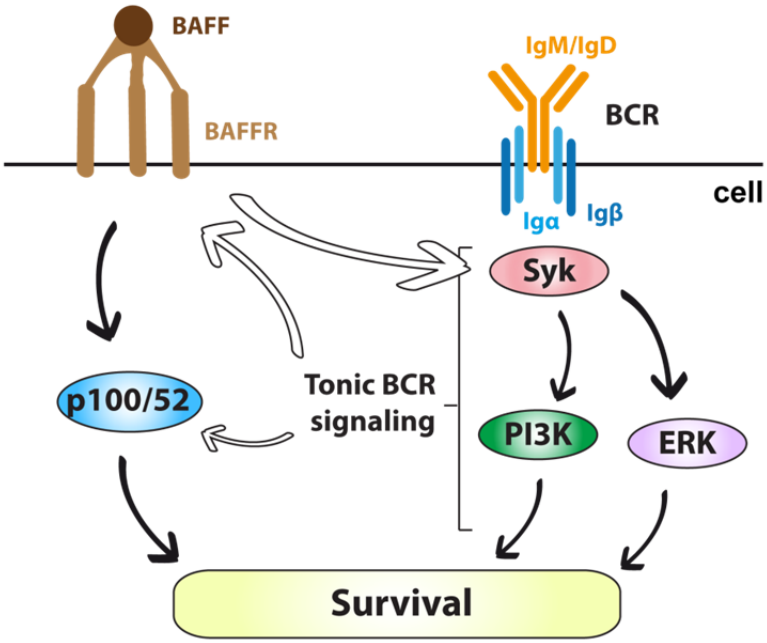

Figure 59. Cooperation between the BAFFR and BCR in B cells. Signals transmitted by the BAFFR can be transduced via the kinase Syk as well as the PI3K and ERK. Tonic BCR signaling is able to regulate the surface expression level of the BAFFR and the level of the NF-κB precursor p100. Interconnected signaling is depicted by white arrows.

4.4.6 SPPL2a is critical for B cell transition from the T1 to the T2 maturation stage

Although immature B cells of *SPPL2a*$^{-/-}$ mice already show compromised BCR signaling with respect to the activation of Syk, the developmental arrest of these B cells does not manifest prior to the splenic T1 stage. Thus, it can be speculated that the impairment in Syk activation does not represent the main cause of the maturation block of SPPL2a-deficient B cells. Instead, defects that arise at the T1 developmental stage or even at the transition from the T1 to the T2 stage might be decisive.

Apparently, the PI3K/Akt pathway is massively impaired in *SPPL2a*$^{-/-}$ T1 B cells and might therefore primarily account for the developmental arrest at exactly this maturation stage. There are several reasons which could explain why the compromised Akt signaling and the maturation arrest of *SPPL2a*$^{-/-}$ B cells arise precisely at the T1 stage. The reduced BAFFR surface levels could contribute to the onset of the maturation block at the T1 stage since signaling via this receptor is reported to be primarily required for the survival of transitional B cells. The dependency of T2 B cells on the cytokine BAFF and its receptor was demonstrated

in mice deficient for either BAFF or the BAFFR. These mice exhibit an arrested B cell development at the T1 stage (Miller & Hayes, 1991; Schiemann *et al.*, 2001; Thompson *et al.*, 2001). Additionally, an up-regulation of BAFFR expression from the T1 to the T2 B cell stage was observed by flow cytometric analysis and emphasizes that BAFFR signaling gains importance at the T1-to-T2 transition. In conclusion, the B cell maturation block at the T1 stage might be collectively provoked by decreased signal transmission by the BAFFR as well as BCR which can both signal via the compromised PI3K/Akt pathway. Additionally, the reduced tonic ligand-independent BCR signaling is reduced in *SPPL2a*$^{-/-}$ B cells and probably contributes to the low surface levels of BAFFR. This theory would be in agreement with studies showing that a synergy between BAFFR and tonic BCR signaling is required for optimal differentiation of T1 into T2 B cells (Rowland, Leahy, *et al.*, 2010). Furthermore, since the B cell maturation arrest can be ascribed to the accumulating CD74 NTF, severe impairments in signaling pathways are expected to correlate with the intensity of fragment accumulation. Flow cytometric analysis revealed that the NTF already accumulates in B220^{+} IgM^{+} immature B cells of *SPPL2a*$^{-/-}$ mice. However, impairments in the PI3K/Akt pathway manifest at the T1 B cell stage indicating that the effects of the high abundant CD74 NTF need a certain time to arise and to fully affect the target pathway. Moreover, flow cytometric analysis showed an increase of CD74 NTF levels from the T1 to the T2 stage in both wild type and the remaining SPPL2a-deficient B cells. Hypothetically, those *SPPL2a*$^{-/-}$ B cells that reach the T2 stage might not withstand the even higher CD74 NTF levels and are eliminated.

Regardless of the detailed mechanism underlying the impaired PI3K/Akt signaling, this compromised signal cascade is suggested to be a major cause for the maturation arrest of *SPPL2a*$^{-/-}$ B cells. In this project, reduced Akt phosphorylation was shown to result in decreased FoxO1 inactivation and an elevated transcription of genes coding for the pro-apoptotic proteins p27 and Bim. This might eventually lead to an imbalance between pro- and anti-apoptotic signals in the B cells and might induce their cell death by apoptosis. Unexpectedly, the number of apoptotic B cells in SPPL2a-deficient spleens is not elevated (data not shown), probably due to a rapid elimination of apoptotic cells. The decreased inactivation of FoxO1 also results in an up-regulated transcription of *RAG1/2*. This is in line with studies demonstrating that tonic signaling down-regulates *RAG1/2* gene expression in B cells beyond the immature stage (Amin & Schlissel, 2008; Grawunder *et al.*, 1995; Verkoczy *et al.*, 2007). Apparently, tonic BCR signaling is considerably compromised in SPPL2a-deficient B cells and is therefore not capable of turning off the transcription of these genes.

Whether the increased mRNA levels of *RAG1/2* finally affect the IgM levels in general or contribute to the changed cellular distribution of the BCR needs to be investigated.

4.5 SPPL2a as regulator of B cell survival – medical relevance

Altogether, the findings presented here emphasize the ability of the intramembrane protease to control the function of CD74 by clearance of its NTF. Thereby, signaling events that are essential for the differentiation and survival of B cells are maintained. In light of this, SPPL2a can be regarded as regulator of B cell survival and might therefore represent a promising target for the treatment of B cell malignancies and autoimmune disorders.

In detail, the development of potent and specific small-molecule inhibitors of SPPL2a could be used to indirectly interfere with BCR signaling pathways resulting in the controlled regulation of B cell differentiation and survival. B cell neoplasms can develop at different stages of B cell maturation and mostly arise due to deregulated signaling downstream of the pre-BCR or BCR (Rickert, 2013). Sustained activation of the PI3K/Akt pathway and the resulting aberrant proliferative and anti-apoptotic signals were shown to be preferentially associated with the formation of malignancies what emphasizes the importance of this signaling cascade for B cell homeostasis (Chang *et al.*, 2003; Pauls *et al.*, 2012). As an example, Syk expression was detected to be enhanced in chronic lymphocytic leukemia (Buchner *et al.*, 2009). By applying Syk inhibitors, activation of Syk downstream targets was reduced leading to the induction of apoptosis. In contrast, a tumor suppressor function has been attributed to PTEN, the antagonist of the PI3K (Cristofano & Pandolfi, 2000). In a selection of human multiple myelomas, PTEN expression was reported to be lost leading to uncontrolled activated Akt activity (Hyun *et al.*, 2000). Moreover, B cell-specific deletion of the *PTEN* allele in mice caused hyper-proliferation of B cells due to a lower threshold for BCR activation and increased signaling via Akt (Anzelon *et al.*, 2003). Additionally, transcription factors are frequently mutated in B cell lymphomas, among them FoxO1 (Morin *et al.*, 2011). In light of the crucial role of these signaling components in the development of B cell malignancies, uncoupling of the BCR signaling by targeting critical factors is of great importance. As example, the PI3K inhibitor idelalisib (GS-1101) (Fruman & Rommel, 2011) and the Syk inhibitor fostamatinib (Friedberg *et al.*, 2010) were proven as effective and safe therapeutics in clinical trials. The development of small inhibitory compounds of SPPL2a could complement the currently available therapeutic approaches for the treatment of B cell neoplasms.

Apart from the development of B cell malignancies due to an enhanced survival and proliferation of cells, B cells are implicated in the development of several autoimmune diseases, e.g. multiple sclerosis, rheumatoid arthritis and systemic lupus erythematosus (Pillai *et al.*, 2011; Townsend *et al.*, 2010). Currently, several therapeutic strategies to directly target B cells are tested in clinical trials or are already approved (Dörner *et al.*, 2009). One of them is the anti-CD20 chimeric antibody rituximab that has been developed for the treatment of non-Hodgkin lymphoma. Since absence of SPPL2a leads to a reduction of splenic B cells in mice, inhibition of the activity of this protease by potent inhibitors might represent a novel target for the regulation and depletion of auto-reactive B cells.

4.6 Outlook

Within this project it could be shown that the B cell maturation arrest of *SPPL2a*$^{-/-}$ mice at the T1 stage is mainly caused by impaired PI3K/Akt signaling and the subsequent elevation of pro-apoptotic gene transcription. However, the final prove of this theory is still pending. In order to unequivocally identify the compromised PI3K/Akt pathway as the main reason for the developmental defect, *SPPL2a*$^{-/-}$ mice could be crossed with *PTEN*$^{-/-}$ mice. In SPPL2a PTEN double-deficient mice, the Akt pathway would be constitutively active and should be able to restore the phenotype of SPPL2a single-deficient mice. In order to prove the theory of a direct effect of the accumulating CD74 NTF, potential interactions between CD74 and the BCR, Syk and Akt can be analyzed by co-immunoprecipitation. Furthermore, an unbiased search for potential additional interaction partners of CD74 could help to identify the detailed mechanism of vesicle accumulation accompanied with impaired endocytic trafficking. To evaluate the fate of endocytosed cargo and to examine a potential endosome maturation defect, the lysosomal delivery of gold-labeled BSA could be monitored in *SPPL2a*$^{-/-}$ and wild type B cells by electron microscopy. In case of an endosomal maturation defect in SPPL2a-deficient B cells caused by the accumulating CD74 NTF, the endocytosed cargo would need a longer time to reach the lysosome when compared to wild type cells. Whether the internalized BSA reaches CD74-containing vesicles could be evaluated by co-staining for CD74. Furthermore, the hypothesized decreased turnover of MHCII in B cells deficient for SPPL2a could be addressed by performing pulse-chase experiments in which the degradation of MHCII is monitored over time in wild type versus *SPPL2a*$^{-/-}$ B cells.

Additionally, the analysis of signaling pathways could be extended to other CD74-expressing cell types, e.g. BMDCs. It would be interesting to examine the effects of CD74 NTF accumulation on signaling cascades that are not dependent on the BCR but still involve the PI3K and Akt. In dendritic cells, a cell type belonging to the innate immune system, PI3K signaling can be induced via Toll-like receptors (Hazeki *et al.*, 2007). In these cells, direct BCR-independent effects of the CD74 NTF in PI3K signaling can be evaluated.

The phenotypic alterations of SPPL2a-deficient mice might not all be related to the absent turnover of the CD74 NTF. Since the expression of CD74 is restricted to APCs and SPPL2a is ubiquitously expressed in different tissues of mice, it is very likely that further *in vivo*-relevant substrates of SPPL2a exist. The identification of new substrates of SPPL2a and its family member SPPL2b can be facilitated by the generation of SPPL2a and SPPL2b knock-in mice which was a side project of this work. Overexpression of the proteases was aimed to be accomplished by a targeted insertion of a cassette coding for either SPPL2a or -b and an upstream stop sequence flanked by Loxp sites into the endogenous ROSA26 locus of mice. Currently, the first mice which are heterozygous for the SPPL2a knock-in are available and can be bred with Cre expressing mice in order to delete the Stop sequence and guarantee expression of SPPL2a. Analysis of these mice will give new insights into the *in vivo* function of SPPL2a and would help to identify new substrates of the protease.

5 Summary

The intramembrane protease SPPL2a mediates the processing of transmembrane proteins in type II orientation. As the first *in vivo* validated substrate of this protease CD74 (invariant chain) was revealed. It functions as chaperone in MHCII-mediated antigen presentation. In the late endosomal membrane, different proteases sequentially process CD74. SPPL2a mediates the turnover of the final membrane-bound N-terminal fragment (NTF) of CD74. Absence of this protease in mice causes an accumulation of CD74 NTF accompanied by a high abundance of intracellular vesicles which is associated with a B cell maturation arrest at the transitional 1 stage and major impairments in the endocytic system. However, the detailed mechanisms underlying these disturbances were unknown.

In this study, a detailed analysis of B cells from *SPPL2a*$^{-/-}$ mice revealed major defects in endocytic trafficking. SPPL2a-deficient B cells show a delayed degradation of the fluid-phase cargo ovalbumin as well as a retention of endocytosed transferrin in intracellular vesicles as compared to wild type cells. Moreover, CD74 NTF accumulation causes enhanced MHCII levels at the cell surface and in intracellular vesicles. To clarify how the accumulated CD74 NTF leads to the B cell maturation block, the impact of SPPL2a-deficiency on signaling pathways which are essential for B cell survival and differentiation were analyzed. It could be demonstrated that tonic and B cell antigen receptor (BCR)-induced signaling via the PI3K/Akt pathway is severely compromised in SPPL2a-deficient B cells. These cells show an altered BCR trafficking leading to a reduction of surface localized IgM and a reduced signal transmission via the BCR and the tyrosine kinase Syk. Decreased IgM surface expression and the diminished activation of Syk in *SPPL2a*$^{-/-}$ B cells are interconnected processes. However, these disturbances do not necessarily account for the impaired PI3K/Akt signaling. Instead, direct effects of the endosomal CD74 NTF accumulation on the PI3K/Akt pathway can be assumed. In agreement with the compromised PI3K/Akt cascade, inactivation of the transcription factor FoxO1 as effector of Akt is reduced in *SPPL2a*$^{-/-}$ B cells leading to an elevated transcription of pro-apoptotic genes. Thus, impairments in the PI3K/Akt cascade most likely represent the major cause of the B cell developmental defect in *SPPL2a*$^{-/-}$ mice.

It can be concluded that clearance of the CD74 NTF by SPPL2a is required to maintain the integrity of the endocytic system. The turnover of this NTF is indispensable to guarantee appropriate levels of tonic BCR signaling which is essential for the maturation and survival of B cells.

6 Zusammenfassung

Die Intramembranprotease SPPL2a prozessiert Transmembranproteine in Typ II Orientierung. Das erste *in vivo* validierte Substrat dieser Protease ist das Molekül CD74, welches als Chaperon bei der MHCII-vermittelten Antigenpräsentation agiert. CD74 wird in späten Endosomen sequenziell prozessiert, wobei SPPL2a den Abbau des membran-ständigen N-terminalen Fragments (NTF) von CD74 reguliert. In Mäusen induziert die Defizienz dieser Protease die Akkumulation des CD74 NTFs sowie die Anreicherung von intrazellulären Vesikeln in B-Zellen. Dies führt zu einer Störung der B-Zellmaturierung im „Transitional 1 Stadium“ in der Milz und einer Beeinträchtigung des endocytischen Systems. Der genaue molekulare Mechanismus ist jedoch unklar.

In dieser Arbeit wurden die Defekte des endosomalen Systems auf Grund der CD74 NTF Akkumulation in B-Zellen aus *SPPL2a*$^{-/-}$ Mäusen näher charakterisiert. Es konnte gezeigt werden, dass SPPL2a-defiziente B-Zellen im Vergleich zu Wildtyp-Zellen eine verlangsamte Degradierung des *Fluid-Phase Cargo* Ovalbumin sowie eine Retention von internalisiertem Transferrin in intrazellulären Vesikeln aufweisen. Des Weiteren zeigen *SPPL2a*$^{-/-}$ B-Zellen erhöhte MHCII Proteinmengen an der Zelloberfläche und in intrazellulären Kompartimenten. Um den Mechanismus des B-Zellreifungsdefekts zu untersuchen, wurde die Auswirkung der SPPL2a-Defizienz auf Signalwege untersucht, welche besonders für das Überleben und Reifen von B-Zellen verantwortlich sind. Hierbei wurde eine stark verminderte tonische und *B cell antigen receptor* (BCR)-induzierte Aktivierung des PI3K/Akt-Weges in *SPPL2a*$^{-/-}$ B-Zellen festgestellt. Weiterhin zeigen diese Zellen im Vergleich zu Wildtyp-Kontrollen einen veränderten Transport des BCR und damit einhergehend eine Reduktion von IgM an der Zelloberfläche. Als Folge ist die Signalübertragung über den BCR und die Proteinkinase Syk in SPPL2a-defizienten B-Zellen stark vermindert. Die reduzierten IgM Oberflächenlevel sowie die verringerte Aktivierung von Syk sind voneinander abhängige Prozesse, welche jedoch Defekte im PI3K/Akt Signalweg nicht unmittelbar bedingen. Stattdessen scheint die Anreicherung des CD74 NTFs einen direkten negativen Effekt auf die Aktivierung dieser Kaskade zu haben. In Übereinstimmung mit den beobachteten Beeinträchtigungen des PI3K/Akt-Weges konnte in *SPPL2a*$^{-/-}$ B-Zellen außerdem eine verminderte Inaktivierung des Transkriptionsfaktors FoxO1 festgestellt werden, welche eine gesteigerte Transkription pro-apoptotischer Gene hervorruft und demnach maßgeblich zum Reifungsdefekt dieser Zellen beiträgt.

Zusammenfassend konnte gezeigt werden, dass der Abbau des CD74 NTF durch SPPL2a essentiell für die Funktionalität des endosomalen Systems ist. Die Beseitigung des Fragments ist unverzichtbar, um eine optimale Intensität an tonischen BCR-vermittelten Signalen zu gewährleisten, welche das Überleben und die Differenzierung von B-Zellen sicherstellen.

7 References

Aiba, Y., Kameyama, M., Yamazaki, T., Tedder, T. F. & Kurosaki, T. (2008) Regulation of B-cell development by BCAP and CD19 through their binding to phosphoinositide 3-kinase. *Blood* **111**(3)

Al-Alwan, M. M., Okkenhaug, K., Vanhaesebroeck, B., Hayflick, J. S. & Marshall, a. J. (2007) Requirement for Phosphoinositide 3-Kinase p110 Signaling in B Cell Antigen Receptor-Mediated Antigen Presentation. *J. Immunol.* **178**(4), 2328–2335

Alessi, D. R., James, S. R., Downes, C. P., Holmes, A. B., Gaffney, P. R., Reese, C. B. & Cohen, P. (1997) Characterization of a 3-phosphoinositide-dependent protein kinase which phosphorylates and activates protein kinase Balpha. *Curr. Biol.* **7**(4), 261–9

Allman, D. & Pillai, S. (2008) Peripheral B cell subsets. *Curr. Opin. Immunol.* **20**(2), 149–57

Alt, F., Oltz, E., Young, F. & Gorman, J. (1992) VDJ recombination. *Immunol. Today* **13**(8), 306–14

Amin, R. H. & Schlissel, M. S. (2008) Foxo1 directly regulates the transcription of recombination-activating genes during B cell development. *Nat. Immunol.* **9**(6), 613–622

Anzelon, A. N., Wu, H. & Rickert, R. C. (2003) Pten inactivation alters peripheral B lymphocyte fate and reconstitutes CD19 function. *Nat. Immunol.* **4**(3), 287–94

Astoul, E., Watton, S. & Cantrell, D. (1999) The dynamics of protein kinase B regulation during B cell antigen receptor engagement. *J. Cell Biol.* **145**(7), 1511–20

Bannish, G., Fuentes-Panana, E. M., Cambier, J. C., Pear, W. S. & Monroe, J. G. (2001) Ligand-independent signaling functions for the B lymphocyte antigen receptor and their role in positive selection during B lymphopoiesis. *J. Exp. Med.***194**(11), 1583–1596

Barkett, M. & Gilmore, T. (1999) Control of apoptosis by Rel/NF-kappaB transcription factors. *Oncogene* **18**, 6910–6924

Beel, a J. & Sanders, C. R. (2008) Substrate specificity of gamma-secretase and other intramembrane proteases. *Cell. Mol. Life Sci.* **65**(9), 1311–34

Behnke, J., Schneppenheim, J., Koch-Nolte, F., Haag, F., Saftig, P. & Schröder, B. (2011) Signal-peptide-peptidase-like 2a (SPPL2a) is targeted to lysosomes/late endosomes by a tyrosine motif in its C-terminal tail. *FEBS Lett.* **585**(19), 2951–7

Beisner, D. R., Langerak, P., Parker, A. E., Dahlberg, C., Otero, F. J., Sutton, S. E., Poirot, L., et al. (2013) The intramembrane protease Sppl2a is required for B cell and DC development and survival via cleavage of the invariant chain. *J. Exp. Med.* **210**(1), 23–30

Bénaroch, P., Yilla, M., Raposo, G., Ito, K., Miwa, K., Geuze, H. J. & Ploegh, H. L. (1995) How MHC class II molecules reach the endocytic pathway. *EMBO J.* **14**(1), 37–49

Bergmann, H., Yabas, M., Short, A., Miosge, L., Barthel, N., Teh, C. E., Roots, C. M., et al. (2013) B cell survival, surface BCR and BAFFR expression, CD74 metabolism, and CD8- dendritic cells require the intramembrane endopeptidase SPPL2A. *J. Exp. Med.* **210**(1), 31–40

Bijlmakers, M. J., Benaroch, P. & Ploegh, H. L. (1994) Mapping functional regions in the lumenal domain of the class II-associated invariant chain. *J. Exp. Med.* **180**(2), 623–9

Bikoff, E. K., Huang, L.-Y., Episkopou, V., Meerwijk, J. van, Germain, R. N. & Robertsin, E. (1993) Defective major histocompatibility complex class II assembly, transport, peptide acquisition, and CD4+ T cell selection in mice lacking invariant chain expression. *J. Exp. Med.* **177**(June)

Bléry, M., Tze, L., Miosge, L. A., Jun, J. E. & Goodnow, C. C. (2006) Essential role of membrane cholesterol in accelerated BCR internalization and uncoupling from NF-kappa B in B cell clonal anergy. *J. Exp. Med.* **203**(7), 1773–83

Boehmer, H. von & Melchers, F. (2010) Checkpoints in lymphocyte development and autoimmune disease. *Nat. Immunol.* **11**(1), 14–20

Brady, O. a, Zhou, X. & Hu, F. (2014) Regulated intramembrane proteolysis of the frontotemporal lobar degeneration risk factor, TMEM106B, by signal peptide peptidase-like 2a (SPPL2a). *J. Biol. Chem.* **289**(28), 19670–80

Bronckers, A. L. J. J., Gueneli, N., Güllmann-Rauch, R., Schneppenheim, J., Moraru, A. P., Himmerkus, N., Bervoets, T. J., et al. (2013) The intramembrane protease SPPL2A is critical for tooth enamel formation. *J. Bone Miner. Res.* **28**(7), 1622–30

Brown, M. S. & Goldstein, J. L. (1997) The SREBP Pathway: Regulation of Cholesterol Metabolism by Proteolysis of a Membrane-Bound Transcription Factor. *Cell* **89**(3), 331–340

Brown, M., Ye, J., Rawson, R. & Goldstein, J. (2000) Regulated intramembrane proteolysis: a control mechanism conserved from bacteria to humans. *Cell* **100**, 391–398

Browne, C. D., Nagro, C. J. Del, Cato, M. H., Dengler, H. S. & Rickert, R. C. (2009) Suppression of phosphatidylinositol 3,4,5-trisphosphate production is a key determinant of B cell anergy. *Immunity* **31**(5), 749–60

Buchner, M., Fuchs, S., Prinz, G., Pfeifer, D., Bartholomé, K., Burger, M., Chevalier, N., et al. (2009) Spleen tyrosine kinase is overexpressed and represents a potential therapeutic target in chronic lymphocytic leukemia. *Cancer Res.* **69**(13), 5424–32

Burkhardt, A. (1991) Anti-immunoglobulin stimulation of B lymphocytes activates src-related protein-tyrosine kinases. *Proc. Natl. Acad. Sci. U. S. A.* **88**(August), 7410–7414

Calamito, M., Juntilla, M. M., Thomas, M., Northrup, D. L., Rathmell, J., Birnbaum, M. J., Koretzky, G., et al. (2010) Akt1 and Akt2 promote peripheral B-cell maturation and survival. *Blood* **115**(20), 4043–4050

Cambier, J. C., Gauld, S. B., Merrell, K. T. & Vilen, B. J. (2007) B-cell anergy: from transgenic models to naturally occurring anergic B cells? *Nat. Rev. Immunol.* **7**(8), 633–643

Castellino, F., Han, R. & Germain, R. N. (2001) The transmembrane segment of invariant chain mediates binding to MHC class II molecules in a CLIP-independent manner. *Eur. J. Immunol.* **31**(3), 841–850

Chambard, J. C., Lefloch, R., Pouysségur, J. & Lenormand, P. (2007) ERK implication in cell cycle regulation. *Biochim. Biophys. Acta - Mol. Cell Res.* **1773**(8), 1299–1310

Chang, F., Lee, J. T., Navolanic, P. M., Steelman, L. S., Shelton, J. G., Blalock, W. L., Franklin, R. a, et al. (2003) Involvement of PI3K/Akt pathway in cell cycle progression, apoptosis, and neoplastic transformation: a target for cancer chemotherapy. *Leukemia* **17**(3), 590–603

Chaturvedi, A., Martz, R., Dorward, D., Waisberg, M. & Pierce, S. K. (2012) Endocytosed BCRs sequentially regulate MAPK and Akt signaling pathways from intracellular compartments. *Nat. Immunol.* **13**(2), 196–196

Cheng, A. M., Rowley, B., Pao, W., Hayday, A., Bolen, J. B. & Pawson, T. (1995) Syk tyrosine kinase required for mouse viability and B-cell development. *Nature* **378**(6554), 303–6

Clark, M., Campbell, K. & Kazlauskas, A. (1992) The B cell antigen receptor complex: association of Ig-alpha and Ig-beta with distinct cytoplasmic effectors. *Science (80-.).* **258**(October), 123–126

Claudio, E., Saret, S., Wang, H. & Siebenlist, U. (2009) Cell-autonomous role for NF-kappa B in immature bone marrow B cells. *J. Immunol.* **182**(6), 3406–13

Clayton, E., Bardi, G., Bell, S. E., Chantry, D., Downes, C. P., Gray, a., Humphries, L. a., et al. (2002) A Crucial Role for the p110 Subunit of Phosphatidylinositol 3-Kinase in B Cell Development and Activation. *J. Exp. Med.* **196**(6), 753–763

Cornall, R. J., Cheng, A. M., Pawson, T. & Goodnow, C. C. (2000) Role of Syk in B-cell development and antigen-receptor signaling. *Proc. Natl. Acad. Sci. U. S. A.* **97**(4), 1713–8

Cristofano, A. Di & Pandolfi, P. P. (2000) The multiple roles of PTEN in tumor suppression. *Cell* **100**(4), 387–90

Dal Porto, J. M., Gauld, S. B., Merrell, K. T., Mills, D., Pugh-Bernard, a E. & Cambier, J. (2004) B cell antigen receptor signaling 101. *Mol. Immunol.* **41**(6-7), 599–613

Dengler, H., Baracho, G., Omori, S., Bruckner, S., Arden, K., Castrillon, D., Depinho, R., et al. (2008) Distinct functions for the transcription factor Foxo1 at various stages of B cell differentiation. *Nat. Immunol.* **9**(12), 1388–1398

Dijkers, P. F., Medema†, R. H., Lammers, J.-W. J., Koenderman, L. & Coffer, P. J. (2000) Expression of the pro-apoptotic Bcl-2 family member Bim is regulated by the forkhead transcription factor FKHR-L1. *Curr. Biol.* **10**(19), 1201–1204

Do, B. R. K. G., Hatada, E., Lee, H., Tourigny, M. R., Hilbert, D. & Chen-kiang, S. (2000) Attenuation of Apoptosis Underlies B Lymphocyte Stimulator Enhancement of Humoral Immune Response. *J. Exp. Med.* **192**(7). 953-64

Dörner, T., Radbruch, A. & Burmester, G. R. (2009) B-cell-directed therapies for autoimmune disease. *Nat. Rev. Rheumatol.* **5**(8), 433–41

Driessen, C., Bryant, R. A., Lennon-Duménil, A.-M., Villadangos, J. A., Bryant, P. W., Shi, G.-P., Chapman, H. A., et al. (1999) Cathepsin S controls the trafficking and maturation of MHC class II molecules in dendritic cells. *J. Cell Biol.* **147**(4), 775–790

Duncan, E. a., Dave, U. P., Sakai, J., Goldstein, J. L. & Brown, M. S. (1998) Second-site Cleavage in Sterol Regulatory Element-binding Protein Occurs at Transmembrane Junction as Determined by Cysteine Panning. *J. Biol. Chem.* **273**(28), 17801–17809

Edbauer, D., Winkler, E., Regula, J. T., Pesold, B., Steiner, H. & Haass, C. (2003) Reconstitution of γ -secretase activity **5**(May), 486–488

Eris, J., Basten, A. & Brink, R. (1994) Anergic self-reactive B cells present self antigen and respond normally to CD40-dependent T-cell signals but are defective in antigen-receptor-mediated functions. *Proc. Natl. Acad. Sci. U. S. A.* **91**(May), 4392–4396

Faure-André, G., Vargas, P., Yuseff, M.-I., Heuzé, M., Diaz, J., Lankar, D., Steri, V., et al. (2008) Regulation of dendritic cell migration by CD74, the MHC class II-associated invariant chain. *Science* **322**(5908), 1705–10

Feng, J., Park, J., Cron, P., Hess, D. & Hemmings, B. A. (2004) Identification of a PKB/Akt hydrophobic motif Ser-473 kinase as DNA-dependent protein kinase. *J. Biol. Chem.* **279**(39), 41189–96

Fluhrer, R., Grammer, G., Israel, L., Condron, M. M., Haffner, C., Friedmann, E., Böhland, C., et al. (2006) A gamma-secretase-like intramembrane cleavage of TNFalpha by the GxGD aspartyl protease SPPL2b. *Nat. Cell Biol.* **8**(8), 894–6

Fluhrer, R., Steiner, H. & Haass, C. (2009) Intramembrane Proteolysis by Signal Peptide Peptidases: A Comparative Discussion of GXGD-type Aspartyl Proteases. *J. Biol. Chem.* **284**(21), 13975-9

Freisewinkel, I. M., Schenck, K. & Koch, N. (1993) The segment of invariant chain that is critical for association with major histocompatibility complex class II molecules contains the sequence of a peptide eluted from class II polypeptides. *Proc. Natl. Acad. Sci. U. S. A.* **90**(20), 9703–6

Friedberg, J. W., Sharman, J., Sweetenham, J., Johnston, P. B., Vose, J. M., Lacasce, A., Schaefer-Cutillo, J., et al. (2010) Inhibition of Syk with fostamatinib disodium has significant clinical activity in non-Hodgkin lymphoma and chronic lymphocytic leukemia. *Blood* **115**(13), 2578–85

Friedmann, E., Hauben, E., Maylandt, K., Schleeger, S., Vreugde, S., Lichtenthaler, S. F., Kuhn, P.-H., et al. (2006) SPPL2a and SPPL2b promote intramembrane proteolysis of TNFalpha in activated dendritic cells to trigger IL-12 production. *Nat. Cell Biol.* **8**(8), 843–8

Friedmann, E., Lemberg, M. K., Weihofen, A., Dev, K. K., Dengler, U., Rovelli, G. & Martoglio, B. (2004) Consensus analysis of signal peptide peptidase and homologous human aspartic proteases reveals opposite topology of catalytic domains compared with presenilins. *J. Biol. Chem.* **279**(49), 50790–8

Fruman, D. A. & Rommel, C. (2011) PI3Kδ inhibitors in cancer: rationale and serendipity merge in the clinic. *Cancer Discov.* **1**(7), 562–72

Fruman, D. A., Snapper, S. B., Yballe, C. M., Davidson, L., Yu, J. Y., Alt, F. W. & Cantley, L. C. (1999) Impaired B cell development and proliferation in absence of phosphoinositide 3-kinase p85alpha. *Science* **283**(5400), 393–7

Gassart, A. De, Camosseto, V., Thibodeau, A., Ceppi, M., Catalan, N., Pierre, P. & Gatti, E. (2008) MHC class II stabilization at the surface of human dendritic cells is the result of maturation-dependent MARCH I down-regulation. *Proc. Natl. Acad. Sci. U. S. A.* (14)

Gold, M. R. (2008) B cell development: important work for ERK. *Immunity* **28**(4), 488–90

Goodnow, C. C., Crosbie, J., Adelstein, S., Lavoie, T. B., Smith-Gill, S. J., Brink, R. A., Pritchard-Briscoe, H., et al. (1988) Altered immunoglobulin expression and functional silencing of self-reactive B lymphocytes in transgenic mice. *Nature* **334**(6184), 676–82

Gore, Y., Starlets, D., Maharshak, N., Becker-Herman, S., Kaneyuki, U., Leng, L., Bucala, R., et al. (2008) Macrophage migration inhibitory factor induces B cell survival by activation of a CD74-CD44 receptor complex. *J. Biol. Chem.* **283**(5), 2784–92

Gorvel, J.-P., Escola, J.-M., Stang, E. & Bakke, O. (1995) Invariant Chain Induces a Delayed Transport from Early to Late Endosomes. *J. Biol. Chem.* **270**(6), 2741–2746

Grawunder, U., Leu, T. M. J., Schatz, D. G., Werner, A., Rolink, A. G., Melchers, F. & Winkler, T. H. (1995) Downregulation of RAG1 and RAG2 Gene Expression in Pre-B cells after Functional Immunoglobulin Heavy Chain Rearrangement. *Immunity* **3**, 601–608

Gregers, T. F., Nordeng, T. W., Birkeland, H. C., Sandlie, I. & Bakke, O. (2003) The cytoplasmic tail of invariant chain modulates antigen processing and presentation. *Eur. J. Immunol.* **33**(2), 277–286.

Grumont, R. J., Rourke, I. J., Reilly, L. A. O., Strasser, A., Miyake, K., Sha, W. & Gerondakis, S. (1998) B Lymphocytes Differentially Use the Rel and Nuclear Cycle Progression and Apoptosis in Quiescent and **187**(5), 663–674

Guo, B., Kato, R. M., Garcia-Lloret, M., Wahl, M. I. & Rawlings, D. J. (2000) Engagement of the Human Pre-B Cell Receptor Generates a Lipid Raft–Dependent Calcium Signaling Complex. *Immunity* **13**(2), 243–253

Haapasalo, A. & Kovacs, D. M. (2011) The many substrates of presenilin/γ-secretase. *J. Alzheimers. Dis.* **25**(1), 3–28

Haass, C. & Steiner, H. (2002) Alzheimer disease γ -secretase : a complex story of GxGD-type presenilin proteases **12**(12), 556–562

Hardy, R. R. & Hayakawa, K. (1991) A developmental switch in B lymphopoiesis. *Proc. Natl. Acad. Sci. U. S. A.* **88**(24), 11550–4

Hardy, R. R., Kincade, P. W. & Dorshkind, K. (2007) The protean nature of cells in the B lymphocyte lineage. *Immunity* **26**(6), 703–14

Hardy, R. R., Kincade, P. W. & Dorshkind, K. (2007) The protean nature of cells in the B lymphocyte lineage. *Immunity* **26**(6), 703–14

Harnett, M. M., Katz, E. & Ford, C. a. (2005) Differential signalling during B-cell maturation. *Immunol. Lett.* **98**(1), 33–44

Hashimoto, A., Okada, H., Jiang, A., Kurosaki, M., Greenberg, S., Clark, E. A. & Kurosaki, T. (1998) Involvement of Guanosine Triphosphatases and Phospholipase C- gamma 2 in Extracellular Signal–regulated Kinase, c-Jun NH2 -terminal Kinase, and p38 Mitogen-activated Protein Kinase Activation by the B Cell Antigen Receptor. *J. Exp. Med.* **188**(7)

Hazeki, K., Nigorikawa, K. & Hazeki, O. (2007) Role of phosphoinositide 3-kinase in innate immunity. *Biol. Pharm. Bull.* **30**(9), 1617–23

He, B., Chadburn, a., Jou, E., Schattner, E. J., Knowles, D. M. & Cerutti, a. (2004) Lymphoma B Cells Evade Apoptosis through the TNF Family Members BAFF/BLyS and APRIL. *J. Immunol.* **172**(5), 3268–3279

Henley, T., Kovesdi, D. & Turner, M. (2008) B-cell responses to B-cell activation factor of the TNF family (BAFF) are impaired in the absence of PI3K delta. *Eur. J. Immunol.* **38**(12), 3543–8

Hinman, R. M., Bushanam, J. N., Whitney, A., Satterthwaite, A. B. & Kinase, T. (2014) B Cell Receptor Signaling Down-Regulates Forkhead Box Transcription Factor Class O 1 mRNA Expression via Phosphatidylinositol 3-Kinase and Bruton's Tyrosine Kinase. *J. Immunol.* **178**(2), 740-7

Hou, P., Araujo, E., Zhao, T., Zhang, M., Massenburg, D., Veselits, M., Doyle, C., et al. (2006) B cell antigen receptor signaling and internalization are mutually exclusive events. *PLoS Biol.* **4**(7), e200

Hsu, B. L., Harless, S. M., Lindsley, R. C., Hilbert, D. M. & Cancro, M. P. (2002) Cutting Edge: BLyS Enables Survival of Transitional and Mature B Cells Through Distinct Mediators. *J. Immunol.* **168**(12), 5993–5996

Huotari, J. & Helenius, A. (2011) Endosome maturation. *EMBO J.* **30**(17), 3481–500

Hutchcroft, J. E., Harrison, M. L. & Geahlenll, R. L. (1991) B Lymphocyte Activation Is Accompanied by Phosphorylation of a 72-kDa Protein-tyrosine. *J. Biol. Chem.* **266**(15), 14846–14849

Hyun, T., Yam, a, Pece, S., Xie, X., Zhang, J., Miki, T., Gutkind, J. S., et al. (2000) Loss of PTEN expression leading to high Akt activation in human multiple myelomas. *Blood* **96**(10), 3560–3568

Jellusova, J., Miletic, A. V, Cato, M. H., Lin, W.-W., Hu, Y., Bishop, G. A., Shlomchik, M. J., et al. (2013) Context-specific BAFF-R signaling by the NF-κB and PI3K pathways. *Cell Rep.* **5**(4), 1022–35

Jorissen, E. & Strooper, B. De. (2010) Gamma-secretase and the intramembrane proteolysis of Notch. *Curr. Top. Dev. Biol.* **92**, 201–30

Jou, S.-T., Carpino, N., Takahashi, Y., Piekorz, R., Chao, J.-R., Wang, D. & Ihle, J. N. (2002) Essential, Nonredundant Role for the Phosphoinositide 3-Kinase p110 in Signaling by the B-Cell Receptor Complex. *Mol. Cell. Biol.* **22**(24), 8580–8591

Jou, S.-T., Carpino, N., Takahashi, Y., Piekorz, R., Chao, J.-R., Wang, D. & Ihle, J. N. (2002) Essential, Nonredundant Role for the Phosphoinositide 3-Kinase p110 in Signaling by the B-Cell Receptor Complex. *Mol. Cell. Biol.* **22**(24), 8580–8591

Keren, Z., Diamant, E. & Ostrovsky, O. (2004) Modification of ligand-independent B cell receptor tonic signals activates receptor editing in immature B lymphocytes. *J. Biol.Chem.* **279**(14), 13418–13424

Kim, K. J., Kanellopoulos-Langevin, C., Merwin, R. M., Sachs, D. H. & Asofsky, R. (1979) Establishment and Characterization of BALB / c Lymphoma Lines with B Cell Properties. *J. Immunol.* **122**(2), 549–554

Kim, S., Wang, R., Gordon, D. J., Bass, J., Steiner, D. F., David, G., Thinakaran, G., et al. (1999) Furin mediates enhanced production of fibrillogenic ABri peptides in familial British dementia. *Nat. Neurosci*. **2**(11), 984-8

Kim, S.-H., Creemers, J. W. M., Chu, S., Thinakaran, G. & Sisodia, S. S. (2002) Proteolytic processing of familial British dementia-associated BRI variants: evidence for enhanced intracellular accumulation of amyloidogenic peptides. *J. Biol. Chem.* **277**(3), 1872–7

Kirkin, V., Cahuzac, N., Guardiola-Serrano, F., Huault, S., Lückerath, K., Friedmann, E., Novac, N., et al. (2007) The Fas ligand intracellular domain is released by ADAM10 and SPPL2a cleavage in T-cells. *Cell Death Differ.* **14**(9), 1678–87

Korade-Mirnics, Ž. & Corey, S. (2000) Src kinase-mediated signaling in leukocytes. *J. Leukoc. Biol.* **68**(November), 603–613

Krawitz, P., Haffner, C., Fluhrer, R., Steiner, H., Schmid, B. & Haass, C. (2005) Differential localization and identification of a critical aspartate suggest non-redundant proteolytic functions of the presenilin homologues SPPL2b and SPPL3. *J. Biol. Chem.* **280**(47), 39515–39523

Kümmel, D. & Ungermann, C. (2014) Principles of membrane tethering and fusion in endosome and lysosome biogenesis. *Curr. Opin. Cell Biol.* **29**, 61–6

Kurosaki, T., Shinohara, H. & Baba, Y. (2010) B cell signaling and fate decision. *Annu. Rev. Immunol.* **28**, 21–55

Labrecque, N., Madsen, L., Fugger, L., Benoist, C. & Mathis, D. (1999) Toxic MHC class II beta chains. *Immunity* **11**, 515–516

Laemmli, U. K. (1970) Cleavage of structural proteins during the assembly of the head of bacteriophage T4. *Nature* **15**(227), 680–5

Lagaudrière-Gesbert, C., Newmyer, S. L., Gregers, T. F., Bakke, O. & Ploegh, H. L. (2002) Uncoating ATPase Hsc70 is recruited by invariant chain and controls the size of endocytic compartments. *Proc. Natl. Acad. Sci. U. S. A.* **99**(3), 1515–1520

Lal, M. & Caplan, M. (2011) Regulated intramembrane proteolysis: signaling pathways and biological functions. *Physiology (Bethesda).* **26**(1), 34–44

Lam, K., Kühn, R. & Rajewsky, K. (1997) In vivo ablation of surface immunoglobulin on mature B cells by inducible gene targeting results in rapid cell death. *Cell* **90**, 1073–1083

Landsverk, O. J. B., Bakke, O. & Gregers, T. F. (2009) MHC II and the endocytic pathway: Regulation by invariant chain. *Scand. J. Immunol.* **70**(3), 184–193

Landsverk, O. J. B., Barois, N., Gregers, T. F. & Bakke, O. (2011) Invariant chain increases the half-life of MHC II by delaying endosomal maturation. *Immunol. Cell Biol.* **89**(5), 619–29

Lee, J. R., Urban, S., Garvey, C. F. & Freeman, M. (2001) and Proteolysis Control EGF Signal Activation in Drosophila **107**, 161–171

Lemberg, M. K. (2013) Sampling the membrane: function of rhomboid-family proteins. *Trends Cell Biol.* **23**(5), 210–7

Lemberg, M. K., Bland, F. a., Weihofen, a., Braud, V. M. & Martoglio, B. (2001) Intramembrane Proteolysis of Signal Peptides: An Essential Step in the Generation of HLA-E Epitopes. *J. Immunol.* **167**(11), 6441–6446

Leng, L., Metz, C. N., Fang, Y., Xu, J., Donnelly, S., Baugh, J., Delohery, T., et al. (2003) MIF signal transduction initiated by binding to CD74. *J. Exp. Med.* **197**(11), 1467–76

Li-Weber, M. & Krammer, P. H. (2003) Function and regulation of the CD95 (APO-1/Fas) ligand in the immune system. *Semin. Immunol.* **15**(3), 145–57

Lutz, M. B., Kukutsch, N., Ogilvie, A. L. J., Roßner, S., Koch, F., Romani, N. & Schuler, G. (1999) An advanced culture method for generating large quantities of highly pure dendritic cells from mouse bone marrow. *J. Immunol. Methods* **223**(1), 77–92

Lyko, F., Martoglio, B., Jungnickel, B., Rapoport, T. A. & Dobberstein, B. (1995) Signal sequence processing in rough microsomes. *J. Biol. Chem.* **270**(34), 19873–8

Ma, J. K., Platt, M. Y., Eastham-Anderson, J., Shin, J.-S. & Mellman, I. (2012) MHC class II distribution in dendritic cells and B cells is determined by ubiquitin chain length. *Proc. Natl. Acad. Sci. U. S. A.* **109**(23), 8820–7

Mackay, F., Figgett, W. A., Saulep, D., Lepage, M. & Hibbs, M. L. (2010) B-cell stage and context-dependent requirements for survival signals from BAFF and the B-cell receptor. *Immunol. Rev.* **237**(1), 205–25

Mackay, F. & Schneider, P. (2009) Cracking the BAFF code. *Nat. Rev. Immunol.* **9**(7), 491–502

Madsen, L., Labrecque, N., Engberg, J., Dierich, A., Svejgaard, A., Benoist, C., Mathis, D., et al. (1999) Mice lacking all conventional MHC class II genes. *Proc. Natl. Acad. Sci.* **96**(August), 10338–10343

Maehr, R., Kraus, M. & Ploegh, H. L. (2004) Mice deficient in invariant-chain and MHC class II exhibit a normal mature B2 cell compartment. *Eur. J. Immunol.* **34**(8), 2230–2236

Martin, L., Fluhrer, R., Reiss, K., Kremmer, E., Saftig, P. & Haass, C. (2008) Regulated intramembrane proteolysis of Bri2 (Itm2b) by ADAM10 and SPPL2a/SPPL2b. *J. Biol. Chem.* **283**(3), 1644–52

Matza, D., Kerem, A. & Shachar, I. (2003) Invariant chain, a chain of command. *Trends Immunol.* **24**(5), 264–268

Mayle, K. M., Le, A. M. & Kamei, D. T. (2012) The intracellular trafficking pathway of transferrin. *Biochim. Biophys. Acta* **1820**(3), 264–81

Medema, R., Kops, G., Bos, J. & Burgering, B. (2000) AFX-like Forkhead transcription factors mediate cell-cycle regulation by Ras and PKB through p27kip1. *Nature* **404**(April), 782-7

Meffre, E. & Nussenzweig, M. C. (2002) Deletion of immunoglobulin beta in developing B cells leads to cell death. *Proc. Natl. Acad. Sci. U. S. A.* **99**(17), 11334–9

Melchers, F., Rolink, A. & Grawunder, U. (1995) Positive and negative selection events during B lymphopoiesis. *Curr. Opin.Immunol.***7**(2), 214–227

Merrell, K. T., Benschop, R. J., Gauld, S. B., Aviszus, K., Decote-Ricardo, D., Wysocki, L. J. & Cambier, J. C. (2006) Identification of Anergic B Cells within a Wild-Type Repertoire. *Immunity* **25**(6), 953–962

Mielenz, D., Ruschel, a., Vettermann, C. & Jack, H.-M. (2003) Immunoglobulin Heavy Chains Do Not Mediate Tyrosine Phosphorylation of Ig from the ER-cis-Golgi. *J. Immunol.* **171**(6), 3091–3101

Miller, D. J. & Hayes, C. E. (1991) Phenotypic and genetic characterization of a unique B lymphocyte deficiency in strain AM7ySnJ mice. *Eur. J. Immunol.* **21**(5), 1123–1130

Mombaerts, P., Iacomini, J., Johnson, R. S., Herrup, K., Tonegawa, S. & Papaioannou, V. E. (1992) RAG-1-deficient mice have no mature B and T lymphocytes. *Cell* **68**(5), 869–77

Monji, T., McCormack, A. L., Yates, J. R. & Pious, D. (1994) Invariant-cognate peptide exchange restores class II dimer stability in HLA-DM mutants. *J. Immunol.* **153**(10), 4468–77

Monroe, J. G. (2004) Ligand-independent tonic signaling in B-cell receptor function. *Curr. Opin. Immunol.* **16**(3), 288–95

Monroe, J. G. (2006) ITAM-mediated tonic signalling through pre-BCR and BCR complexes. *Nat. Rev. Immunol.* **6**(4), 283–94

Morin, R. D., Mendez-Lago, M., Mungall, A. J., Goya, R., Mungall, K. L., Corbett, R. D., Johnson, N. A., et al. (2011) Frequent mutation of histone-modifying genes in non-Hodgkin lymphoma. *Nature* **476**(7360), 298–303

Morrison, M. D., Reiley, W., Zhang, M. & Sun, S.-C. (2005) An atypical tumor necrosis factor (TNF) receptor-associated factor-binding motif of B cell-activating factor belonging to the TNF family (BAFF) receptor mediates induction of the noncanonical NF-kappaB signaling pathway. *J. Biol. Chem.* **280**(11), 10018–24

Murphy, J. E., Padilla, B. E., Hasdemir, B., Cottrell, G. S. & Bunnett, N. W. (2009) Endosomes: a legitimate platform for the signaling train. *Proc. Natl. Acad. Sci. U. S. A.* **106**(42), 17615–22

Murphy, K. (2012) *Janeway's Immunobiology*, 8th ed. New York.

Neefjes, J., Jongsma, M., Paul, P. & Bakke, O. (2011) Towards a systems understanding of MHC class I and MHC class II antigen presentation. *Nat. Rev. Immunol.* **11**(12), 823–36

Niel, G. van, Wubbolts, R., Broeke, T. Ten, Buschow, S. I., Ossendorp, F. a, Melief, C. J., Raposo, G., et al. (2006) Dendritic cells regulate exposure of MHC class II at their plasma membrane by oligoubiquitination. *Immunity* **25**(6), 885–94

Niiro, H. & Clark, E. a. (2002) Regulation of B-cell fate by antigen-receptor signals. *Nat. Rev. Immunol.* **2**(12), 945–56

Nordeng, T. W., Gregers, T. F., Kongsvik, T. L., Méresse, S., Gorvel, J.-P., Jourdan, F., Motta, A., et al. (2002) The cytoplasmic tail of invariant chain regulates endosome fusion and morphology. *Mol. Biol. Cell* **13**(6), 1846–1856

Novak, R., Jacob, E., Haimovich, J., Avni, O. & Melamed, D. (2010) The MAPK/ERK and PI3K pathways additively coordinate the transcription of recombination-activating genes in B lineage cells. *J. Immunol.* **185**(6), 3239–3247

Nyborg, A. C., Kornilova, A. Y., Jansen, K., Ladd, T. B., Wolfe, M. S. & Golde, T. E. (2004) Signal peptide peptidase forms a homodimer that is labeled by an active site-directed gamma-secretase inhibitor. *J. Biol. Chem.* **279**(15), 15153–60

O'Keefe, T. L., Williams, G. T., Davies, S. L. & Neuberger, M. S. (1996) Hyperresponsive B cells in CD22-deficient mice. *Science* **274**(5288), 798–801

Ohnishi, K. & Melchers, F. (2003) The nonimmunoglobulin portion of lambda5 mediates cell-autonomous pre-B cell receptor signaling. *Nat. Immunol.* **4**(9), 849–56

Okkenhaug, K., Bilancio, A., Farjot, G., Priddle, H., Sancho, S., Peskett, E., Pearce, W., et al. (2002) Impaired B and T cell antigen receptor signaling in p110delta PI 3-kinase mutant mice. *Science* **297**(5583), 1031–4

Pauls, S. D., Lafarge, S. T., Landego, I., Zhang, T. & Marshall, A. J. (2012) The phosphoinositide 3-kinase signaling pathway in normal and malignant B cells: activation mechanisms, regulation and impact on cellular functions. *Front. Immunol.* **3**, 224

Petro, J. B. & Khan, W. N. (2001) Phospholipase C-gamma 2 couples Bruton's tyrosine kinase to the NF-kappaB signaling pathway in B lymphocytes. *J. Biol. Chem.* **276**(3), 1715–9

Piatelli, M. J., Doughty, C. & Chiles, T. C. (2002) Requirement for a hsp90 chaperone-dependent MEK1/2-ERK pathway for B cell antigen receptor-induced cyclin D2 expression in mature B lymphocytes. *J. Biol. Chem.* **277**(14), 12144–50

Pillai, S. & Cariappa, A. (2009) The follicular versus marginal zone B lymphocyte cell fate decision. *Nat. Rev. Immunol.* **9**(11), 767–77

Pillai, S., Cariappa, A. & Moran, S. T. (2005) Marginal zone B cells. *Annu. Rev. Immunol.* **23**, 161–96

Pillai, S., Mattoo, H. & Cariappa, A. (2011) B cells and autoimmunity. *Curr. Opin. Immunol.* **23**(6), 721–31

Pogue, S. L., Kurosaki, T., Bolen, J. & Herbst, R. (2000) B Cell Antigen Receptor-Induced Activation of Akt Promotes B Cell Survival and Is Dependent on Syk Kinase. *J. Immunol.* **165**(3), 1300–1306

Ponting, C., Hutton, M. & Nyborg, A. (2002) Identification of a novel family of presenilin homologues. *Hum. Mol.Genet.* **11**(9), 1037–1044

Radons, J., Faber, V., Buhrmester, H., Völker, W., Horejsí, V. & Hasilik, A. (1992) Stimulation of the biosynthesis of lactosamine repeats in glycoproteins in differentiating U937 cells and its suppression in the presence of NH4Cl. *Eur. J. Cell Biol.* **57**(2), 184–92

Rawson, R. B., Zelenski, N. G., Nijhawan, D., Ye, J., Sakai, J., Hasan, M. T., Chang, T. ., et al. (1997) Complementation Cloning of S2P, a Gene Encoding a Putative Metalloprotease Required for Intramembrane Cleavage of SREBPs. *Mol. Cell* **1**(1), 47–574

Richards, J. D., Davé, S. H., Chou, C. H., Mamchak, a a & DeFranco, a L. (2001) Inhibition of the MEK/ERK signaling pathway blocks a subset of B cell responses to antigen. *J. Immunol.* **166**(6), 3855–3864

Rickert, R. C. (2013) New insights into pre-BCR and BCR signalling with relevance to B cell malignancies. *Nat. Rev. Immunol.* **13**(8), 578–91

Roche, P. A., Teletski, C. L., Stang, E., Bakke, O. & Long, E. O. (1993) Cell surface HLA-DR-invariant chain complexes are targeted to endosomes by rapid internalization. *Proc. Natl. Acad. Sci. U. S. A.* **90**(18), 8581–5

Rolink, A. & Melchers, F. (1996) B-cell development in the mouse. *Immunol. Lett.* **54**(2-3), 157–61

Romagnoli, P. & Germain, R. N. (1994) The CLIP region of invariant chain plays a critical role in regulating major histocompatibility complex class II folding, transport, and peptide occupancy. *J. Exp. Med.* **180**(3), 1107–13

Roth, D. & Craig, N. (1998) VDJ recombination: a transposase goes to work. *Cell* **94**, 411–414

Rowland, S. L., DePersis, C. L., Torres, R. M. & Pelanda, R. (2010) Ras activation of Erk restores impaired tonic BCR signaling and rescues immature B cell differentiation. *J. Exp. Med.* **207**(3), 607–621

Rowland, S. L., Leahy, K. F., Halverson, R., Torres, R. M. & Pelanda, R. (2010) BAFF receptor signaling aids the differentiation of immature B cells into transitional B cells following tonic BCR signaling. *J. Immunol.* **185**(8), 4570–4581

Sadofsky, M. (2001) The RAG proteins in V (D) J recombination: more than just a nuclease. *Nucleic Acids Res.* **29**(7), 1399–1409

Sadowski, L., Pilecka, I. & Miaczynska, M. (2009) Signaling from endosomes: location makes a difference. *Exp. Cell Res.* **315**(9), 1601–9

Saijo, K., Schmedt, C., Su, I.-H., Karasuyama, H., Lowell, C. a, Reth, M., Adachi, T., et al. (2003) Essential role of Src-family protein tyrosine kinases in NF-kappaB activation during B cell development. *Nat. Immunol.* **4**(3), 274–9

Sakai, J., Duncan, E. A., Rawson, R. B., Hua, X., Brown, M. S. & Goldstein, J. L. (1996) Sterol-Regulated Release of SREBP-2 from Cell Membranes Requires Two Sequential Cleavages , One Within a Transmembrane Segment. *Hum. Mol. Genet.* **11**(9), 1037–1046

Sanger, F. & Nicklen, S. (1977) DNA sequencing with chain-terminating. *Proc Natl Acad Sci U S A.* **74**(12), 5463–5467

Sarbassov, D. D., Guertin, D. A., Ali, S. M. & Sabatini, D. M. (2005) Phosphorylation and regulation of Akt/PKB by the rictor-mTOR complex. *Science* **307**(5712), 1098–101

Sato, S., Miller, A. S., Inaoki, M., Bock, C. B., Jansen, P. J., Tang, M. L. K. & Tedder, T. F. (1996) CD22 Is Both a Positive and Negative Regulator of B Lymphocyte Antigen Receptor Signal Transduction: Altered Signaling in CD22-Deficient Mice. *Immunity* **5**(6), 551–562

Schägger, H. (2006) Tricine-SDS-PAGE. *Nat. Protoc.* **1**(1), 16–22

Schiemann, B., Gommerman, J. L., Vora, K., Cachero, T. G., Shulga-Morskaya, S., Dobles, M., Frew, E., et al. (2001) An essential role for BAFF in the normal development of B cells through a BCMA-independent pathway. *Science* **293**(5537), 2111–4

Schneppenheim, J. (2013) Die Bedeutung der Intramembranprotease SPPL2a für die Entwicklung muriner B-Lymphozyten. *Dissertation* Christian–Albrechts–University of Kiel, Kiel.

Schneppenheim, J., Dressel, R., Hüttl, S., Lüllmann-Rauch, R., Engelke, M., Dittmann, K., Wienands, J., et al. (2013) The intramembrane protease SPPL2a promotes B cell development and controls endosomal traffic by cleavage of the invariant chain. *J. Exp. Med.* **210**(1), 41–58

Schneppenheim, J., Hüttl, S., Kruchen, A., Fluhrer, R., Müller, I., Saftig, P., Schneppenheim, R., et al. (2014) Signal-peptide-peptidase-like 2a is required for CD74 intramembrane proteolysis in human B cells. *Biochem. Biophys. Res. Commun.* **451**(1), 48-53

Schneppenheim, J., Hüttl, S., Mentrup, T., Lüllmann-Rauch, R., Rothaug, M., Engelke, M., Dittmann, K., et al. (2014) The intramembrane proteases signal Peptide peptidase-like 2a and 2b have distinct functions in vivo. *Mol. Cell. Biol.* **34**(8), 1398–411

Schweighoffer, E., Vanes, L., Nys, J., Cantrell, D., McCleary, S., Smithers, N. & Tybulewicz, V. L. J. (2013) The BAFF receptor transduces survival signals by co-opting the B cell receptor signaling pathway. *Immunity* **38**(3), 475–88

Shi, G. P., Villadangos, J. A., Dranoff, G., Small, C., Gu, L., Haley, K. J., Riese, R., et al. (1999) Cathepsin S Required for Normal MHC Class II Peptide Loading and Germinal Center Development Targeting of Mouse Cathepsin S Gene. *Immunity* **10**(2), 197–206

Shinkai, Y., Rathbun, G., Lam, K. P., Oltz, E. M., Stewart, V., Mendelsohn, M., Charron, J., et al. (1992) RAG-2-deficient mice lack mature lymphocytes owing to inability to initiate V(D)J rearrangement. *Cell* **68**(5), 855–67

Slot, J. W. & Geuze, H. J. (2007) Cryosectioning and immunolabeling. *Nat. Protoc.* **2**(10), 2480–2491

Srinivasan, L., Sasaki, Y., Calado, D. P., Zhang, B., Paik, J. H., DePinho, R. a., Kutok, J. L., et al. (2009) PI3 Kinase Signals BCR-Dependent Mature B Cell Survival. *Cell* **139**(3), 573–586

Stadanlick, J. E., Kaileh, M., Karnell, F. G., Scholz, J. L., Miller, J. P., Quinn, W. J., Brezski, R. J., et al. (2008) Tonic B cell antigen receptor signals supply an NF-kappaB substrate for prosurvival BLyS signaling. *Nat. Immunol.* **9**(12), 1379–87

Stang, E. & Bakke, O. (1997) MHC class II-associated invariant chain-induced enlarged endosomal structures: a morphological study. *Exp. Cell Res.* **235**(1), 79–92

Starlets, D., Gore, Y., Binsky, I., Haran, M., Harpaz, N., Shvidel, L., Becker-Herman, S., et al. (2006) Cell-surface CD74 initiates a signaling cascade leading to cell proliferation and survival. *Blood* **107**(12), 4807–4816

Steiner, H., Fluhrer, R. & Haass, C. (2008) Intramembrane proteolysis by gamma-secretase. *J. Biol. Chem.* **283**(44), 29627–31

Stepanek, O., Draber, P., Drobek, A., Horejsi, V. & Brdicka, T. (2013) Nonredundant roles of Src-family kinases and Syk in the initiation of B-cell antigen receptor signaling. *J. Immunol.* **190**(4), 1807–18

Su, Y., Hao, Z., Yamamoto, K., Lin, W., Young, A., Duncan, S., Yoshida, H., et al. (2011) 14-3-3 regulates B-cell homeostasis through stabilization of FOXO1. *Proc. Natl. Acad. Sci.* **108**(16), 6689–6689

Sun, H., Lesche, R., Li, D.-M., Liliental, J., Zhang, H., Gao, J., Gavrilova, N., et al. (1999) PTEN modulates cell cycle progression and cell survival by regulating phosphatidylinositol 3,4,5,-

trisphosphate and Akt/protein kinase B signaling pathway. *Proc. Natl. Acad. Sci.* **96**(11), 6199–6204

Suzuki, H., Terauchi, Y., Fujiwara, M., Aizawa, S., Yazaki, Y., Kadowaki, T. & Koyasu, S. (1999) Xid-like immunodeficiency in mice with disruption of the p85alpha subunit of phosphoinositide 3-kinase. *Science* **283**(5400), 390–2

Szydłowski, M., Jabłońska, E. & Juszczyński, P. (2014) FOXO1 transcription factor: a critical effector of the PI3K-AKT axis in B-cell development. *Int. Rev. Immunol.* **33**(2), 146–57

Thompson, J. S., Bixler, S. a, Qian, F., Vora, K., Scott, M. L., Cachero, T. G., Hession, C., et al. (2001) BAFF-R, a newly identified TNF receptor that specifically interacts with BAFF. *Science* **293**(5537), 2108–11

Townsend, M. J., Monroe, J. G. & Chan, A. C. (2010) B-cell targeted therapies in human autoimmune diseases: an updated perspective. *Immunol. Rev.* **237**(1), 264–83

Tsang, E., Giannetti, A. M., Dinh, M., Tse, J. K. Y., Ho, H., Wang, S., Bradshaw, J. M., et al. (2008) Molecular mechanism of the Syk activation switch. *J. Biol. Chem.* **283**(47), 32650–32659

Turner, M., Gulbranson-Judge, A., Quinn, M. E., Walters, a. E., MacLennan, I. C. M. & Tybulewicz, V. L. J. (1997) Syk tyrosine kinase is required for the positive selection of immature B cells into the recirculating B cell pool. *J. Exp. Med.* **186**(12), 2013–2021

Turner, M., Mee, P. J., Costello, P. S., Williams, O., Price, A. A., Duddy, L. P., Furlong, M. T., et al. (1995) Perinatal lethality and blocked B-cell development in mice lacking the tyrosine kinase Syk. *Nature* **378**(6554), 298–302

Tze, L. E., Baness, E. A., Hippen, K. L. & Behrens, T. W. (2000) Ig light chain receptor editing in anergic B cells. *J. Immunol.* **165**(12), 6796–802

Vascotto, F., Lankar, D., Faure-André, G., Vargas, P., Diaz, J., Roux, D. Le, Yuseff, M.-I., et al. (2007) The actin-based motor protein myosin II regulates MHC class II trafficking and BCR-driven antigen presentation. *J. Cell Biol.* **176**(7), 1007–1019

Verkoczy, L., Duong, B., Skog, P., Ait-Azzouzene, D., Puri, K., Vela, J. L. & Nemazee, D. (2007) Basal B Cell Receptor-Directed Phosphatidylinositol 3-Kinase Signaling Turns Off RAGs and Promotes B Cell-Positive Selection. *J. Immunol.* **178**(10), 6332–6341

Vidal, R., Frangione, B., Rostagno, A. & Mead, S. (1999) A stop-codon mutation in the BRI gene associated with familial British dementia. *Nature* **399**(6738),776-81

Villadangos, J. A. & Ploegh, H. L. (2000) Proteolysis in MHC Class II Antigen Presentation. Who's in Charge? *Immunity* **12**(3), 233–239

Vogt, A. & Kropshofer, H. (1999) Quality control of MHC class II associated peptides by HLA-DM/H2-M. *Semin. Immunol.* **11**(6), 391-403

Voss, M., Schröder, B. & Fluhrer, R. (2013) Mechanism, specificity, and physiology of signal peptide peptidase (SPP) and SPP-like proteases. *Biochim. Biophys. Acta* **1828**(12), 2828–39

Weihofen, a, Lemberg, M. K., Ploegh, H. L., Bogyo, M. & Martoglio, B. (2000) Release of signal peptide fragments into the cytosol requires cleavage in the transmembrane region by a protease

activity that is specifically blocked by a novel cysteine protease inhibitor. *J. Biol. Chem.* **275**(40), 30951–6

Weihofen, A. & Martoglio, B. (2003) Intramembrane-cleaving proteases: controlled liberation of proteins and bioactive peptides. *Trends Cell Biol.* **13**(2), 71–78

Wienands, J., Larboletite, O., Reth, M. & Larbolette, O. (1996) Evidence for a preformed transducer complex organized by the B cell antigen receptor. *Proc. Natl. Acad. Sci. U. S. A.* **93**(15), 7865–7870

Wolfe, M. S. (2009) Intramembrane Proteolysis. *Chem. Rev.* **109**(4), 1599-612

Wolfe, M. S. (2009) Intramembrane-cleaving proteases. *J. Biol. Chem.* **284**(21), 13969–73

Wolfe, M. S., Angeles, J. D. L., Miller, D. D., Xia, W. & Selkoe, D. J. (1999) Are Presenilins Intramembrane-Cleaving Proteases ? Implications for the Molecular Mechanism of Alzheimer's Disease. *Biochemistry* **38**(35), 11223-30

Wolfe, M. S. & Selkoe, D. J. (2002) Biochemistry. Intramembrane proteases--mixing oil and water. *Science* **296**(5576), 2156–7

Yamamoto, K., Floyd-Smith, G., Francke, U., Koch, N., Lauer, W., Dobberstein, B., Schäfer, R., et al. (1985) The gene encoding the Ia-associated invariant chain is located on chromosome 18 in the mouse. *Immunogenetics* **21**(1), 83–90

Yamanashi, Y., Kakiuchi, T., Mizuguchi, J., Yamamoto, T. & Toyoshima, K. (1991) Association of B cell antigen receptor with protein tyrosine kinase Lyn. *Science* **251**(4990), 192–4

Yankee, T. M. & Clark, E. A. (2000) Signaling through the B cell antigen receptor in developing B cells. *Rev. Immunogenet.* **2**(2), 185–203

Yasuda, T., Sanjo, H., Pagès, G., Kawano, Y., Karasuyama, H., Pouysségur, J., Ogata, M., et al. (2008) Erk Kinases Link Pre-B Cell Receptor Signaling to Transcriptional Events Required for Early B Cell Expansion. *Immunity* **28**(4), 499–508

Yokozeki, T., Adler, K., Lankar, D. & Bonnerot, C. (2003) B cell receptor-mediated Syk-independent activation of phosphatidylinositol 3-kinase, Ras, and mitogen-activated protein kinase pathways. *J. Immunol.* **171**(3), 1328–35

Yusuf, I., Zhu, X., Kharas, M. G., Chen, J. & Fruman, D. a. (2004) Optimal B-cell proliferation requires phosphoinositide 3-kinase-dependent inactivation of FOXO transcription factors. *Blood* **104**(3), 784–787

Zachos, C., Blanz, J., Saftig, P. & Schwake, M. (2012) A critical histidine residue within LIMP-2 mediates pH sensitive binding to its ligand β-glucocerebrosidase. *Traffic* **13**(8), 1113–23

Zahn, C., Kaup, M., Fluhrer, R. & Fuchs, H. (2013) The transferrin receptor-1 membrane stub undergoes intramembrane proteolysis by signal peptide peptidase-like 2b. *FEBS J.* **280**(7), 1653–63

Zhang, Y., Diwo, Z., Mao, F., Leung, W. & Haugland, R. (1994) Novel fluorescent acidic organelle-selective dyes and mitochondrion-selective dyes that are well retained during cell fixation and permeabilization. *Mol. Biol. Cell*

8 Supplement

8.1 List of figures

8.2 List of tables

9 List of publications

Parts of the presented dissertation have been published previously:

Schneppenheim J, Dressel R, **Hüttl S**, Lüllmann-Rauch R, Engelke M, Dittmann K, Wienands J, Eskelinen E. L, Hermans-Borgmeyer I, Fluhrer R, Saftig P, Schröder B (2013). The intramembrane protease SPPL2a promotes B cell development and controls endosomal traffic by cleavage of the invariant chain. *J. Exp. Med.,* 210, 41-58.

Own contribution: Figure 4A, B, F, G

Parts of the dissertation were submitted for publication and are currently under revision:

Hüttl S, Schweizer M, Schneppenheim J, Saftig P, Schröder B. Processing of CD74 by the intramembrane protease SPPL2a is critical for B cell receptor signaling in transitional B cells. *JI, in revision*

Own contribution: All figures, electron microscopy in cooperation with Dr. Michaela Schweizer (ZMNH, Hamburg)

Additional data which are not included in the dissertation have been published previously:

Schneppenheim J, **Hüttl S**, Kruchen A, Fluhrer R, Müller I, Saftig P, Schneppenheim R, Martin CL, Schröder B. (2014) Signal-peptide-peptidase-like 2a is required for CD74 intramembrane proteolysis in human B cells. *Biochem. Biophys. Res. Commun.,* 451 (1), 48-53

Own contribution: Figure 3C

Schneppenheim J, **Hüttl S**, Lüllmann-Rauch R, Mentrup T, Engelke M, Dittmann K, Dressel R, Araki M, Araki K, Wienands J, Fluhrer R, Saftig P, Schröder B. (2014) The intramembrane proteases signal-peptide-peptidase-like 2a and b 2 (SPPL2a/b) have distinct functions *in vivo*. *Mol. Cell. Biol.,* 34 (8). 1398-411

Own contribution: Figure 5D, 7B, C

10 Declaration

Herewith I declare that:

I apart from the supervisor's guidance, the content and design of this dissertation is my own work.

II this thesis has not been submitted partially or wholly as part of a doctoral degree to another examining body.

III parts of this work have been submitted for scientific publication.

IV this thesis has been prepared according to the Rules of Good Scientific Practice of the German Research Foundation.

Kiel, February 2015

Susann Hüttl

11 Acknowledgement

Es ist vollbracht: 4 Jahre und 4 Monate intensive Arbeit sind nun auf insgesamt 150 Seiten abgedruckt. An dieser Stelle möchte ich mich bei den Personen bedanken, die mich während dieser spannenden Zeit tatkräftig unterstützt haben.

Besonderer Dank gilt meinen beiden „Doktorvätern“ Dr. Bernd Schröder und Prof. Dr. Paul Saftig. Vielen Dank für die unzähligen konstruktiven Diskussionen und die ergebnisorientierte Betreuung. Herrn Prof. Dr. Matthias Leippe danke ich für die Bereitschaft, die Begutachtung der Dissertation zu übernehmen.

Ich danke besonders meiner Mitstreiterin Dr. Janna Schneppenheim für die tolle Teamarbeit, die großartige Einarbeitung in das Projekt und so manch unvergessliches Laborerlebnis.

Ebenso geht mein Dank an Sebastian Held und Marlies Rusch für ihre exzellente technische Unterstützung im Laboralltag. Auch möchte ich den Mitarbeitern des Viktor-Hensen-Hauses, im Speziellen Andrea Henke, für die kompetente Durchführung der Mauszucht danken. Dr. Michaela Schweizer möchte ich für die Anfertigung der EM-Bilder danken. Weiterhin danke ich meinen lieben Kollegen und Freunden für die tolle Arbeitsatmosphäre, die großartige Unterstützung sowie für die vielen schönen Erlebnisse auch außerhalb der Arbeitswelt.

Besonders möchte ich mich auch bei meiner Freundin Dr. Susann Voigt für die tolle gemeinsame Zeit in Kiel und die große private und berufliche Unterstützung bedanken.

Nicht minder aufregend waren die letzten Jahre für meine Familie. Ich danke besonders meinen Eltern Ines und Bernd, meinem Bruder Max und meinem Freund Fabi von ganzem Herzen für ihre Liebe, ihren Rückhalt und ihr Vertrauen.

12 Scientific Career

Name:	Susann Hüttl
Birth:	30th October 1985 in Gera
Residence:	Dorf 1, 24159 Kiel
Nationality:	german

PhD studies

Since 11/2010	PhD project in the working group of Prof. Dr. Paul Saftig, financed by the Sonderforschungsbereich 877 ("Proteolysis as a Regulatory Event in Pathophysiology")

Academic studies

03/2010 – 10/2010	Max-Delbrück-Centrum for Molecular Medicine Berlin-Buch - Master-Thesis, topic: "Sleeping Beauty transposition in mammalian cells"
03/2009 – 11/2010	Master studies in Biotechnology at the Brandenburg University of Technology Cottbus-Senftenberg - Degree: Master of Science
09/2008 – 01/2009	Department of Molecular Biology, Stockholm University, Sweden - Bachelor-Thesis, topic: "Homing endonucleases in bacteriophages"
09/2007 – 01/2008	Department of Biochemistry and Molecular Biology, University of Southern Denmark, Odense - Practical semester, topic: "Cloning, purification and characterization of a peptide substrate for the protein kinase CK2"
09/2005 – 02/2009	Bachelor studies in Biotechnology at the Brandenburg University of Technology Cottbus-Senftenberg - Degree: Bachelor of Science

Education

08/1998 – 06/2005	Oberschule „Am Elsengrund", Berlin - Graduation: University-Entrance Diploma
08/1992 – 08/1998	primary school